Agnes Rita Koller, BSc.

Investigations of ocean tide models in satellite gravimetry: Modeling minor tides and estimation of major tides from GRACE data

Master's Thesis

to achieve the university degree of
Diplom-Ingenieurin
Master degree programme: Geomatics Science

submitted to
Graz University of Technology

Supervisor:
Univ.-Prof. Dr.-Ing. Torsten Mayer-Gürr
Working Group Theoretical Geodesy and Satellite Geodesy of
Institute for Geodesy

Graz, Juni 2017

Acknowledgments

I want to thank my supervisor Univ.-Prof. Dr.-Ing. Torsten Mayer-Gürr for his continuous support, motivation and knowledge during my thesis.

Besides my supervisor, I would like to thank my family and my friends a lot, for believing in me and encouraging me all the time.

Thank you!

Eidesstattliche Erklärung

AFFIDAVIT

Ich erkläre an Eides statt, dass ich die vorliegende Arbeit selbstständig verfasst, andere als die angegebenen Quellen/Hilfsmittel nicht benutzt, und die den benutzten Quellen wörtlich und inhaltlich entnommenen Stellen als solche kenntlich gemacht habe. Das in TUGRAZonline hochgeladene Textdokument ist mit der vorliegenden Masterarbeit identisch.

I declare that I have authored this thesis independently, that I have not used other than the declared sources/resources, and that I have explicitly indicated all material which has been quoted either literally or by content from the sources used. The text document uploaded to TUGRAZonline is identical to the present master‘s thesis.

Graz, am _____ _____

Datum/Date Unterschrift/Signature

Abstract

As the system Earth is a dynamic one, ocean tides refer to the relocation of water masses relative to the sea floor as a result of tide generating forces. When modeling gravity field model (e.g. [10, ITSG-Grace2016]), several background models get subtracted during the data processing procedure. It pointed out, that one source of trouble is represented by the global ocean tide model (T. Mayer-Gürr, personal communication, May 2017). Therefore profound knowledge of ocean tides is required, to understand the dynamic system Earth.

Furthermore minor tides shall be computed with a new approach in this field of interest, instead of the standard linear admittance approach. In this thesis prediction of minor tides by least square collocation in application of collocation for the determination of minor ocean tides is presented. The developed approach is applied to major tides out of the FES2014, which are not available at the EOT11a model.

Since the EOT11a model is in use for the GRACE-only gravity field model [22, ITSG-Grace2016], this global ocean tide model gets compared with a newer assimilated one - the FES2014. Both ocean tide models are are provided in form of tidal maps. Those differences are also collated with residual major tidal constituents, estimated by diurnal solutions of GRACE.

Kurzfassung

Ozeangezeiten beziehen sich auf die Verlagerung von Wassermassen in Bezug auf den Meeresboden, da das System Erde dynamisch ist. Für die Bestimmung des statischen Gravitationsfeldes (z.B.: [10, ITSG-Grace2016]), müssen diverse Hintergrundmodelle vorab subtrahiert werden. Es stellte sich heraus, dass das globale Ozeangezeitenmodell einen großen Fehlereinfluss darstellen könnte (T. Mayer-Gürr, persönliches Gespräch, Mai 2017). Daher ist es wichtig, fundierte Kenntnisse über Ozeangezeiten zu haben, um das dynamische System Erde besser zu verstehen.

In weiterer Folge sollen kleinere Tiden mittels eines neuen Ansatzes berechnet werden, anstatt mit dem Ansatz der linearen Admittanz. In dieser Arbeit wird die Prädiktion von Gezeiten mittels Kollokation am Beispiel der Bestimmung von Ozeangezeiten präsentiert. Der entwickelte Ansatz wird angewandt auf jene Haupttiden des FES2014, welche nicht im EOT11a Modell verfügbar sind.Das globale Ozeangeitenmodell EOT11a wird als Hintergrundmodell für das GRACE-only Schwerefeld [22, ITSG-Grace2016] verwendet. Daher wird ebendieses gegen ein neueres assimiliertes Modell getestet - das FES2014. Beide Modelle stehen als tidal maps zur Verfügung. Die daraus berechneten Differenzen werden auch mit den residualen Haupttiden, welche aus täglichen GRACE Lösungen geschätzt werden, verglichen.

Contents

1 Introduction

Since oceans cover almost 71% of Earth's surface, they contribute a huge amount to model the dynamic system Earth. Therefore precise knowledge of ocean tides is crucial, because they cause of 75% of the sea level change.
Several ocean tide models exist, which are computed by different methods, but none of them do include observations of the satellite mission GRACE. This brings up the first question, if a known ocean tide model can be improve considerably, if more than 15 years observations of GRACE are considered in addition.
All models do provide a set of major tides, which represent about 95% of the the ocean tide magnitudes. The remaining 5% are represented by minor tides, which may also interfere the related major tide [1, Allain D.]. As yet they are computed under the assumption of linearity within several frequency bands. This is realized by the approach of linear, quadratic or spline admittance - depending on the ocean tide model. This thesis deals with the evaluation of this assumption. It's known, that some tidal constituents are highly correlated with some other, therefore it's necessary to do a detailed study about the questions - can improvements be achieved, if the known correlations of the modeled major tides are taken into account too.
The goal of this thesis is to estimate major constituents out of GRACE observations and developing a new approach to determine minor tides without the assumption of linearity.

The present thesis is structured in the following sections: Section 2 deals with the fundamentals of potential theory, the principle of least squares collocation and a brief overview of the satellite mission GRACE. The available and used ocean tide models are described in detail, including the specifications of the different data types of the given netCDF-files and of course the available different major tides.
In chapter 3 the theory of tides is discussed. It shows an overview of the different types of tides and a detailed explanation how they originate and the principle of modelling ocean tides (major and minor tides).
Section 4 deals with the proceeding of the available datasets of different ocean tide models, to retrieve individual tidal constituents in terms of equivalent water heights, which are following the IERS conventions 2010 [16]. Moreover minor tides, calculated by the admittance approach, are discussed.
In chapter 6 the estimation of long-periodic, diurnal and semi-diurnal residual tidal constituents from GRACE observations, to improve the EOT11a model, is discussed and validated.
Section 5.3 deals with the least squares collocation of minor tides in terms of equivalent water heights. Chapter 7 contains a summary and a conclusion of all received results, a statement of the developed method and last but nor least an outlook on possible prospective research.

2 Theoretical Background

This section deals with the theoretical background of the satellite mission GRACE, the used ocean tide models, the fundamentals of potential theory and the principle of collocation, which are used in this thesis.

2.1 GRACE

The **G**ravity **R**ecovery **A**nd **C**limate **E**xperiment - GRACE - gravity field satellite mission is a joint project of the National Aeronautics and Space Administration - NASA - and the Deutsches Zentrum für Luft- und Raumfahrt -DLR. It was launched in 2002 and it's accurately mapping variations in Earth's gravity field [22, Tapley].

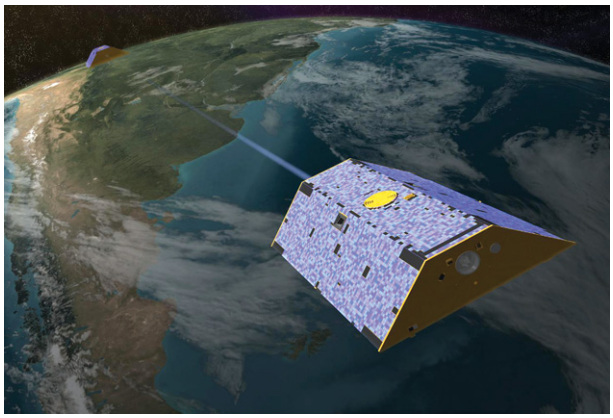

Figure 2.1: scenario of the GRACE mission source:

GRACE consists of two identical satellites - a twin satellite mission - in the same polar orbit (inclination of 89°) in a height of 500 kilometers (at the beginning of the mission) above Earth. The twin satellites are separated by a distance of round 220 km. This orbit configuration guarantees a global regular data distribution. A homogeneous data coverage can be obtained after a period of 30 days of observations.

Both satellites have a microwave distance measurement system (K-Band and Ka-Band). The measuerements principle is known as low-low satellite to satellite tracking (SST) system.The distance between the two satellites changes due to mass anomalies. To gather additional influences, which change the orbital parameters of GRACE, the mission has an accelerometer on board, to measure non-gravitational forces too. Additionally there are GPS receiver to measure the satellite's position to enable high-low satellite to satellite tracking [22, Tapley].

Because of possible determination of the time variable gravity field it seems to be meaningful to have a closer look on estimation of tidal constiutents using GRACE observations - if the aliasing problems allow it - see in more detail section 6.1.

2.2 Ocean tide models

In general there exist three different types of ocean tide models [9, Mazdak M.]:

- **pure hydrodynamic models:** dynamic equations are solved to derive tidal heights and currents consistent with predescribed physics,
- **assimilated models:** observations of ocean surface (e.g. altimetry) are used in additional to the pure hydrodynamic model (=assimilated models) and
- **empirical models:** only observations of oceans surface are used to determine tides.

In this thesis two out of three models are used - the empirical model EOT11a (see EOT11a in 2.2) and the assimilated model FES2014 (see FES2014 in section 2.2). similiar behaviour.

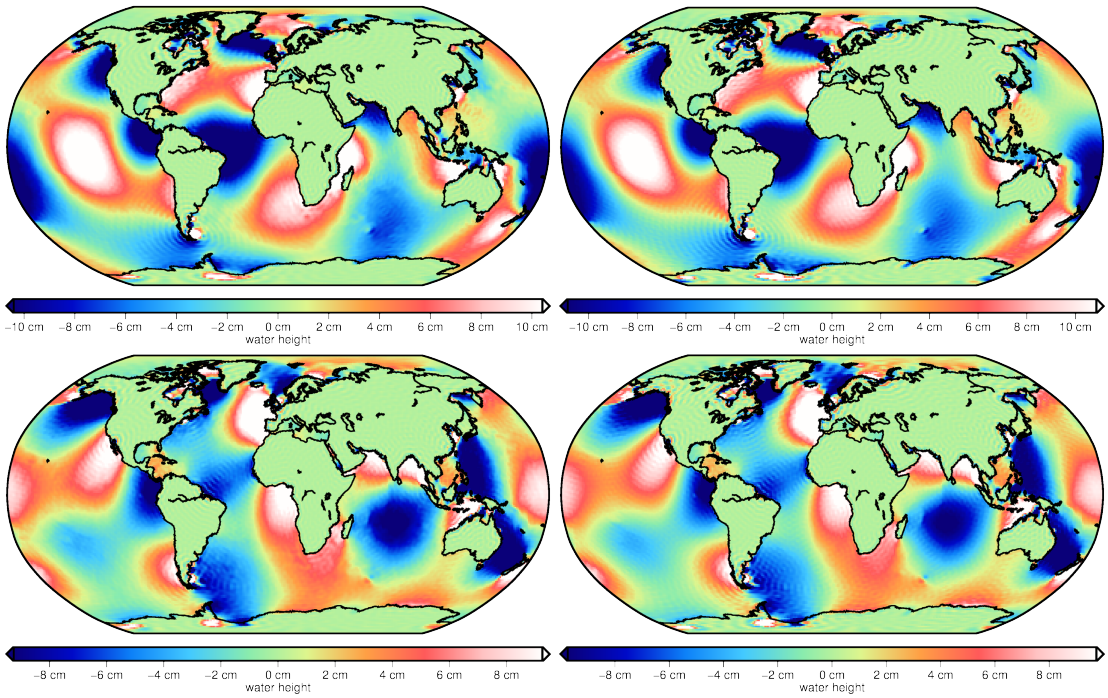

(a) EOT11a, cosine and sine **(b)** FES2014, cosine and sine

Figure 2.2: semi-diurnal constiuent N2 from EOT11a and FES2014

Figure 2.2 shows the semi-diurnal tide N2 in cosine and sine of both handled models.

At first appearance it shows, that the FES2014 model (right side) has a better resolution than the EOT11a model (left side). More differences will be disucussed in section 2.2.

EOT11a - Empirical Ocean Tide Model from Multi-Mission Satellite Altimetry

This model is a global solution for tidal constituents based on an empirical analysis of multi-mission satellite altimetry data (see Table 2.1). EOT11a provides a spatial resolution of 7.5'x 7.5'for all nineteen provided tidal constituents [17, Technical Note EOT11a].

Table 2.1: Overview of satellite alitimetry missions for EOT11a, [19, DGFI Report No.89]

Mission	Operation period [m.yy]	Latitude coverage [°]
TOPEX/Poseidon	09.92 – 10.05	±66.1
Jason-1	01.02 – 12.09	±66.1
Jason-2	07.08 – 04.10	±66.1
ERS-2	04.95 – 07.03	±81.5
ENVISAT	09.02 – 01.08	±81.5

The grids are stored as coards in NetCDF-3files. Each file has informations/data about number of nodes in west-east- and south-north-directions, longitudes and latitudes of grid nodes [°] , real part of tidal constants [cm] and imaginary part of tidal constants [cm] (see figure 2.3).

```
dimensions:
        x = 2881 ;
        y = 1441 ;
variables:
        float x(x) ;
                x:long_name = "Longitude" ;
                x:units = "degrees_east" ;
                x:actual_range = 0., 360. ;
        float y(y) ;
                y:long_name = "Latitude" ;
                y:units = "degrees_east" ;
                y:actual_range = -90., 90. ;
        float re(y, x) ;
                re:long_name = "ampl*cos(phas)" ;
                re:units = "cm" ;
                re:scale_factor = 1.f ;
                re:add_offset = 0.f ;
                re:_FillValue = NaNf ;
        float im(y, x) ;
                im:long_name = "ampl*sin(phas)" ;
                im:units = "cm" ;
                im:scale_factor = 1.f ;
                im:add_offset = 0.f ;
                im:_FillValue = NaNf ;

// global attributes:
                :Conventions = "COARDS, CF-1.0" ;
                :title = "EOT11a: 2N2 load tide " ;
                :source = "------" ;
                :node_offset = 0 ;
```

Figure 2.3: header-informations of netcdf file EOT11a

EOT11a includes the main astronomical tides Q_1, O_1, P_1, S_1, K_1, $2N_2$, N_2, M_2, S_2, K_2, the non-linear constituent M_4 ($2xM_2$), the long period tides M_m and M_f and four long periodic tidal waves (Ω_1, Ω_2, S_a and S_{sa}).

Table 2.2: list of main tides in EOT11a

Darwin notation	Doodson number	frequency[°/h]	Source
long period waves			
Ω_1	055.565	0.002206	HW95
Ω_2	055.575	0.004412	HW95
S_a	056.554	0.041066	HW95
S_{sa}	057.555	0.082137	HW95
M_m	065.455	0.544375	EOT11a
M_f	075.555	1.098033	EOT11a
M_{tm}	085.455	1.642407	FES2004
M_{sqm}	093.555	2.113928	FES2004
diurnal waves			
Q_1	135.655	13.398661	EOT11a
O_1	145.555	13.943036	EOT11a
P_1	163.555	14.958931	EOT11a
K_1	165.555	15.041069	EOT11a
semi-diurnal waves			
$2N_2$	235.755		EOT11a
N_2	245.655	28.439730	EOT11a
M_2	255.555	28.984104	EOT11a
S_2	273.555	30.000000	EOT11a
K_2	275.555	30.082137	EOT11a
quarter-diurnal waves			
$M4$	455.555		EOT11a

Two long periodic waves (M_{tm} and M_{sqm}) are further included to complete the tidal spectrum (see table 2.2). Those tidal constituents are taken from the Tide Generating Potential catalog (HW95 - [7]) or from the global oceantide model FES2004.

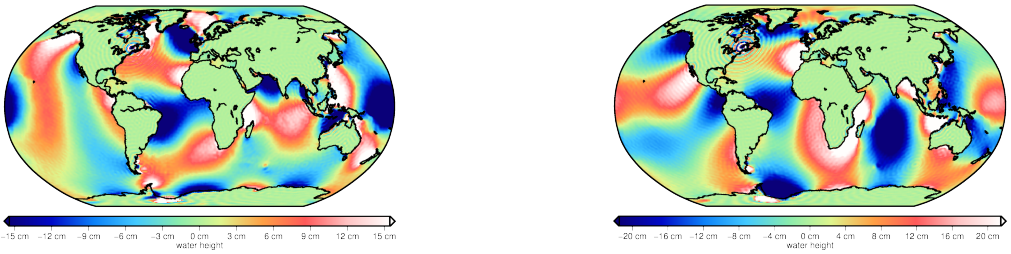

Figure 2.4: semi-diurnal constituent S2 derived from EOT11a in terms of water equivalent heights in cosine and sine

Minor tides are calculated by the approach of linear admittance.

FES2014 - Finite Element Solution

The global ocean tide model FES2014 uses a longer altimeter time series, compared to the empirical model EOT11a. Satellite altimetry observations are assimilated into a global hydrodynamic model. It provides a more accurate model in most of shallow water regions (source: www.aviso.com). Since the missions Jason-1(from cycle 262 on) and Topex/Poseidon (from cycle 369 on) are on their new orbit, those dates are also included into calculations. FES2014 provides a spatial resolution of 3.75'x 3.75'for all 27 tidal constituents.

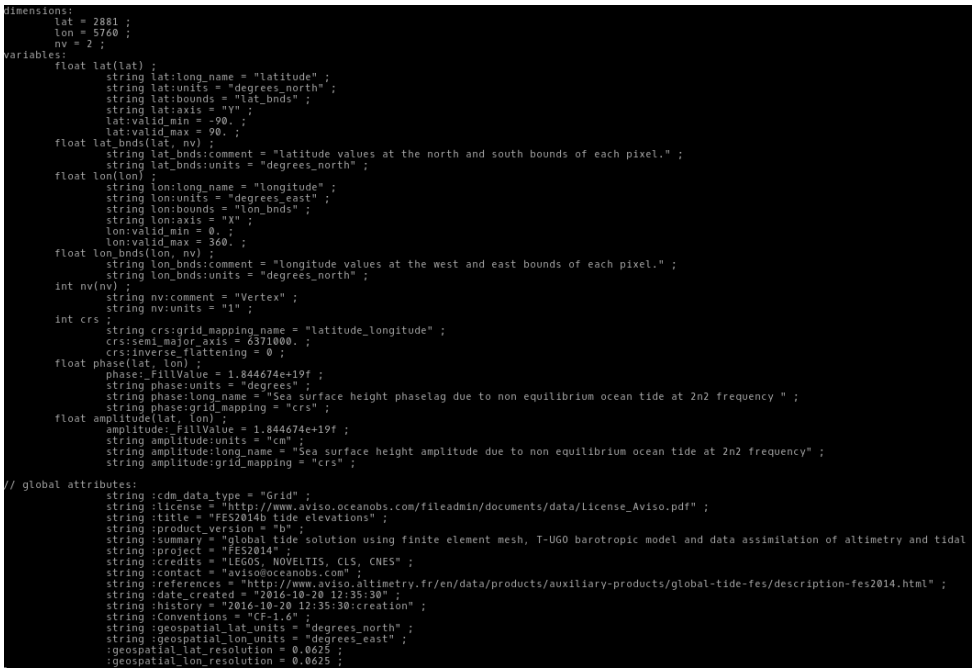

Figure 2.5: header-informations of netcdf file FES2014

The grids are stored as coards in NetCDF-4 files. Each file has informations/data about number of nodes in west-east direction and south-north-directions, longitudes and latitudes of grid nodes [°] , amplitude [cm] and phase [°] of tidal constituents (see figure 2.5). There are much more datasets stored in this file compared to the EOT11a netcdf files.

FES2014 provides one additonal diurnal tide (J_1) and eight additional semi-dirunal tides (ϵ_2, μ_2, ν_2, M_{KS2}, λ_2, L_2, T_2 and R_2), compared to EOT11a.

Table 2.3: list of additional main tides in FES2014 w.r.t. EOT11a

Darwin notation	**Doodson number**	**frequency[°/h]**
long period waves		
M_{sf}	073.555	0.544375
diurnal waves		
J_1	175.455	0.043293
semi-diurnal waves		
ϵ_2	227.555	
μ_2	237.555	0.0776897
ν_2	247.455	0.0792009
M_{KS2}	257.555	0.080739
λ_2	263.655	
L_2	265.455	0.0820239
T_2	272.556	0.0832193
R_2	274.556	
quarter-diurnal waves		
M_{N4}	445.655	0.1595109
M_{S4}	473.555	0.1638446
S_4	491.555	0.1666663
tre-diurnal waves		
M_3	355.555	

There are also one tre-dirunal tide (M_3 - 355.555), one shallow water overtide of principal lunar (M_6 - 655.555) and one eight-diurnal tides (M_8 - 855.555) provided. In total there are 34 tides available at the global ocean tide model FES2014.

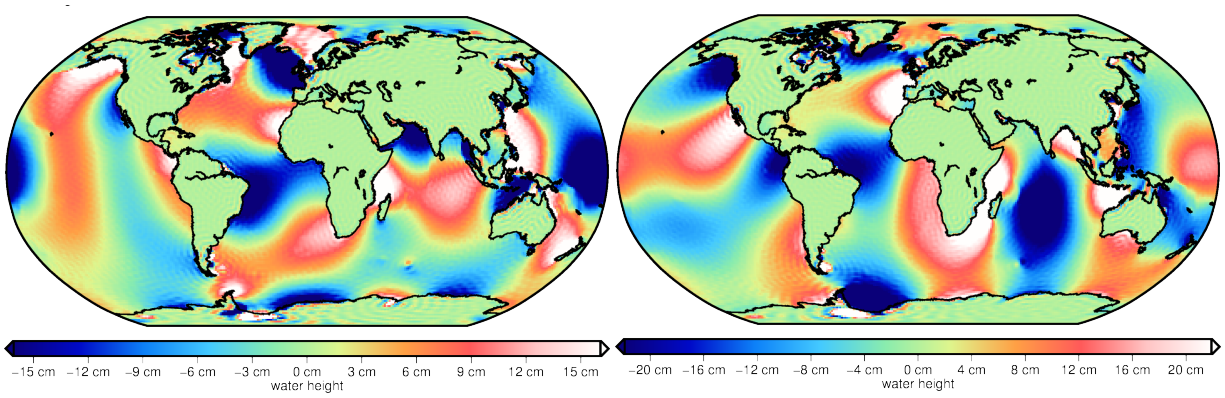

Figure 2.6: semi-diurnal constitutent S2 derived from FES2014 in terms of equivalent water heights in cosine and sine

2.3 Fundamentals of potential theory

The gravitational field is a conservative vector field. It can be described mathematically by Newton's law of universal gravitation, which implies that two distanced points attract each other with a force

$$f = G\frac{m_1 m_2}{l^2}\frac{\mathbf{l}}{l} \tag{2.1}$$

where $G = 6.6742 \cdot 10^{-11} m^3 kg^{-1} s^{-2}$ is Newton's gravitational constant, l represents the distance between the points centers and m_1, m_2 are the respective masses. This means, that all point masses attract an other point mass by a force directed along the distance between the interacting point masses. The force F is directly proportional to the two point's masses and inversely proportional to the square of the separation distance l^2. Since the attraction of the masses m_1 and m_2 is symmetrically, no distinguishing between the attracted mass and the attracting mass is necessary, which means, that the force is performed by the mass m on a unit mass of the point of view $P(x, y, z)$. Therefore equation (2.1) can be rewritten as

$$F(x, y, z) = G\frac{m}{l^2} = \nabla V. \tag{2.2}$$

Under consideration of all mass elements $dm(\xi,\ \eta,\ \theta)$ in a volume v and their local density ρ, equation (2.2) becomes an integral (Newton integral)

$$V(x, y, z) = G \int\int\int_{\nu} \frac{d\rho}{l} d\nu, \tag{2.3}$$

with the density of the volume $\rho = \frac{dm}{d\nu}$. Equation (2.3) requires the detailled knowledge of the density function. In reality it's just known for the upper layers of the Earth [21, Torge, 2001]

Spherical Harmonic Expansion of the Gravitational Potential

As already mentioned it's necessary to know the density function $\rho(r)$ of the earth to compute the gravitational potential V using equation (2.3). Assuming that the gravitational potential is a continuous function - outside the attracting masses - V is a solution of the Laplace equation

$$\Delta V = 0. \tag{2.4}$$

This solutions are called harmonic functions, hence the gravitational potential is a harmonic function outside the attracting masses [8, Hofmann-Wellenhof et al.].

It's common to express the potential V in terms of spherical harmonics

$$V(r, \lambda, \theta) = \frac{GM}{R} \sum_{n=0}^{\infty} \left(\frac{R}{r}\right)^{n+1} \sum_{m=0}^{n} c_{nm}\, C_{nm}(\lambda, \theta) + s_{nm}\, S_{nm}(\lambda, \theta) \tag{2.5}$$

with the geocentric constant GM, earth's radius R and the basis functions

$$\begin{aligned} C_{nm}(\lambda, \theta) &= \cos(m\lambda)\, P_{nm}(\cos\theta) \\ S_{nm}(\lambda, \theta) &= \sin(m\lambda)\, P_{nm}(\cos\theta). \end{aligned} \tag{2.6}$$

The respective associated Legendre functions $P_{nm}(\cos\theta)$ in formula (2.6) of degree n and order m can be computed by

$$P_{nm}(t) = \left(1 - t^2\right)^{m/2} \frac{d^m P_n(t)}{dt^m} \tag{2.7}$$

with $t = \cos\theta$. $P_n(t)$ are Legendre polynomials [8, Hofmann-Wellenhof et al].

2.4 Collocation

This sections deals with collocation - the least-squares prediction of a quantity. The basic idea of collocation is, that every geodetic observation can be split up into

1. a systematic part, which depends from unknown parameters (trend, Ax),
2. an irregular part, which expresses the influence of the gravitational disturbing potential

$$T = \frac{GM}{R} \sum_{n=0}^{\infty} \left(\frac{R}{r}\right)^{n+1} \sum_{m=0}^{n} c_{nm} C_{nm}(\lambda, \theta) + s_{nm} S_{nm}(\lambda, \theta) \tag{2.8}$$

   on the considered quantity (signal, t) and
3. random part (noise, n).

Hence, the basic mathematical model can be written as

$$l = Ax + t + n. \tag{2.9}$$

Equation (2.9) is visualized in figure 2.7 below:

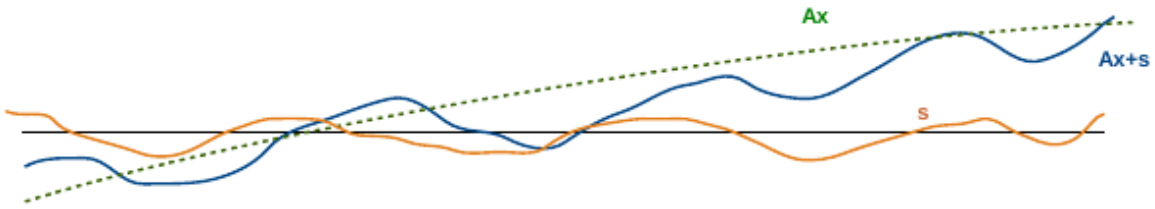

Figure 2.7: basic model collocation

In this thesis the scenario $A = 0$ and $n = 0$ is handled, therefore the observation equation changes to just on problem - estimating the signal t, to receive predicted quantities.

Generals

Many problems of gravimetric geodesy are formulated and solved in terms of integrals over the whole earth (e.g. Stokes formula). To solve those problems, measurements of the considered item must be theoretically available at every point of Earth's surface. This is practically not possible - either on land or at the ocean. Hence it's necessary to estimate functionals of the disturbing potential nor the disturbing potential itself for other points of Earth's surface. Especially in oceanic regions extrapolations beside interpolations are required. As said by Hofmann-Wellenhof and Moritz in physical geodesy [8]:

> Prediction (i.e., interpolation or extrapolation) cannot give exact values; hence, the problem is to estimate the errors that are to be expected in the gravity g or in the gravity anomaly Δg.

This begs following questions:

- How accurate are the prediction methods (estimation errors of e.g. δg)?
- What influence does the prediction error have on derived quantities?
- What is the best prediction method?

Therefore it's necessary to have a closer look on statistical treatment, because those errors/problems which are mentioned above, can be described by one function - the covariance function.

Accuracy of prediction methods

One functional of the disturbing potential $l = \mathcal{F}\{T\}$ at point P can be calculated by a linear combination of all other measurements.

$$\tilde{l}_P = \mathcal{F}\{l_i\} = \sum_{i=1}^{n} \alpha_{Pi} \cdot l_i \tag{2.10}$$

The task is to determine α_{Pi} in a kind of way, that they represent a minimum, therefore it has to be considered the quadratic prediction error

$$\epsilon_P^2 = (l_P - \tilde{l}_P)^2 = (l_P - \sum_{i=1}^{n} \alpha_{Pi} \cdot l_i) \cdot (l_P - \sum_{k=1}^{n} \alpha_{Pk} \cdot l_k). \tag{2.11}$$

The expansion of the product in (2.11) gives

$$\epsilon_P^2 = l_P^2 - 2 \sum_i \alpha_{Pi}\, l_P\, l_i + \sum_i \sum_k \alpha_{Pi}\, \alpha_{Pk}\, l_i\, l_k. \tag{2.12}$$

By applying the average operator $\mathcal{M}\{\cdots\}$ on equation (2.12) and Einstein's summation convention, the result is

$$m_P^2 = C_0 - 2\alpha_{Pi}\, C_{Pi} + \alpha_{Pi}\, \alpha_{Pk}\, C_{ik} \quad \text{with} \tag{2.13}$$

$$\begin{array}{lcl} m_P^2 & = & \mathcal{M}\{\epsilon_P^2\}, \\ C_0 \equiv C(0) & = & \mathcal{M}\{l_P^2\}, \\ C_{Pi} \equiv C(Pi) & = & \mathcal{M}\{l_P\, l_i\}, \\ C_{ik} \equiv C(ik) & = & \mathcal{M}\{l_i\, l_k\}. \end{array} \tag{2.14}$$

Equation (2.13) is the basic formula for the standard error of the prediction formula (2.10) above, where C_{Pi} is the covariance between observations and the quantity which shall be predicted and C_{ik} is the covariance between known quantities.

Thus it could be shown, that the covariance function is essential to determine the accuracy of prediction methods.

Least - squares prediction of functionals of the disturbing potential

Section 2.4 dealed with the accuracy of prediction methods and forms the basis for collocation. The values α_{Pi} can be obtained by minimizing the standard error of the prediction formula (2.13),

$$\frac{\partial m_P^2}{\partial \alpha_{Pi}} = -2\, C_{Pi} + \alpha_{Pk}\, C_{ik} \tag{2.15}$$

Rearranging equation (2.15) yields to

$$\alpha_{Pk} = C_{ik}^{-1} C_{Pi}\,, \tag{2.16}$$

which represents the solution of formula (2.15) , which is a system of linear equations with unknown α_{Pk}. Substituting formula (2.16) into formula (2.10), gives

$$\tilde{l}_P = \alpha_{Pk} l_i = C_{ik}^{-1} C_{Pi}\, l_k \tag{2.17}$$

in matrix-notation. This fundamental formula for least-squares prediction shows, that it is necessary to know statistical behavior of the quantities through the covariance function, to estimate functionals of the disturbing potential T.

Covariance function

As shown before (see section 2.4), the covariance function

$$C(\Delta s) \equiv cov_{\Delta s}\{l\} \; = M\{l \cdot l'\} \quad \text{with} \tag{2.18}$$

$cov_s\{\}$	operator of covariance
$M\{\}$	operator of mean
$\Delta\omega$	frequency
l	observation (functional of T)

has great importance for predicting functionals of the disturbing potential. The covariance function depends on the distance differences Δs. .

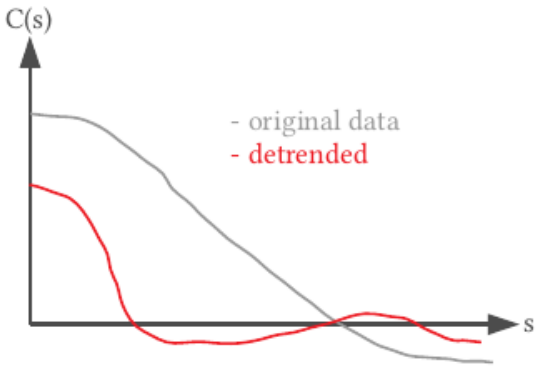

Figure 2.8: The covariance function

In figure 2.8 can be seen, that the covariance function decreases with increasing distance differences. The observations become more and more independent. The highest peak in the figure above represents the mean variance

$$C(0) \equiv var\{l\} \; = \mathcal{M}\{l \cdot l\} \tag{2.19}$$

of all considered observations l.

The input data have to be without any trend and mean value. The determination of the covariance function is problematic, hence it can be estimated only from available samples (e.g. measurements of gravity anomalies or like treated in this thesis, in terms of equivalent water heights).

For Earths surface on land, there are estimations of covariance functions available (e.g. Kaula - 1959, Hirvonen - 1962, Tscherning-Rapp model - 1974, Kühtreiber 2002).

The mentioned covariance functions are available in a global and also local way for free-air anomalies or gravity anomalies. Field of interests mainly are regional geoid determinations or regional Moho-estimations as done in several projects, but there is none for estimating minor tides in frequency domain.

3 Theory of Tides

Tidal movements (verical and horizontal) are caused by gravitational attraction of celestial bodies, in particular by the Moon and the Sun. This attraction can be expressed mathematically by Newtons's law of gravitation, which is described in detail in section 3.1. The Earth responses to the acting forces by means of various deformations, principled following different types of tides exist [2, lecture notes GGOS]:

- **Solid earth tides** are defined as the response of the solid Earth (deformation of land-masses) on external - direct forces (caused by Sun and Moon).
- **Ocean tides** are the relocation of water masses relative to the sea floor caused by tidal forces.
- **Ocean tide loading** is defined as the response of the solid Earth (seafloor and coastal areas) and on the relocation of ocean masses caused by ocean tides. Hence it's an indirect effect. It causes two differents effects - the deformation of Earth's crust and changes of the gravitational potential.
- **Elastic ocean tides** represent the sum of ocean tides and ocean tide loading.
- **Earth tides** are defined by the sum of solid Earth tides and ocean tide loading, therefore they are also called total deformation of the Earth.
- **Atmospheric tides:** represent pressure fluctations in the atmosphere.

All deformations lead to a disturbance in the gravitational potential. Furthermore can be distinguished between astronomic waves, radiational waves and non-linear waves. The former are generated by the gravitational attraction by sun and moon (e.g. M_2). The latter ones are generated by cyclic geophysical phenomens (e.g. atmosphere - S_2) and last the non-linear-waves are generated by a non-linear interaction of several waves. It has to be mentioned, that all tidal constituents have non-linear components [20, Schureman P.].

For example the tidal constituent S_2 belongs to all three wave types mentioned above.

3.1 Tidal acceleration

Due to gravitational attraction of celestial bodies, tidal forces arise. Tides are periodic motions of the solid or fluid Earth. The Moon has the biggest influence, because comapred to the other celestial bodies, his distance to Earth is the smallest. Therefore the schmeatic scenario for tides in system Earth-Moon is shown in the illustration below.

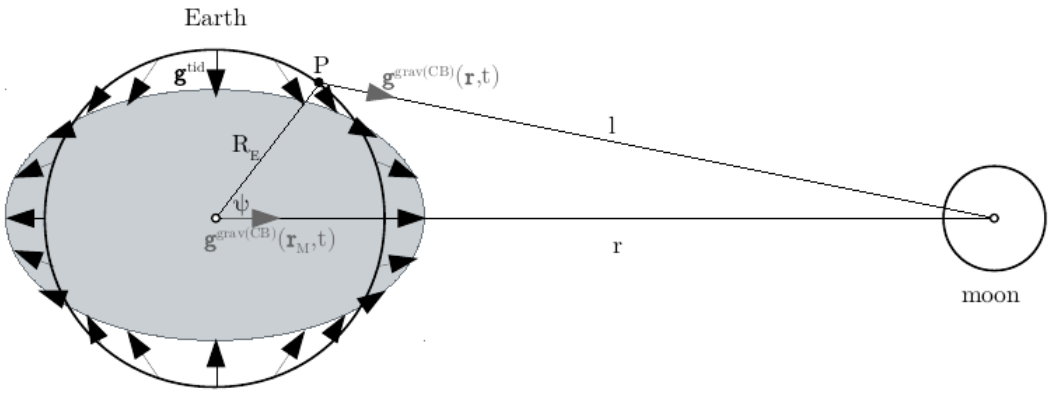

Figure 3.1: schematic tidal force acting on a point of the Earth's surface due to the moon

According to Newton's law of gravitation, the acceleration $\mathbf{g}^{grav(CB)}(\mathbf{r})$ on a point P on Earth's surface in direction of l caused by a celestial body (CB) is

$$\mathbf{g}^{grav(CB)}(\mathbf{r}) = \frac{GM_{CB}}{l^2}\frac{\mathbf{r}_{CB} - \mathbf{r}_P}{l} \tag{3.1}$$

where G is the gravitational constant, M_{CB} the mass of the attracting body , r_{CB} and r_P are the position vectors of the center of mass of the CB and the point P on Earth's surface. Arising thereby $l = |r_{CB} - r_P|$ is the distance between the points mentioned before.

The tidal acceleration g^{tid} in point P is defined as the difference between the gravitational attraction of CB in P and the acceleration of Earth's center of mass $\ddot{r}_M$. Due to Earth's rotation and the orbital motion as well, the tidal acceleration depends on time and can be written as

$$\mathbf{g}^{tid}(\mathbf{r}, t) = \mathbf{g}^{grav(CB)}(\mathbf{r}, t) - \ddot{r}_M(t). \tag{3.2}$$

The acceleration of the Earth's center of mass $\ddot{r}_M$ can be approximated by $g^{grav(CB)}(r_M, t)$ and this yields to

$$\mathbf{g}^{tid}(\mathbf{r}, t) = \mathbf{g}^{grav(CB)}(\mathbf{r}, t) - \mathbf{g}^{grav(CB)}(\mathbf{r}_M, t) \tag{3.3}$$

Caused by the huge distance, the gravitational field can be assumed to be radially symmetric. Hence the tidal acceleration can be written as

$$\mathbf{g}^{tid}(\mathbf{r}, t) = -GM_{CB}\frac{\mathbf{r} - \mathbf{r}_{CB}}{\| \mathbf{r} - \mathbf{r}_{CB} \|^3} + \frac{GM_{CB}}{GM}\mathbf{g}(\mathbf{r}_{CB}). \tag{3.4}$$

3.2 Tide Generating Potential

To calculate functionals of the tidal potential ephemerides of the celestial bodies can be used, or the tidal potential can be expended into spherical harmonics. The first noted method is restricted to precise applications [24, Wenzel], the second method is used and described in this thesis.

Considering computing equation (3.3) on every point of Earth's surface, a gravitational force vector field comes into existence, which is conservative. Hence the tidal acceleration $\mathbf{g}^{tid}(\mathbf{r},t)$ can be expressed as gradient of the gravitational potential V^{tid} (compare 2.3).

$$\mathbf{g}^{tid}(\mathbf{r},t) = \operatorname{grad} V = \nabla V^{tid} \tag{3.5}$$

and represents the direct link between the tidal acceleration (3.3) and the tide generating potential. Equation 3.5 satisfies the Laplace equation

$$\nabla V^{tid} = 0, \tag{3.6}$$

since the potential is considered to be a harmonic function outside the attracting masses. In case of point masses this yields to

$$V^{tid}_{CB_i}(\mathbf{r},\mathbf{t}) = -GM_{CB}\left(\frac{\mathbf{r}\cdot\mathbf{r}_{CB}}{\parallel \mathbf{r}_{CB} \parallel^3} - \frac{1}{\parallel \mathbf{r} - \mathbf{r}_{CB} \parallel^3}\right) \tag{3.7}$$

and can be expanded into a series of spherical harmonics

$$V^{tid}_{CB_i}(\mathbf{r},t) = \frac{GM_{CB_i}}{r_{CB_i}} \sum_{n=2}^{\infty}\sum_{m=0}^{n} \frac{1}{2n+1}\left(\frac{r}{r_{CB_i}}\right)^n \bar{P}_{nm}(\cos\theta)\bar{P}_{nm}(\cos\theta_{CB_i})(\bar{c}^{tid}_{nm}\cos m\lambda + \bar{s}^{tid}_{nm}\sin m\lambda). \tag{3.8}$$

which represents the tide generating potential. The function depends on the mass and the position of the celestial body.

The tide generating potential is dominated by terms of degree $n = 2$

$$\begin{aligned} V^{tid,2}_{CB_i}(r,\theta,\lambda,t) = \; & \tfrac{1}{5}GM_{CB_i}\tfrac{r^2}{r^3_{CB_i}} \; [\bar{P}_{20}(\cos\theta)\bar{P}_{20}(\cos\theta_{CB_i}) \\ & + \bar{P}_{21}(\cos\theta)\bar{P}_{21}(\cos\theta_{CB_i})\cos(\lambda-\lambda_{CB_i}) \\ & + \bar{P}_{22}(\cos\theta)\bar{P}_{22}(\cos\theta_{CB_i})\cos(2(\lambda-\lambda_{CB_i}))] \end{aligned} \tag{3.9}$$

The term $\lambda - \lambda_{CB_i}$ has a period of approximately one day, caused by the Earth's rotation. There exists also a permanent zonal term

$$V^{tid,2}_{CB_i}(r,\theta,\lambda) = \frac{GM_{CB_i}}{4}\frac{r^2}{r^3_{CB_i}}(1-3\cos\theta), \tag{3.10}$$

which is independent of time, since it's just dependend on the observed point on the Earth and not - in contrast to the time dependent part - on the position of the celestial body.

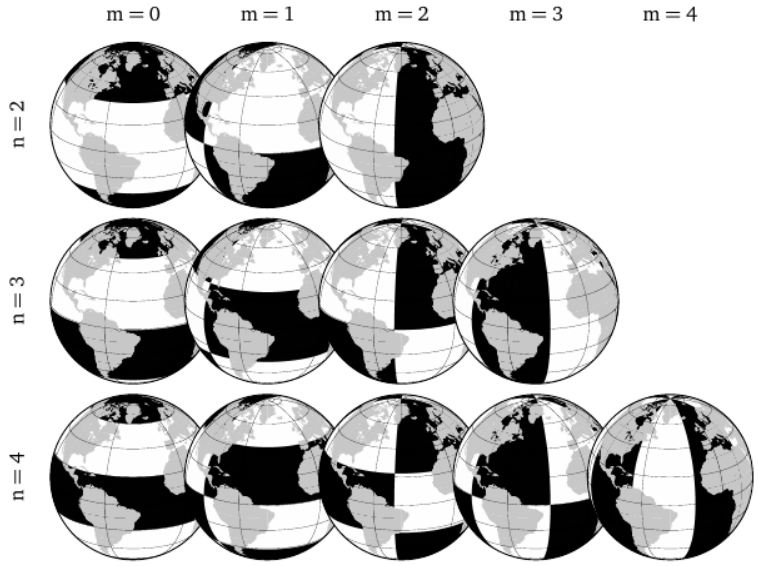

Figure 3.2: illustration of spherical harmonics up to D/O 4 [9, Mazdak M.,]

The zonal parts ($m = 0$) reflects the long-periodic tides, which have a maximum at the pole. The tesseral term ($m = 1$) reflects the diurnal tides with a period of one day and shows a maximum at $\pm 45°$ latitude. The semi-diurnal tides are reflected by the sectorial term ($m = 2$) and have a period of half a day and have a maximum at the equator [24, Wenzel].

Caused by the time dependence of the celestial body's position - see section 3.1 - it's quite difficult to model tides by equation (3.9). Therefore investigations have been done to express the time dependency by orbital parameters of the celestial body. The first research is done by Darwin, but his development was not harmonic, because the amplitudes and phases changed within time. Arthur Doodson accomplished it first, to originate harmonic algebraic expansion - under considerations of Newcomb and Brown - which was sufficient enough for former calculations [4, Cartwright] (see in detail in section 3.3).

harmonic representation of the tide generating potential

Since celestial dynamics according to periodic behaviour, an expansion of $V_{CB_i}^{tid}$ in a Fourier series is possible:

$$V_{CB_i}^{tid}(r,\theta,\lambda,t) = \sum_{n=2}^{\infty}\sum_{m=0}^{n}\left(\frac{r}{R}\right)^n P_{nm}(\cos\theta)\sum_j\left(c_{nm,j}^{tid(CB_i)}\cos(arg_j(t)) + s_{nm,j}^{tid(CB_i)}\sin(arg_j(t))\right), \tag{3.11}$$

because the tide generating potential is composed of j superposed waves [2, lecture notes GGOS, 2012]. The amplitudes $c_{nm,j}^{tid(CB_i)}$ and $s_{nm,j}^{tid(CB_i)}$ and the argument

$$arg_j(t) = \Phi_j + \omega_j t \tag{3.12}$$

represent an individual wave. Φ_j and ω_j denote the phase and the frequency. The dependency of the evaluation point is contained in the argument.

3.3 Astronomical arguments

The harmonic development of the tide generating potential is fundamental for tidal analysis. Charles Darwin developed some harmonic constants, which yields to discrepancies between observations and predictions of tides. Therefore Arthur Doodson gained luni-solar elements to describe the position of the celestial body with respect to the Earth subjected to time. [5, Doodson]

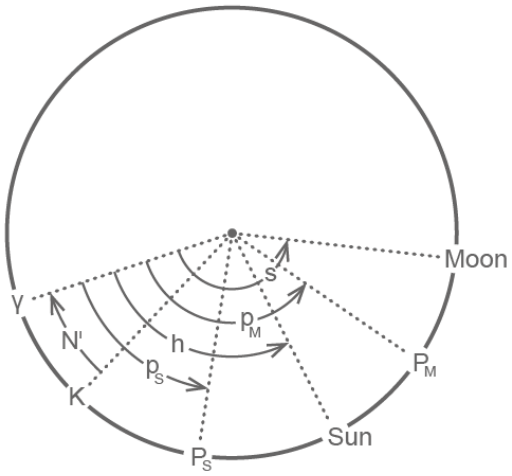

Figure 3.3: Doodson arguments

As described in section 3.2, the time-dependecy of the evaluation point (longitude of the celestial body) can be described by the phase and the amplitude. The results of his investigations are, that phases and frequencies of each individual tide can be expressed by an integer linear combination

$$\Phi_j = \sum_{l}^{6} k_{j,l} \Phi_l \tag{3.13}$$

and

$$\omega_j = \sum_{l}^{6} k_{j,l} \Omega_l \tag{3.14}$$

of so called luni-solar Doodson elements, which are shown in illustration 3.3. The six independet variables of table 3.1 are describing the relative positions of the Sun and the Moon with respect to the Earth. The mean longitude of the moon s, the longitude of the lunar perigee p and the longitude of the ascending lunar ascending node N' describe the lunar orbit.

The mean longitude of the Sun h and the longitude of the solar perigee p_s specify the solar orbit. The local mean lunar time τ is the dominating part of the Doodson elements, it contains the Earth's rotation and dominates the classification of the tidal constituents.

Table 3.1: periods and definitions of the luni-solar Doodson elements at J2000.0, with d denoting a mean solar day, a denoting tropical year

Element	Period	Definition
τ	1.0351d	local mean lunar time
s	27.322 d	mean longitude of the moon
h	1 a	mean longitude of the sun
p	8.847 a	longitude of the lunar perigee
$N' = -\Omega$	18.613 a	longitude of the ascending node of the moon
p_s	20936 a	longitude of the solar perigee

The Doodson elements can be computed by

$$\begin{aligned} \tau &= 15°t + h - s - L \\ s &= 277.0248° + 481267.8906°T + 0.0020°T^2 + \cdots \\ h &= 280.1895° + 36000.7689°T + 0.0003°T^2 + \cdots \\ p &= 334.3853° + 4069.0340°T - 0.0103°T^2 + \cdots \\ N' &= 100.8432° + 1934.1420°T - 0.0021°T^2 + \cdots \\ p_s &= 281.2209° + 1.7192°T + 0.0005°T^2 + \cdots \end{aligned} \tag{3.15}$$

where T is Julian centuries since January 1, 1990 at midnight in Greenwich and t is the Greenwich mean solar time (GST) [5, Doodson].

According to equations (3.12) - (3.14) the argument can be calculated for each individual tide by

$$arg_j(t) = k_{j,1}\,\tau(t) + k_{j,2}\,s(t) + k_{j,3}\,h(t) + k_{j,4}\,p(t) + k_{j,5}\,N'(t) + k_{j,6}\,p_s(t). \tag{3.16}$$

The coefficient $k_{j,1}$ is identical to the order m of the tide generating potential, hence those coefficients can be classified just like the tide generating potential in equation (3.9).

The coefficient $k_{j,1} = 0$ represent the long-periodic part of tides, it's independent of τ. The diurnal tides depent on 1τ and are represented by the coefficient $k_{j,1} = 1$. If the coefficient $k_{j,1}$ has the numerical value 2, it performs the semi-diurnal tides and is dependent on 2τ. The remaining coefficients $(k_{j,2} \ldots k_{j,6})$ can be either positive or negative. To avoid negative numbers, each of them get added the value five, this yields to $d_{j,l} = k_{j,l}+5$. The coefficient $d_{j,1} = k_{j,1}$.

Each individual tides are represented by the Doodson code:

$$d_{j,1}d_{j,2}d_{j,3}.d_{j,4}d_{j,5}d_{j,6}. \tag{3.17}$$

For example the diurnal lunar tide K_1 can be written as 165.555.

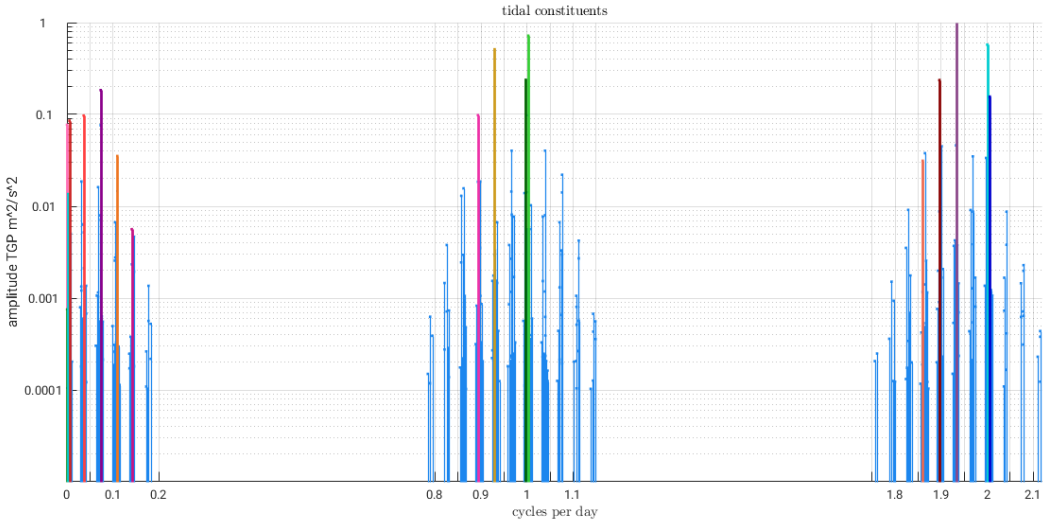

Figure 3.4: tidal spectrum from the HW95 tidal potential catalog in all three frequency bands

The amplitudes and frequencies of each tidal constituents can be retaliated in luni-solar tidal catalogs, i.e. of Hartmann and Wenzel [7, 1995]. 12932 tidesare listed; the expansion in spherical harmonics for the Moon is six and three for the Sun (see table 3.2).

Table 3.2: luni-solar tidal catalogs [24, Wilhelm (1997)], [18, RATGP95]

catalog	**#tides**	**D/O Moon**	**D/O Sun**
Doodson (1921)	377	3	2
Cartwright et al. (1971, 1973)	505	3	2
Büllesfeld (1985)	656	4	2
Tamura (1987)	1200	4	3
Xi(1989)	3070	4	3
Tamura (1993)	2060	4	3
Roosbeek(1996)	6499	5	3
Hartmann & Wenzel (1995a,b)	12932	6	3

3.4 Ocean tides

Ocean tides refer to the relocation of water masses (motion of the ocean's surface) relative to the sea floor as a result of tide generating forces. These deformations lead to a disturbance in the potential. The reaction of the ocean to the tide generating potential can be described by tidal heights at a point on the Earth at a specific time t

$$\zeta(\lambda, \phi, t) = \sum_s \xi_s(\lambda, \phi) \cos\left[\Theta_s(t) + \chi_s - \delta_s(\lambda, \phi)\right] \tag{3.18}$$

which are frequency dependent and can be represented by the correspondending amplitude ξ_s and phase δ_s. The subscript s denotes a single tidal wave. The Doodson argument Θ_s can be computed easily by formula 3.16. The term χ_s is the Doodson-Wartburg phase correction

$$\chi_s = \begin{cases} 0 & \text{for semi-diurnal and longperiodic tides: } d_{1,s} = 0, 2 \\ \frac{\pi}{2} & \text{for diurnal tide } K_1 \text{ (165.555)} \\ -\frac{\pi}{2} & \text{for remaining diurnal tides: } d_{1,s} = 1 \end{cases} \tag{3.19}$$

as defined in the IERS conventions 2010 [16]. Hence a single tidal height at a specific point on Earth can be written as

$$\zeta_s = \xi_s \left[\cos(\delta_s) \cos(\Theta_s + \chi_s) + \sin(\delta_s) \sin(\Theta_s + \chi_s)\right]. \tag{3.20}$$

The particular products of the amplitude ξ_s and the term in the bracket - containing the phase δ_s, can be expanded into spherical harmonics [6, Dow (1988)]

$$\begin{aligned} \xi_s \cos(\delta_s) &= \sum_{n=0}^{\infty} \sum_{m=0}^{n} \left(a_{nm,s} \cos m\lambda + b_{nm,s} \sin m\lambda\right) P_{nm}(\sin \Phi) \\ \xi_s \sin(\delta_s) &= \sum_{n=0}^{\infty} \sum_{m=0}^{n} \left(c_{nm,s} \cos m\lambda + d_{nm,s} \sin m\lambda\right) P_{nm}(\sin \Phi), \end{aligned} \tag{3.21}$$

where the coefficients $a_{nm,s}$, $b_{nm,s}$, $c_{nm,s}$ and $d_{nm,s}$ represent the spherical harmonics coefficients. The associated Legendre polynomials P_{nm} can be calculated by equation (2.7).

Combining equation (3.21) and (3.20), doing some rearranging and applying trigonometric theorems, yields to [17, TN36]

$$\zeta_s = \sum_{n=0}^{\infty} \sum_{m=0}^{m} \sum_{+}^{-} \left[C^{\pm}_{nm,s} \cos(\Theta_s + \chi_s \pm m\lambda) + S^{\pm}_{nm,s} \sin(\Theta_s + \chi_s \pm m\lambda)\right] P_{nm}(\sin \Phi) \tag{3.22}$$

with the coefficients

$$\begin{aligned} C^{\pm}_{nm,s} &= \hat{C}^{\pm}_{nm,s} \sin(\epsilon^{\pm}_{nm,s}) = \tfrac{1}{2}\left(a^{\pm}_{nm,s} \mp d^{\pm}_{nm,s}\right) \\ S^{\pm}_{nm,s} &= \hat{C}^{\pm}_{nm,s} \cos(\epsilon^{\pm}_{nm,s}) = \tfrac{1}{2}\left(c^{\pm}_{nm,s} \mp b^{\pm}_{nm,s}\right). \end{aligned} \tag{3.23}$$

where $\hat{C}^{\pm}_{nm,s}$ are the amplitudes and $\epsilon^{\pm}_{nm,s}$ are the phases.

The effect of the relocation of water masses relative to the seafloor on Earth's gravitational potential can be described by

$$\Delta V^O_s = \frac{GM}{R} \sum_{n=0}^{\infty} \left(\frac{R}{r}\right)^{n+1} \sum_{m=0}^{m=n} \left[\Delta c_{nm,s} \cos m\lambda + \Delta s_{nm,s} \sin m\lambda\right] P_{nm}(\sin \Phi). \tag{3.24}$$

where GM is the geocentric gravitational constant and R the radius of the Earth. The dimensionless potential coefficients or Stokes coefficients $\Delta c_{nm,s}$ and $\Delta s_{nm,s}$ can be obtained by

$$\begin{aligned}\Delta c_{nm,s} &= \tfrac{4\pi R^2\rho_w}{M}\tfrac{1+k'_n}{2n+1}\left[(C^+_{nm,s}+C^-_{nm,s})\cos(\Theta_s+\chi_s)+(S^+_{nm,s}+S^-_{nm,s})\sin(\Theta_s+\chi_s)\right]\\ \Delta s_{nm,s} &= \tfrac{4\pi R^2\rho_w}{M}\tfrac{1+k'_n}{2n+1}\left[(S^+_{nm,s}+S^-_{nm,s})\cos(\Theta_s+\chi_s)-(C^+_{nm,s}+C^-_{nm,s})\sin(\Theta_s+\chi_s)\right]\end{aligned} \tag{3.25}$$

to calculate the mass redistribution effect of ocean tides on the Earth's gravitational potential (with ρ_w is the water density and k'_n the load love numbers). Since the load love k'_n numbers are the ratio between the loading the resultant disurbances [15], the factor $1+k'_n$ denotes the mass effect of ocean tides and the deformation of the solid Earth as well [17, TN36]. The coefficients, amplitudes and phases can be obtained from the relations of formulas in equation (3.23).

3.5 Theory of Admittance

In global ocean tide models only major tides of the tidal spectrum are determined, but there exist lots more minor tides, which should not be neglected, because their influences are significant. Hence minor tides have to be interpolated related to main tides by response analysis method (Munk & Cartwright, 1966). This methodology allows a connection between main tides and minor tides - the qoutient of input (tidal potential) and output defines the admittance

$$Z(\omega) = \frac{H(\omega)}{G(\omega)}, \tag{3.26}$$

where $H(\omega)$ is the tidal height and $G(\omega)$ the tidal potential and is assumed to be a smooth function of frequency within the same frequency band. Based on this method unknown admittances of minor tides can be determined from those major tides, which are given in the global tide model (e.g. EOT11a - see table 2.2). Figure 3.5 below shows schematically how to linearly interpolate one minor tide by two known major tides. In general minor tides will be interpolated separately for each frequency band (diurnal, long-periodic and semi-diurnal) to ensure a small frequency-span, so the regression is not skewed. Hence the assumption of linear variations between closely spaced tidal frequencies is still valid.

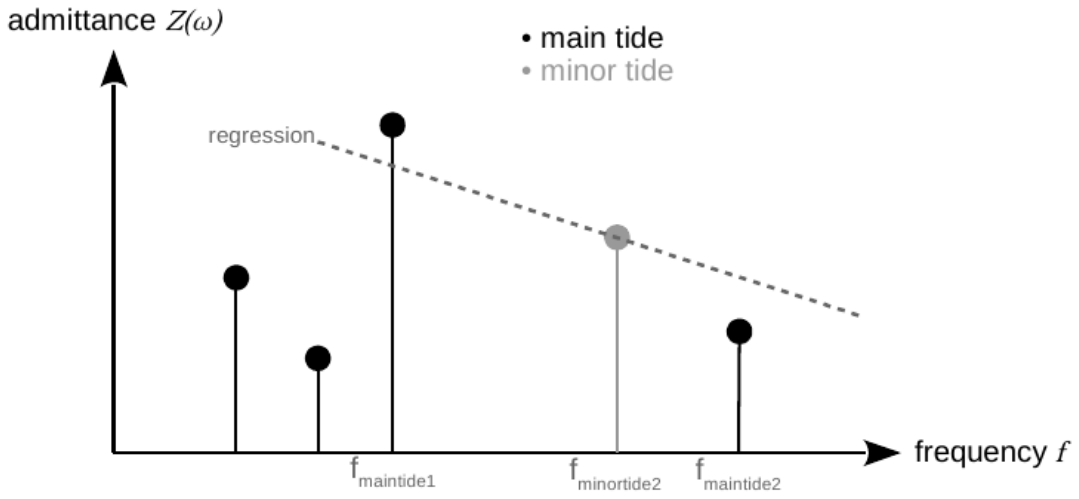

Figure 3.5: schematic illustration of the theory of admittance by linearly interpolating one minor tide by two main tides based on [3, Baur O.]

The interpolations coefficients can be calculated by a weighted average:

$$Z_s = \left(\frac{\omega_1 - \omega_s}{\omega_2 - \omega_1}\right)\frac{H_1}{G_1} + \left(\frac{\omega_s - \omega_1}{\omega_2 - \omega_1}\right)\frac{H_2}{G_2}\ , \text{ with} \tag{3.27}$$

$\omega_{1,2}$	tidal frequencies of main tides
ω_s	tidal frequency of minor tide
$G_{1,2}$	tidal potential main tides
$H_{1,2}$	tidal height main tides.

Rearranging equation (3.27) with respect to equation (3.26) leads to the following formula for interpolated tidal heights:

$$H_s = \left(\frac{\omega_1 - \omega_s}{\omega_2 - \omega_1}\,\frac{G_s}{G_1}\right) H_1 + \left(\frac{\omega_s - \omega_1}{\omega_2 - \omega_1}\,\frac{G_s}{G_2}\right) H_2 \tag{3.28}$$

The product of the quotient of the differences of frequencies and the quotient of the tidal potential are denoted as scalar weighted interpolating coefficients

$$\begin{aligned} a_{s,oceanTideModel} &= \frac{\omega_1 - \omega_s}{\omega_2 - \omega_1}\,\frac{G_s}{G_1} \\ b_{s,oceanTideModel} &= \frac{\omega_s - \omega_1}{\omega_2 - \omega_1}\,\frac{G_s}{G_2}. \end{aligned} \tag{3.29}$$

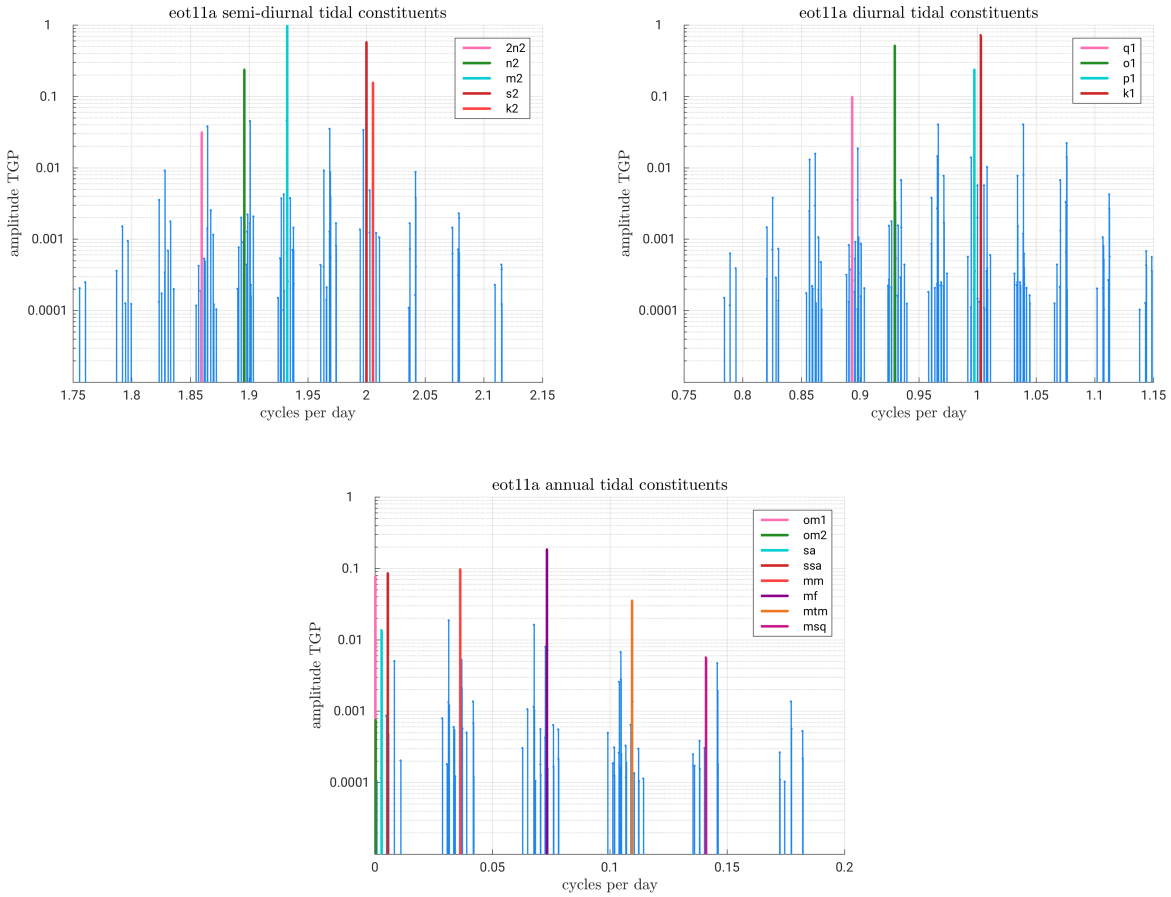

Figure 3.6: linearly interpolated minor tides from EOT11a w.r.t. HW95 catalog

Figure 3.6 shows the tidal spectrum of FES2014. The main tides, which are available at the model are drawn in colour. The IERS Conventions suggest using a linear admittance based on the assumption of linear variations between closely spaced tidal frequencies (see [16, IERS Technical Note, No.36]). The EOT11a follows this advice. Diurnal minor tides from the FES2014 ocean tide model are derived by linear interpolation and semi-diurnal tides are determined by a quadratic spline interpolation [9, Madzak M.]. Different interpolation methods lead to different results, which will be discussed in detail in section 4.3.

4 Estimation of tidal constituents in terms of water heights deduced from oceantide models

This section deals with the proceeding of the available datasets of the different oceantide models, which are mentioned in detail in section 2.2, to retrieve individual tidal constituents in terms equivalent water heights, which are following the IERS conventions 2010 [16]. Moreover minor tides, calculated by the admittance approach, are discussed. The results of these to computations are represented in sections 4.2 and 4.3.

4.1 Transforming input parameters to equivalent water heights

As described in section 2.2, the two considered ocean tide models are stored in a netCDF format - either as phase and amplitude (FES2014) or as real and imaginary part (EOT11a) of the tidal constituents. Hence it's necessary to convert each file for each constituent to a same base, to be able to compare those furthermore.

In a first step, the amplitudes and phases of the FES2014 global oceantide model, have to be converted to the same components as in the global model EOT11a by

$$\begin{aligned} re_s(\phi,\lambda) &= A_s \cos\delta_s \\ im_s(\phi,\lambda) &= A_s \sin\delta_s. \end{aligned} \tag{4.1}$$

Next up, the tidal constituents, in form of the real and imaginary part of equation (4.1), get transformed to potential coefficients by a least squares adjustment. To confirm the IERS conventions of 2010 [16], the Doodson Wartburg phase correction has to be applied. The coefficients can be obtained by using formula (3.25) with

$$\begin{aligned} c_{nm}^{cos},\ s_{nm}^{cos} &\equiv C_{nm,s}^{+} + C_{nm,s}^{-} \\ c_{nm}^{sin},\ s_{nm}^{sin} &\equiv S_{nm,s}^{+} + S_{nm,s}^{-}. \end{aligned} \tag{4.2}$$

To evaluate tidal constituents in terms of equivalent water heights, equation (3.24) changes to

$$\mathrm{ewh_s} = \frac{M}{4\pi R^2 \rho_w} \frac{2n+1}{1+k_n'} \sum_{n=0}^{\infty} \left(\frac{R}{r}\right)^{n+1} \sum_{m=0}^{m=n} \left[\Delta c_{nm,s} \cos m\lambda + \Delta s_{nm,s} \sin m\lambda\right] P_{nm}(\sin\Phi). \tag{4.3}$$

4.2 Evaluation and validation of EOT11a w.r.t FES2014

Illustrations 4.1 and 4.2 show the major tide P_1 and $2N_2$ of the EOT11a model, the FES2014 model and their respective differences in terms of equivalent water heights. The behaviour of those two different models and tidal constituents are similar. The differences mainly occur in regions of high currents or other geophysical phenomens (e.g. plate tectonics Scotia Plate) and of course at the pole regions just because the EOT11a model - compared to the FES2014 model, is a satellite altimetry model only.

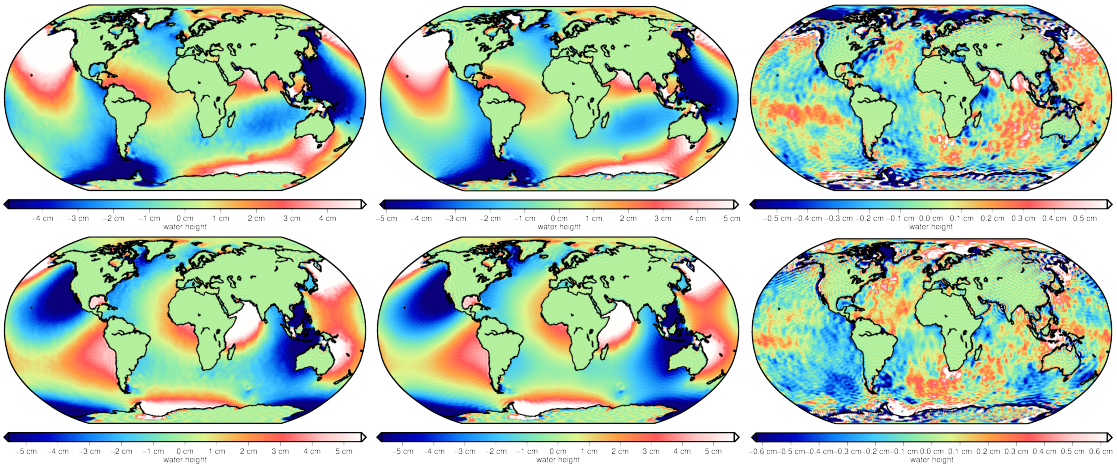

(a) EOT11a **(b)** FES2014 **(c)** differences

Figure 4.1: diurnal tidal constituent P_1 derived by different ocean tide models in cosine and sine in terms of equivalent water heights

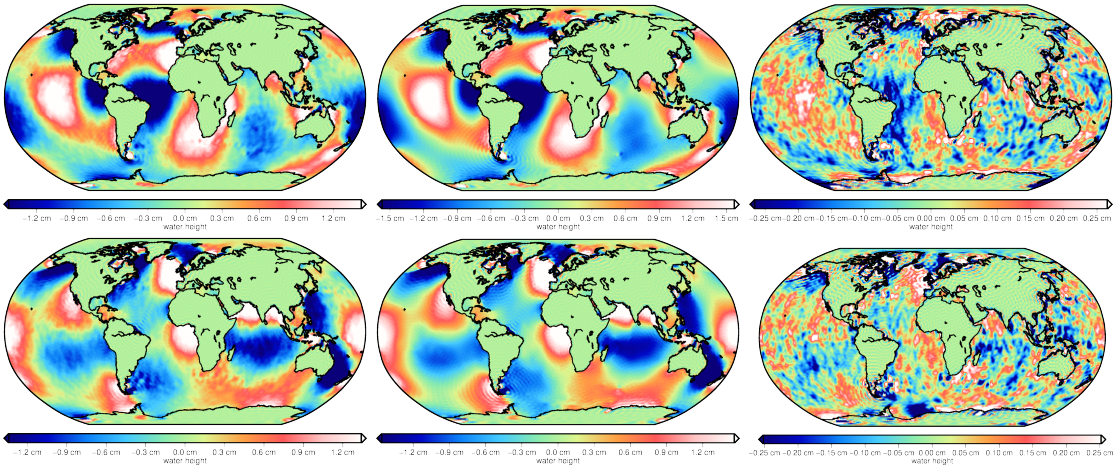

(a) EOT11a **(b)** FES2014 **(c)** differences

Figure 4.2: semi-diurnal tidal constituent $2N_2$ derived by different ocean tide models in cosine and sine in terms of equivalent water heights

It turns out clearly, that more investigations are meaningful, to improve the EOT11a model as a background model for ITSG-Grace2016 gravity field [10] , so that the dynamic system Earth can get described in a better way.

The other results do not differ from the results above, hence they are illustrated in the ap-

pendix A.1 for the sake of completeness.

4.3 Minor tides & Admittance

As described in section 2.2 at the EOT11a model are less tides available than in FES2014 (compare 3.6 with figure 4.3 below).

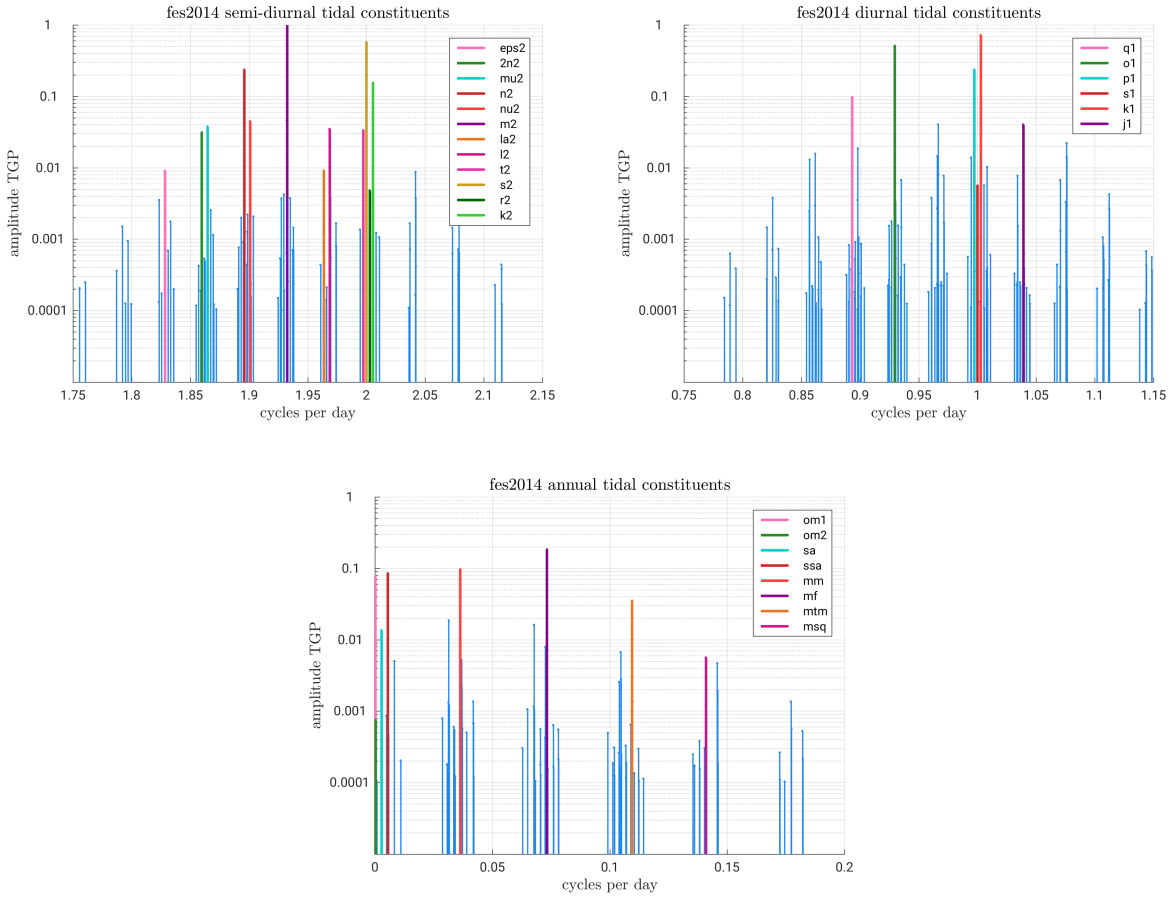

Figure 4.3: linearly interpolated minor tides from FES2014 w.r.t. HW95 catalog

linear Admittance

To evaluate EOT11a it is necessary to calculate those tides with admittance, which are available as major tides in FES2014. Therefore the interpolating-coefficients can be computed as following:

$$\begin{aligned} c_{nm_s}^{cos,sin} &= a_s \; c_{nm_{1,FES2014}}^{cos,sin} + b_s \; c_{nm_{2,FES2014}}^{cos,sin} \\ s_{nm_s}^{cos,sin} &= a_s \; s_{nm_{1,FES2014}}^{cos,sin} + b_s \; s_{nm_{2,FES2014}}^{cos,sin} \end{aligned} \tag{4.4}$$

where a, b (compare with equation (3.28) in section 4.3) denote the scalar interpolation coefficients, the subscripts $1, 2$ denote the two used main tides for interpolating the minor tide with subscript s.

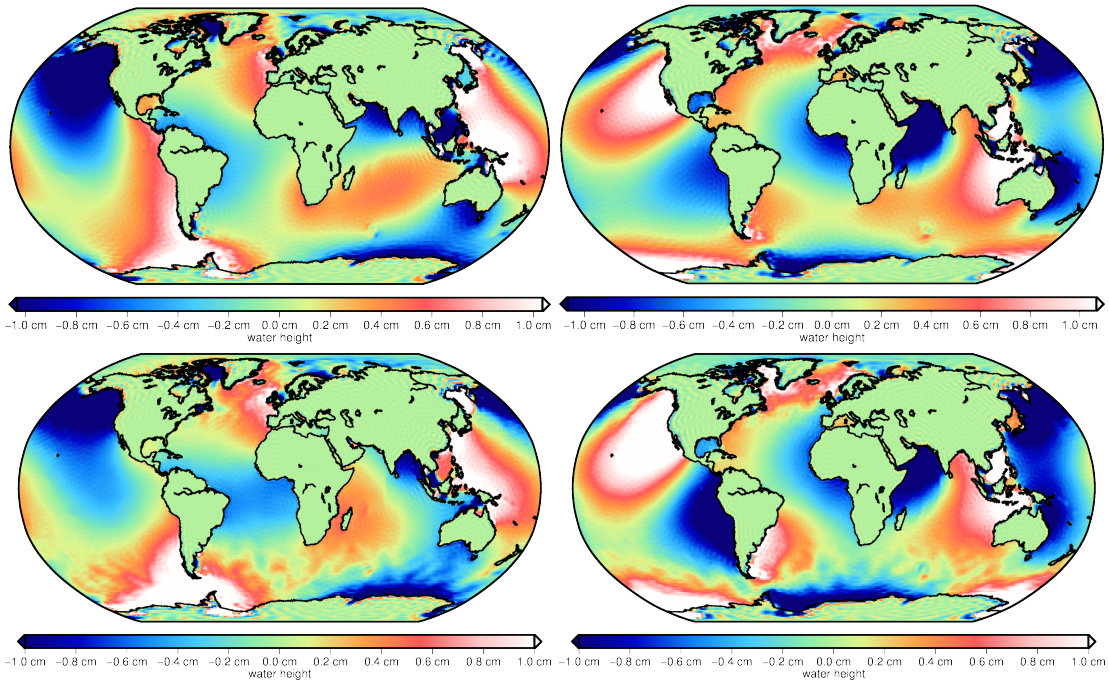

(a) cosine **(b)** sine

Figure 4.4: diurnal constituent J1 derived by linear admittance based on FES2014 main tides potential coefficients (upper block), from FES2014 major tides potential coefficients directly(lower block) in cosine and sine

Figures 4.4 shows the diurnal constituent J_1 derived by linear admittance from EOT11a with FES2014 main tides potential coefficients (left) and derived from FES2014 main tides potential coefficients directly (right). It can be clearly seen, that there are differences between the two models. Both Figures are plottet between ±1 cm, to clarify the differences of both models. The differences in detail are shown for both oscillations in figure 4.5 below.

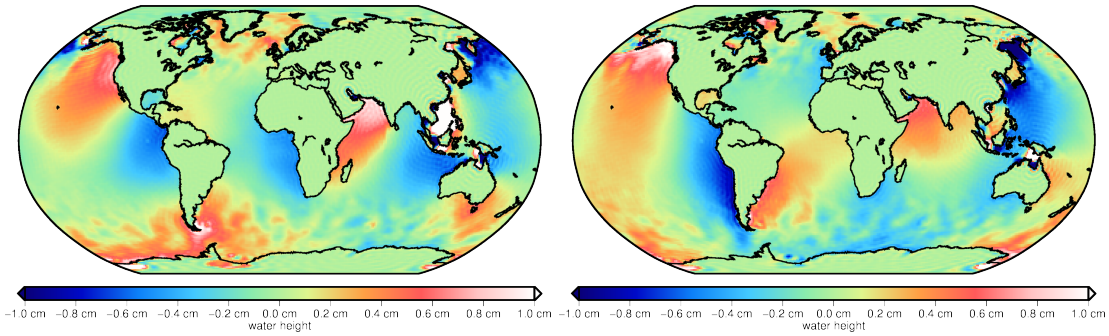

(a) cosine **(b)** sine

Figure 4.5: difference between J_1 out of FES2014 directly and calculated by linear admittance based FES2014 in terms of water heights

For a better possibility of interpretation and appreciation, the differences between FES2014-original and minor tides derived by linear admittance are calculated and illustrated in figure 4.5. The tidal constituent J_1 is extrapolated by O_1 and K_1 (see figure 4.3). There are huge differences up to ±4 cm in specific areas. Those differences are already identifiable in figure 4.4. They mainly occur in areas where ocean currents are present.

Therefore it's explicable that the tidal constituents estimated by FES2014 are better modeled, since this model also includes hydrodynamic models in contrast to the EOT11a model.

Table 4.1 shows how the listed minor tides (column one) gets interpolated. Each minor tide has different coefficients for interpolating. The magnitude of the differences of interpolated minor tides are between ca. ±12 cm. It depends on the size of the minor tide. The rms of all interpolated constituents are similar in scale of a few subcentimenters.

Table 4.1: interpolated minor tides with linear admittance with FES2014 potential coefficients and their differences to FES2014 main tides in terms of minima, maxima and rms

minor tide	**main tide 1**	**main tide 2**	**trig.function**	**differences [cm]**		
				min	max	rms
J_1	O_1	K_1	cos	-4.193	4.647	0.344
			sin	-4.615	4.778	0.327
ϵ_2	$2N_2$	N_2	cos	-3.113	4.446	0.177
			sin	-3.282	4.429	0.197
μ_2	$2N_2$	N_2	cos	-11.524	6.917	0.440
			sin	-8.329	9.299	0.415
ν_2	N_2	M_2	cos	-2.207	2.733	0.154
			sin	-2.848	2.227	0.129
λ_2	M_2	K_2	cos	-4.086	1.893	0.143
			sin	-4.023	3.860	0.164
L_2	M_2	K_2	cos	-6.066	4.300	0.278
			sin	-10.256	9.014	0.308
T_2	M_2	K_2	cos	-1.148	1.144	0.108
			sin	-1.631	1.065	0.097
R_2	M_2	K_2	cos	-0.106	0.158	0.013
			sin	-0.158	0.238	0.013

The biggest differences are in the diurnal constituent J_1 and the semi-diurnal constituents L_2 and μ_2. This fact can be also seen in the extrema in terms of minima and maxima and in their rms. Caused of this fact those particular mentioned tides are discussed in detail on the following pages. The behaviour of the remaining ones is similar, hence they are represented in the appendix at section A.2 from figure A.14 to A.21.

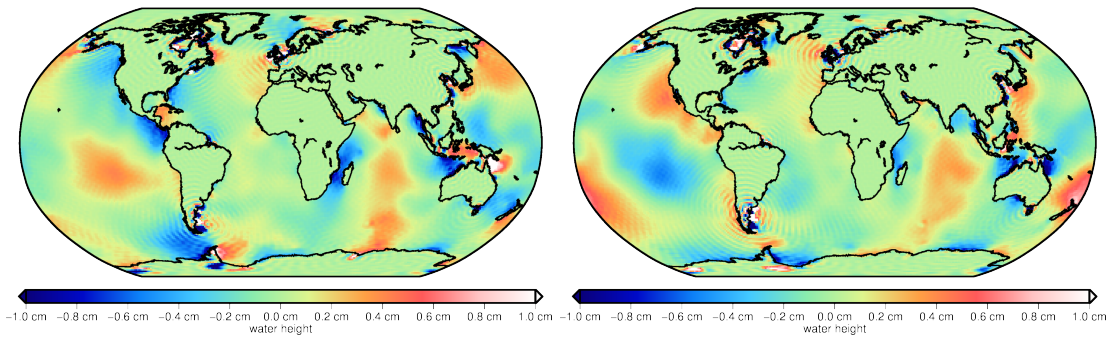

Figure 4.6: differences of semi-diurnal constituent L_2 derived from FES2014 in terms of water height in cosine and sine

The illustration above shows the differences of the two L_2 tides (FES2014 - $FES_{linear\,Admittance}$).

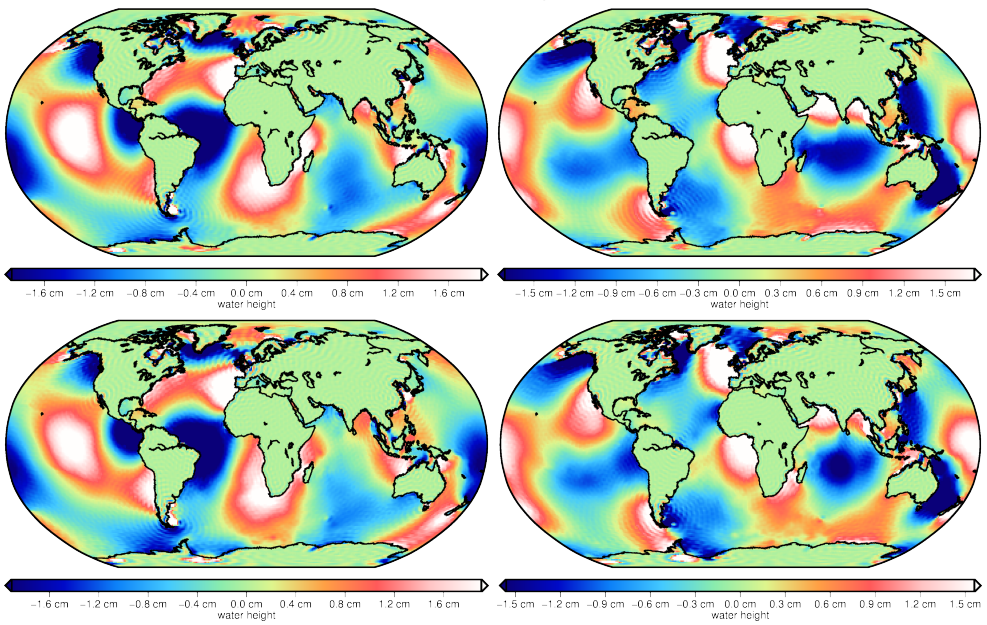

(a) cosine **(b)** sine

Figure 4.7: semi-diurnal constituent μ_2 derived by linear admittance with FES2014 major tides potential coefficients (upper block), from FES2014 main tides potential coefficients directly (lower block)

Figure 4.7 shows the semi-diurnal constituent μ_2 derived by linear admittance based on FES2014 main tides potential coefficients (left) and derived from FES2014 main tides potential coefficients directly (right). At first the differences between the illustrations seem to be smaller compared to the diurnal-tide J_1 (compare with figures 4.4 and 4.5). The main varieties are located on the west coast of South-America and in South-Africa.

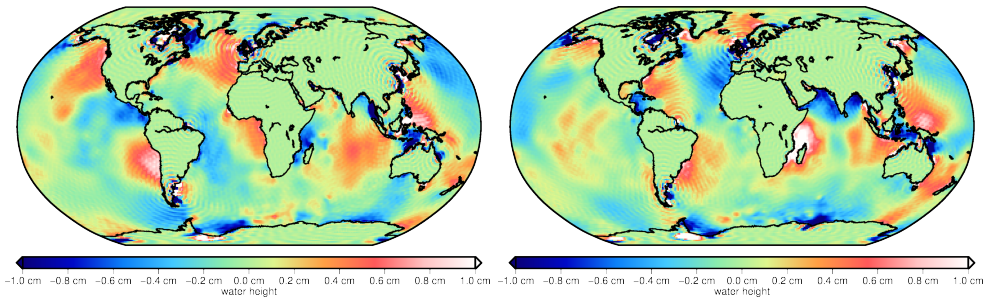

Figure 4.8: difference between μ_2 out of FES2014 and calculated by linear admittance from EOT11a with FES2014 in terms of water heights in cosine and sine

The figure above shows the differences between FES2014 and minor tides derived by linear admittance from EOT11a with FES2014 main tides as input. First assumptions are confirmed by considering figure 4.8. The same conclusion can be drawn like at the lunar diurnal tide J_1 before.

More investigations seem to be meaningful to minimize those discrepancies. An other interpolation-method or different major tides as supporting points could be taken into account.

Therefore more investigations are performed by having a closer look on the frequency spectra of the tidal consitutents. Those investigations are done at the semi-diurnal tidal constituent μ_2.

linear Admittance of μ_2 by using main tides M_2 and $2N_2$

The tidal constituent μ_2 gets linearly interpolated by the main tides $2N_2$ and N_2, which are directly next to considered tide (see figure 4.3 in section 4.3). The origin of μ_2 is a variation of M_2. Hence it's questionable if the choice of interpolation's supporting points was the right and for that reason μ_2 was calculated by using M_2 instead of N_2 in a first step.

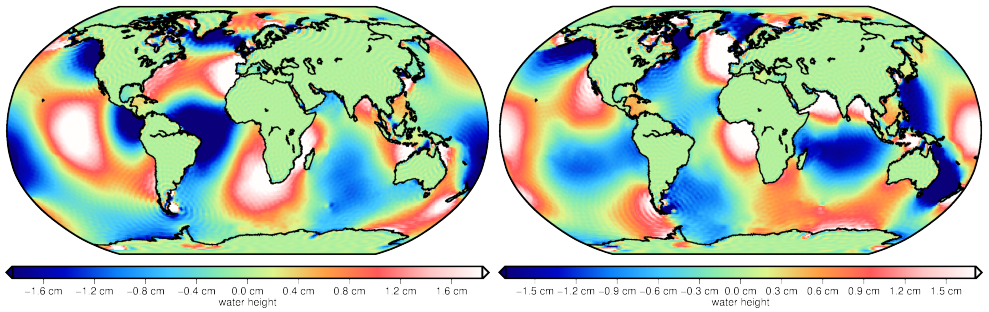

Figure 4.9: μ_2 linearly interpolated by M_2 and $2N_2$ in cosine and sine

Figure 4.9 shows the semi-diurnal constituent μ_2 derived by linear admittance from FES2014 main tides potential coefficients directly with interpolations-coefficients out of EOT11a in cosine (left) and sine (right). Compared with figure 4.7 upper block, the root mean square changes in a minimal positively way from 0.9439 cm to 0.9347 cm for cosine and from 0.8704 cm to 0.8703 cm for sine.

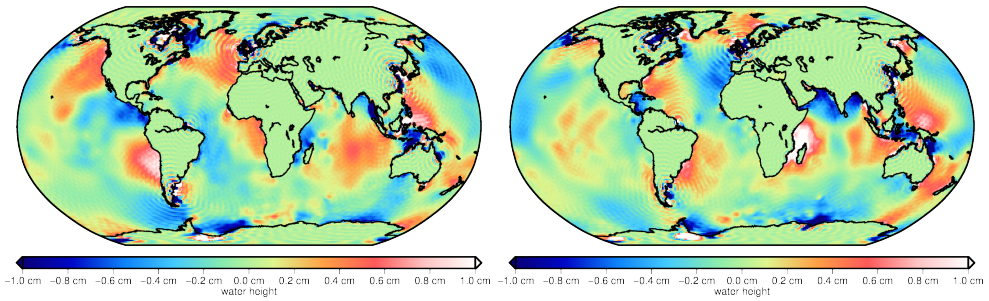

Figure 4.10: difference between μ_2 out of FES2014 and calculated by linear admittance from EOT11a with FES2014 in terms of water heights by main tides M_2 and $2N_2$ in cosine and sine

Comparison of the differences (figure 4.8 and 4.10) also display minimal improvements.

Caused by that fact more investigatons are considered - how does the result change if it's computed by a quadratic interpolation including $2N_2$, N_2 and M_2 .

quadratic Admittance of μ_2 by using main tides $2N_2$, N_2 and M_2

In this section the results of interpolating μ_2 by a quadratic polynom are discussed and visualized. The supporting points for the mentioned constituent are $2N_2$, N_2 and M_2. The quadratic interpolation Admittance can be computed by

$$H_s = \sum_{i=1}^{3} \frac{G_s}{G_i} \prod_{k=1,k\neq i}^{3} \frac{\omega_s - \omega_k}{\omega_i - \omega_k} \tag{4.5}$$

and the three interpolating coefficients c, d, e can be derived out of it, to calculate the potential coefficients for each minor tide in cosine and sine.

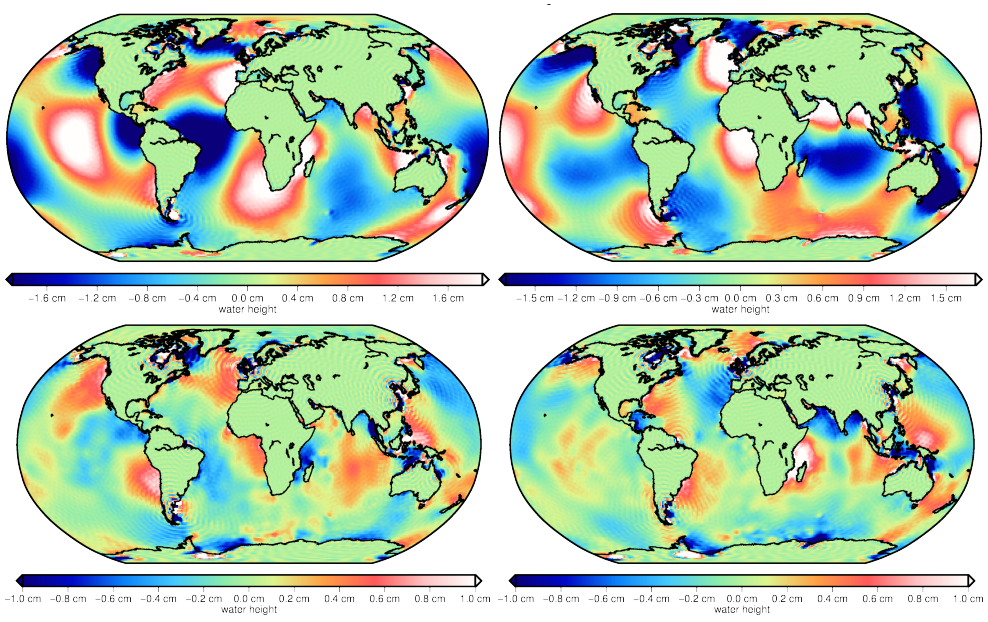

(a) cosine **(b)** sine

Figure 4.11: semi-diurnal constituent μ_2 derived by quadratic admittance with FES2014 main tides potential coefficients (upper block) and their differences to FES2014.

Illustration 4.11 shows the tidal constituent μ_2 derived by quadratic interpolation (upper block) and their differences to FES2014 (lower block) in sine and cosine. Although the root mean square get's higher compared to the linearly interpolated calculations, the minima and maxima of the differences get smaller. Altogether the result seems to be smoother than before. Table 4.2 shows the results of the qudratic interpolated minor tides.

Table 4.2: interpolated minor tides with quadratic admittance EOT11a combined with FES2014 potential coefficients and their differences to FES2014 main tides in terms of minima, maxima and rms

minor tide	**main tide 1**	**main tide 2**	**main tide 3**	**trig.function**	**differences [cm]**		
					min	max	rms
J_1	Q_1	O_1	K_1	cos	-6.374	3.797	0.433
				sin	-8.135	4.005	0.422
ϵ_2	$2N_2$	N_2	M_2	cos	-3.021	4.638	0.188
				sin	-3.309	4.318	0.209
μ_2	$2N_2$	N_2	M_2	cos	-11.463	6.881	0.444
				sin	-8.405	9.341	0.416
ν_2	$2N_2$	N_2	M_2	cos	-1.872	2.561	0.140
				sin	-2.830	2.119	0.125
λ_2	N_2	M_2	K_2	cos	-4.158	1.789	0.134
				sin	-3.657	3.468	0.151
L_2	N_2	M_2	K_2	cos	-5.714	3.487	0.235
				sin	-8.825	7.481	0.254
T_2	M_2	S_2	K_2	cos	-0.156	0.141	0.014
				sin	-0.187	0.236	0.013

This validates the assumption, that more investigations are important and meaningful if calculating minor tides. Therefore it brings up another question, what if the whole tidal spectrum is considered in computations with an included functional model, instead of linear interpolation. This will be discussed in detail in section 5.3.

5 Prediction of minor tides by least squares collocation

This section deals with the least squares collocation in terms of equivalent water heights. As described in detail in section 2.4, the datasets, which are used for the determination of minor tides by collocation, have to be without trend and mean value, to determine the covariance function.

To facilitate the validation of this method, the major tides of the global ocean tide model FES2014, which are also available at the EOT11a model, are used as input for computations. Hence the remaining major tides of FES2014 (ϵ_2, μ_2, ν_2, λ_2, L_2, T_2, R_2 and J_1) are treated as minor tides, which shall be estimated through this statistical approach.

So far, the covariance function was determined for functionals of the disturbing potential as a function of the distance s. Now, a covariance function must be found in dependency of the frequency.

Therefore a pre-assumption is necessary:

The behaviour of all observed points is similar and they just depend on their frequencies and not on their position on Earth's surface. To meet those requirement, the partial tides in terms of equivalent water heights, are ranged to the same level by deviding each tide by it's related tide generating potential

$$ewh_s^{same\,level} = \frac{ewh_s}{TGP_s}. \tag{5.1}$$

Furthermore a spatial trend gets calculated for each tidal constituent in form of a hyperplane

$$z_s = a_0 + a_1\phi + a_2\lambda + a_3\phi^2 + a_3\lambda^2 + a_4\phi\lambda \tag{5.2}$$

and gets subtracted as a mean trend of the used partial tide by

$$ewh_s^{trend\,reduced} = ewh_s^{same\,level} - \frac{1}{N}\sum_{n=1}^{N} z_n. \tag{5.3}$$

Those trend-reduced datasets (in time domain) build the foundation for all upcoming calculations.

In a next step, to be up to par, the main tides must be trend-reduced in frequency domain. Hence it's unalterable to estimate a trend for all observed points for each frequency.

5.1 Estimating trend in frequency domain

For this purpose, a trend was removed (in a linearly way) since one of collocation's requirements is, that the data is mean-centric and without any trend. This is necessary to validate the input datas behaviour and to estimate a more dense grid of equivalent water heights at specific frequencies.

Each tidal constituent (regardless of whether if it's a minor or major tide) has different origins and are located at different frequencies, therefore it's relevant to compute different trends (varying weighted major tides) for different minor tides. The table below shows a brief explanation of the considered minor tides.

Table 5.1: explanation of the used harmonic constituents [23, UKHO]

minor tide	**origin**	**description**
J_1	diurnal, smaller lunar elliptic	modulates the effect of the lunar declination of the major tides K_1 and O_1 in combination with M_1 and Q_1
ϵ_2	semi-diurnal lunar	minor tide component, may interfere with 2N2, μ_2 and L_2
μ_2	semi-diurnal variational, lunar	modulates the effect of M_2 and represents a modification of the lunar orbit due to gravitational effects of the Sun
ν_2	semi-diurnal larger evectional, lunar	
λ_2	semi-diurnal smaller evectional, lunar	
L_2	semi-diurnal smaller elliptic, lunar	together with N_2, the circular orbit of M_2 gets converted into an elliptical, in equatorial plane
T_2	semi-diurnal larger solar elliptic	modulates variation of Earth's orbital speed of S_2
R_2	smaller solar elliptic	

E.g. it doesn't make sense to give the solar major tide S_2 a high weight (when calculating trend), if the lunar minor tide μ_2 shall be estimated. μ_2 is located near the major tide $2N_2$ in frequency domain and modulates the amplitude of M_2, together with the partial tides ν_2 and λ_2.

In this thesis two scenarios are tested:

Calculating a linear trend in frequency domain through

1. direct amplitude weighting and
2. inverse amplitude weighting,

by a Gauß Markoff model:

$$\hat{x} = (A^T P A)^{-1} A^T P l \,, \tag{5.4}$$

where the designmatrix A represents the functional model, P the weight matrix with the amplitudes (T_2 and R_2) or inverse amplitudes (J_1, ϵ_2, μ_2, ν_2, λ_2 and L_2) in it's main diagonal and l denotes the observations of each point at one specific frequency.

Those weightings are chosen, because they seem to be sufficient enough for first investigations to check if estimating minor tides by collocation make sense at all.

The magnitudes of the amplitudes can be seen in figure 4.3. The figure below shows the empirical covariances for both scenarios. On the right side the dataset got reduced by a direct weighting of the amplitudes and the left side shows the dataset reduced by the inverse amplitude weighted linear trend.

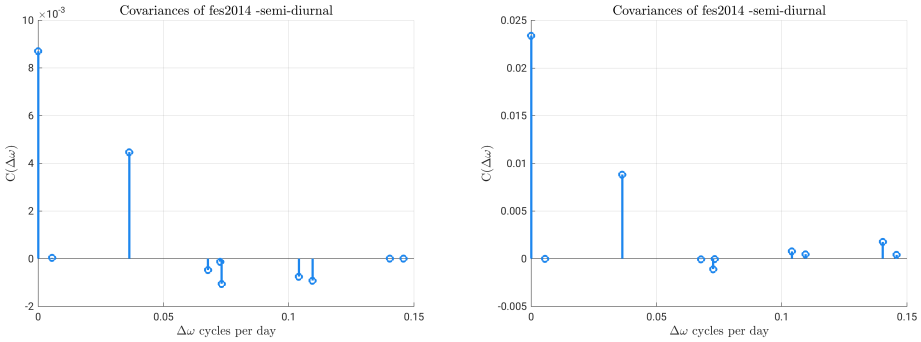

Figure 5.1: empirical covariances for semi diurnal tides reduced by different weighted linear trend

It can be seen, that there aren't huge differences in the shape of the empirical covariances and $C(\Delta\omega)$ decreases with increasing $\Delta\omega$. Therefore just one analytical covariance function must be developed, which plays the main role in collocation.

5.2 Determination of an analytical covariance function

The determination of an analytical covariance function is quite difficult - as already mentioned in section 2.4. It has to be attempted to fit the empirical covariance function to an yet unknown covariance function model, since the already designed ones are mainly valid for functions in dependency of the distance. In every field of research, where statistical methods in physical geodesy are applied, this is the key problem in this context.

First the empirical covariance function (see figure 5.1) got approximated by a simple harmonic oscillation

$$C(\Delta\omega) = \sum_{i=1}^{n} c_n \cos\left(\frac{2\pi}{f} n\Delta\omega\right), \tag{5.5}$$

where $\Delta\omega$ is the frequency difference, f the maximal frequency difference of the whole spectrum and c_n the unknown coefficients, which shall be estimated by a least-squares adjustment. It turned out, that this representation doesn't fit for the present empirical covariance (see figure 5.2 below).

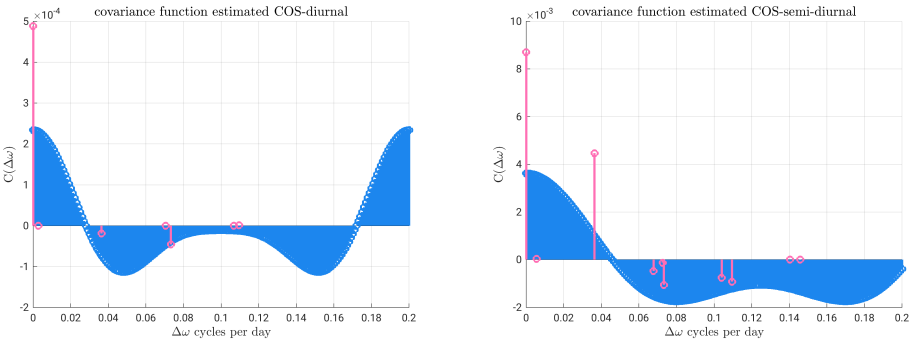

Figure 5.2: analytical covariances for diurnal and semi diurnal tides formed by equation (5.5)

.

Therefore, in a second turn, an already known covariance model was used for estimating tides by collocation - a modified analytical expression for Hirvonen's covariance function in form of

$$C(\Delta\omega) = \frac{C_0}{1 + \left(\frac{\Delta\omega}{d}^2\right)}. \tag{5.6}$$

with the model parameters of the variance C_0 and the half width at half maximum d. The variance can be calculated empirical by formula (2.18) and the half width at half maximum gets interpolated.

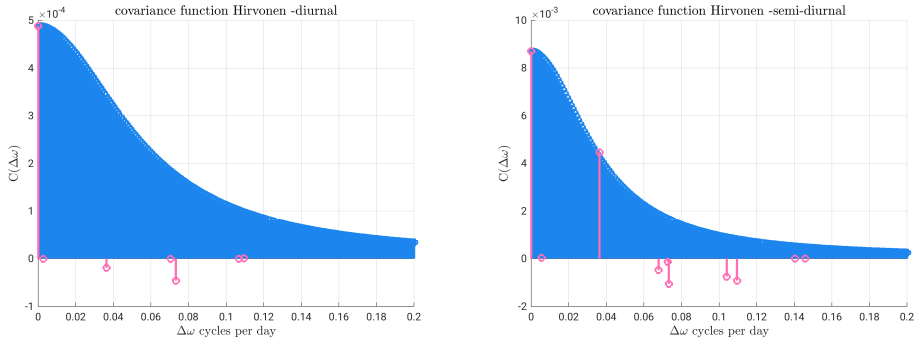

Figure 5.3: analytical covariances for diurnal and semi diurnal tides formed by equation (5.6)

.

The results based on this covariance function do fit, but it does not produce better results than with the approach of linear admittance in terms of root mean squares w.r.t to FES2014. This can be explained by having a look on the analytical covariance function in illustration 5.3.

By having a closer look on the empirical covariances in figure 5.1, their shapes look partly as a cardinal sine (sinc) function. Since the harmonical behaviour of the tidal constituents, should not be neglected, equation (5.5) gets combined with a sinc function as an experiment:

$$C(\Delta\omega) = \sum_{i=1}^{n} c_n \left[\frac{1}{C_0^2} \operatorname{sinc}\left(\frac{2\pi}{f} n\Delta\omega\right) - \cos\left(\frac{2\pi}{f} n\Delta\omega\right) \right]. \tag{5.7}$$

The coefficients c_n are the unknown parameters as before. For first investigatons with this function, the numerical value for the factor f is considered as the maximal frequency difference which occur in each frequency band (between major tides and minor tides). Hence it can be numberated with $f = 0.25$.

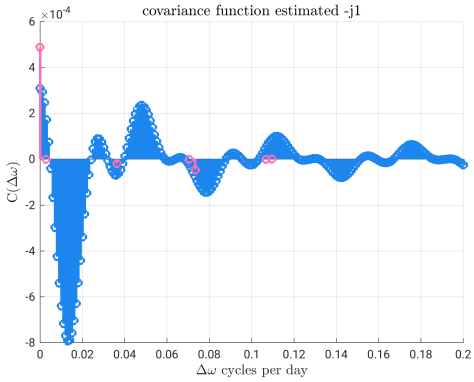

Figure 5.4: covariances for diurnal tides formed by equation (5.7) with $f = 0.25$ (weighted by inverse amplitude).

Figure 5.4 shows the covariance function for diurnal tides with $f = 0.25$. It apparently fits way better than before with the two other coveriances. It's a debatable point if all other diurnal covariances can be described by equation 5.7 with one factor f, since there's is just one testing tide available.

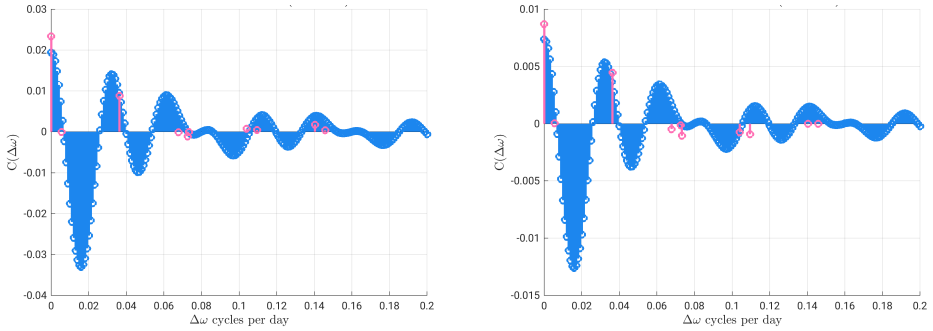

Figure 5.5: covariances for semi diurnal tides formed by equation (5.7) with $f = 0.25$ (left side: weighted by amplitude, right side: weighted by inverse amplitude).

Illustration 5.5 confirmed the assumption, that just one factor is not sufficient to estimate all tidal constituents, because the covariance function changes depending on this factor. Therefore more investigations are done, how the covariances change, if this factor gets changed for each tidal constituent. This research was done empirically, based on the result of the estimated minor tides w.r.t to FES2014 (see table 5.2).

Table 5.2: kind of weighting for trend calculations in frequency domain and numerical values for f to adjust the analytical covariance function

tidal constituent	**f [cycles per day]**	**weighting**
J_1	0.25	A^{-1}
ϵ_2	0.17	
μ_2	0.28	
ν_2	0.25	
λ_2	0.29	
L_2	0.29	
T_2	0.09	A
R_2	0.08	

In figure 5.6 can be seen the graphical results of the different covariances, with the correspondening factor f for each tidal constituent.

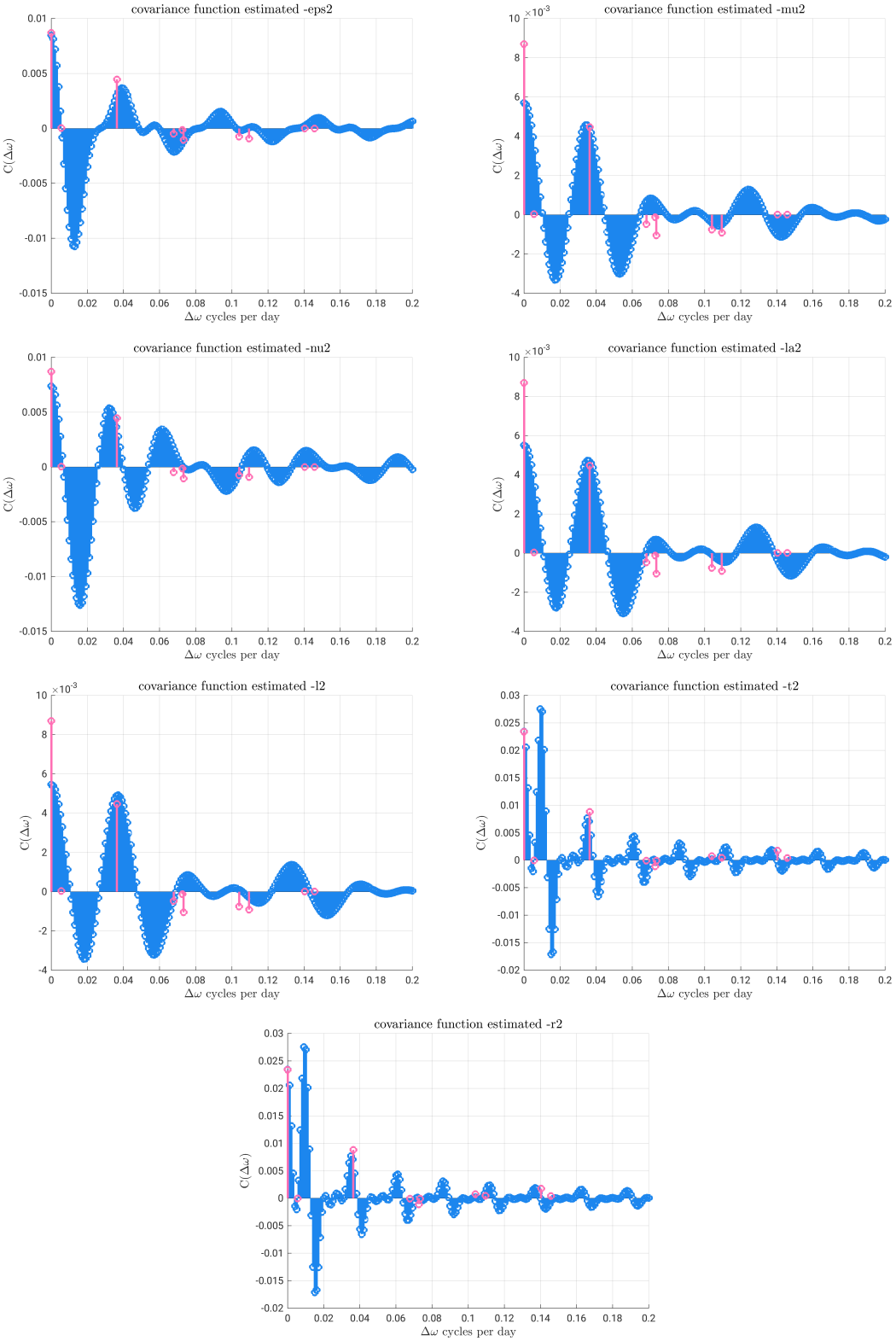

Figure 5.6: covariances for semi diurnal tides formed by equation (5.7) with different numerical values for f (see table 5.2).

5.3 Application of collocation to determination of minor ocean tides

In this section the results of estimating minor tides by least squares collocation are represented and discussed. They get computed in terms of trend reduced and TGP-leveled equivalent water heights by equation 2.17 and looks like

$$\tilde{ewh}_{s,P}^{trend\,reduced} = [C_{P1}^s, C_{s2}^s, \dots C_{Pn}^s] \begin{bmatrix} C_{11} & C_{12} & \dots & C_{1n} \\ C_{21} & C_{22} & \dots & C_{2n} \\ \vdots & \vdots & & \vdots \\ C_{n1} & C_{n2} & \dots & C_{nn} \end{bmatrix}^{-1} \begin{bmatrix} ewh_1 \\ ewh_2 \\ \vdots \\ ewh_n \end{bmatrix} \tag{5.8}$$

in matrix notation. The covariances are calculated by formula (5.7) with different factors f, as pointed out in table 5.2. To obtain equivalent water heights, the calculated trends (spatial - $trend_s$ and frequency based - $trend_{fb}$) have to be restored in a first step

$$ewh_s^{same\,level} = ewh_s^{trend\,reduced} + trend_s + trend_{fb}. \tag{5.9}$$

As a second step, the respective TGP has to be applied by

$$ewh_s = ewh_s^{same\,level} \cdot TGP \tag{5.10}$$

to gain the uniqueness of each tidal constituent.

Table below shows the numerical results of LSC and also the differences out of the linear admittance approach. The graphical representation is shown on the upcoming pages.

Table 5.3: differences of minor tides of LSC w.r.t FES2014 in terms of minima, maxima and rms and the rms of linear admittance for comparison

minor tide	**trig.function**	**differences [cm]**			**rms Δewh lin.A [cm]**
		min	max	rms	
J_1	cos	-3.494	4.229	0.286	0.344
	sin	-3.688	5.296	0.280	0.327
ϵ_2	cos	-3.298	4.274	0.178	0.177
	sin	-3.045	4.217	0.189	0.197
μ_2	cos	-11.656	6.970	0.437	0.440
	sin	-8.199	9.212	0.406	0.415
ν_2	cos	-2.179	3.343	0.162	0.154
	sin	-3.717	3.020	0.190	0.129
λ_2	cos	-3.123	1.677	0.133	0.143
	sin	-3.281	3.330	0.153	0.164
L_2	cos	-5.289	3.690	0.247	0.278
	sin	-8.967	7.789	0.267	0.308
T_2	cos	-1.178	1.149	0.119	0.108
	sin	-1.484	1.505	0.093	0.097
R_2	cos	-0.161	0.158	0.013	0.013
	sin	-0.173	0.397	0.012	0.013

In figure 5.7 can be seen the diurnal tidal constituent J_1 calculated by least square collocation and the differences to FES2014.

For better comparison, the differences of the linear admittance approach w.r.t to FES2014 is also visualized. In terms of the root mean square and minima and maxima, the result, received by collocation gets better, compared to the linear admittance approch. The biggest improvements are near Greenland and Sweden for both oscillations. The sine oscillation has additional betterments near India.

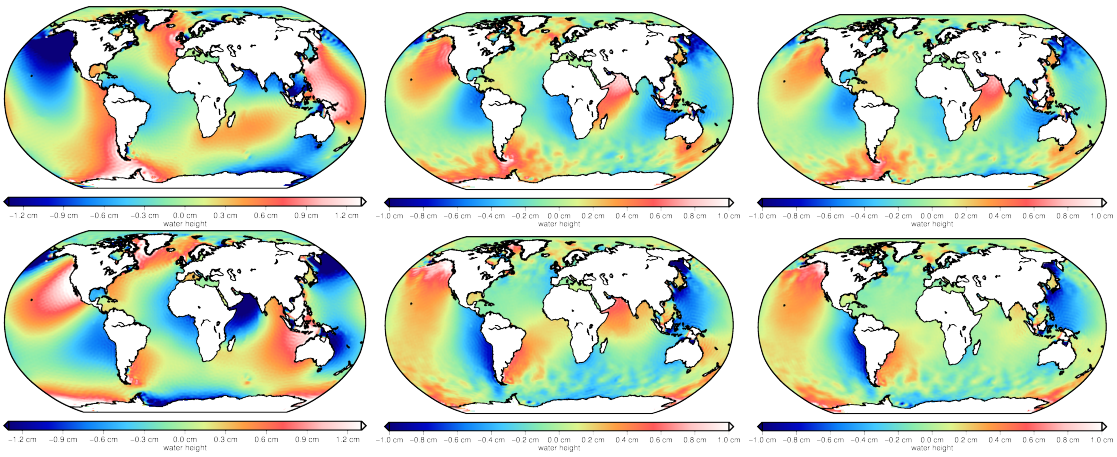

(a) collocation **(b)** FES2014 - lin. admittance **(c)** FES2014 - collocation

Figure 5.7: diurnal tidal constituent J_1 estimated by least squares collocation in cosine (above) and sine (below) and their differences to FES2014 of the linear admittance apporach and LSC

Illustration 5.8 shows the partial tide ϵ_2 in terms of equivalent water heights. The input data set got reduced by a weighted trend. The weighting is the inverse amplitude of the major tides. It seems like this weighting does fit very well for this purpose.

First, because the the nearest major tide $2N_2$ gets the heighest weight and second also the covariance function fits in a good way (see figure 5.1).

The results in the figure below substantiate that - in particular, the behaviour of the sine oscillation gets much better than the results of the linear admittance approach.

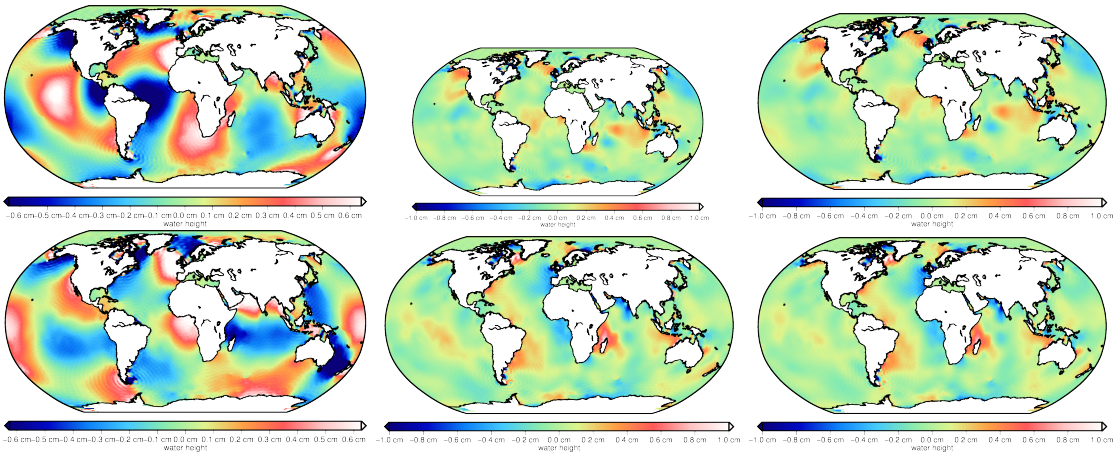

(a) collocation **(b)** FES2014 - lin. admittance **(c)** FES2014 - collocation

Figure 5.8: semi - diurnal tidal constituent ϵ_2 estimated by least squares collocation in cosine (above) and sine (below) and their differences to FES2014 of the linear admittance apporach and LSC

The fact, that the EOT11a model does not deliver good results in the pole regions, does not affect the represented results, since the major tides of the global assimilated model FES2014 are used as input, instead of the EOT11a model - precisely because of that reason.

The assumption, which is formulated in table 5.1, that the major tide $2N_2$ may interfere the partial tide ϵ_2, is hardend by this result.

All in all it can be said, that the minor tide ϵ_2 - determined by collocation - has improved over the results of the linear admittance approach. The solution gets smoother and exhibits minimal enhancements against the standard practice.

Considering the tidal spectrum of semi-diurnal tides and the explanations of minor tides in table 5.1, the tidal constiuents μ_2, ν_2 and λ_2 are modelling the effect of solar gravitation on the Moon's orbital speed of the major tide M_2, since M_2 moves in a circular orbit in the equatorial plane.

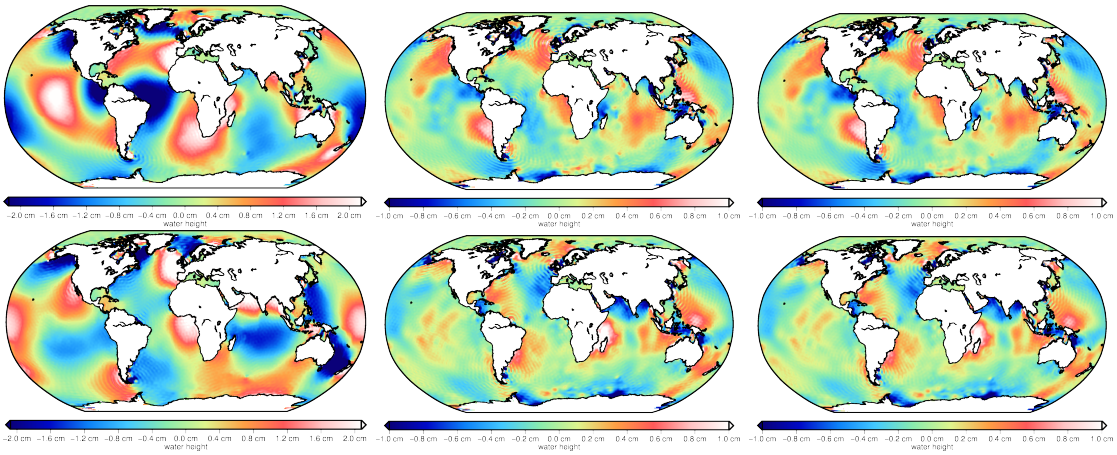

(a) collocation **(b)** FES2014 - lin. admittance **(c)** FES2014 - collocation

Figure 5.9: semi - diurnal tidal constituent μ_2 estimated by least squares collocation in cosine (above) and sine (below) and their differences to FES2014 of the linear admittance apporach and LSC

Hence it's quite difficult to find a fast proper weighting for those three partial tides. Also their determined covariances show this fact in higher frequency differences. It doesn't fit as good, as e.g. for the tidal constiuent ϵ_2, which is described previous.

Even if the rms gets better, the end solution is worse - the minima and maxima get higher.

During the fitting process, by adjusting the factor f, the solution seems to be random. There's no scheme, compared with the other minor tides. Therefore it's clear, that the covariance function does not match those three tidal constituents and it needs much more investigations.

On the next page, the other two minor tides (ν_2 and λ_2) of the triple mentioned above are illustrated.

The behaviour and results of the illustrated partial tides (ν_2 - 5.10 and λ_2 - 5.11) are similar to the μ_2 partial tide as described before. In particular ν_2 has huge differences w.r.t. FES2014 (figure 5.10), compared to the linear approach.

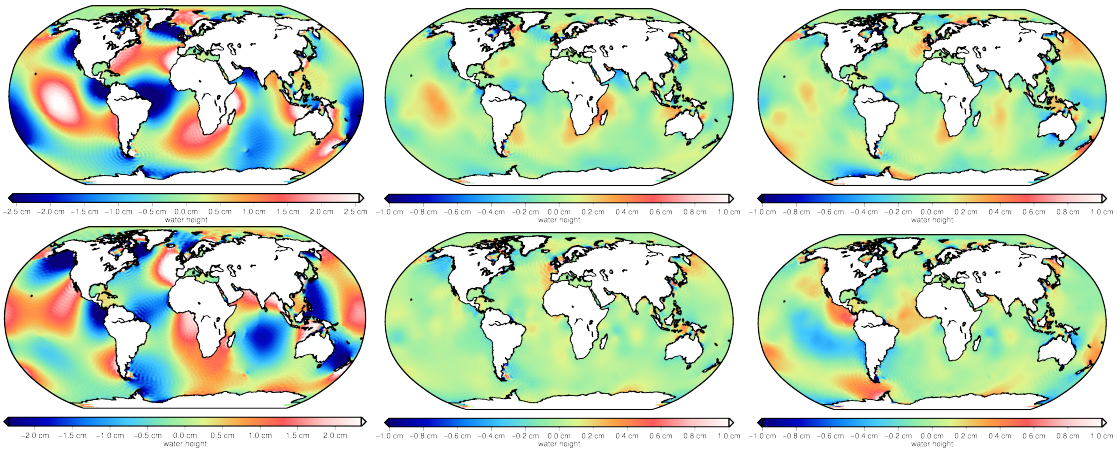

(a) collocation **(b)** FES2014 - lin. admittance **(c)** FES2014 - collocation

Figure 5.10: semi - diurnal tidal constituent ν_2 estimated by least squares collocation in cosine (above) and sine (below) and their differences to FES2014 of the linear admittance apporach and LSC

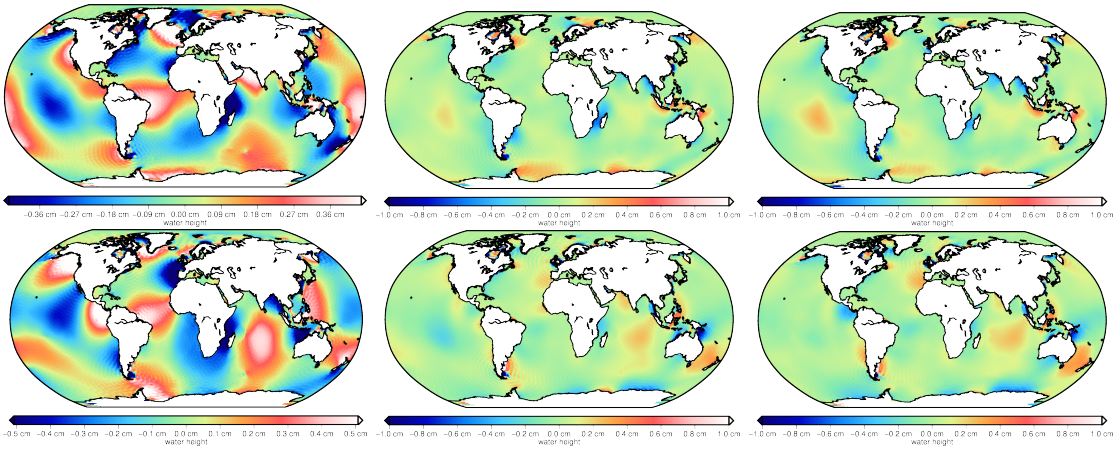

(a) collocation **(b)** FES2014 - lin. admittance **(c)** FES2014 - collocation

Figure 5.11: semi - diurnal tidal constituent λ_2 estimated by least squares collocation in cosine (above) and sine (below) and their differences to FES2014 of the linear admittance apporach and LSC

In illustration 5.12 the tidal constituent L_2 can be seen. It's determination by least squares collocation works very well, which turns out by the graphical representation and by it's numerical values (see table 5.3).

Its rms has betterments of a round 0.3 millimeters and it's extrema get smaller compared to the reults of the linear admittance approach.

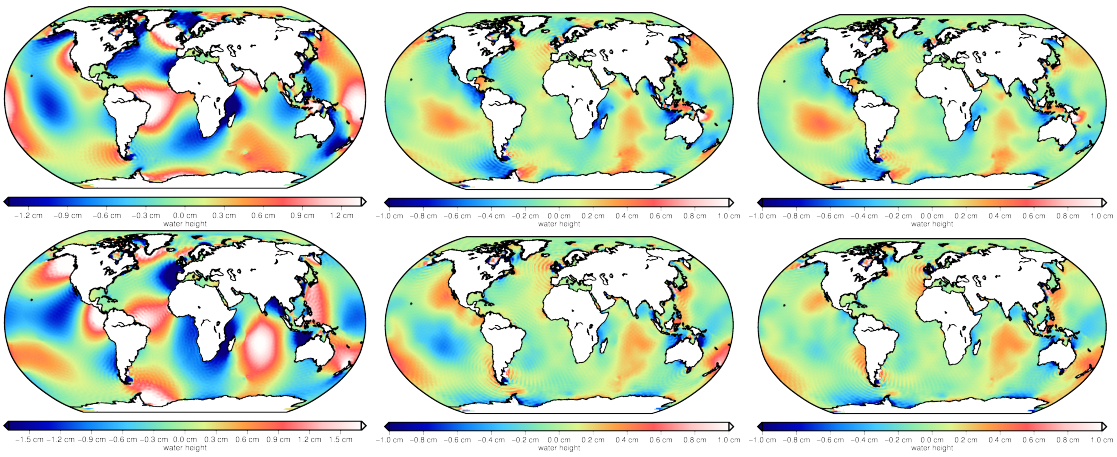

(a) collocation **(b)** FES2014 - lin. admittance **(c)** FES2014 - collocation

Figure 5.12: semi - diurnal tidal constituent L_2 estimated by least squares collocation in cosine (above) and sine (below) and their differences to FES2014 of the linear admittance apporach and LSC

The tidal constituents T_2 - figure 5.13 and R_2 - figure 5.14 are illustrated on the next page. T_2 show improvements for both oscillations in the range of a few submillimeters. All in all the results get smoother.

Since the magnitude of the tidal constituent R_2 is round 10 mm, it's quite difficult to separate this partial tide. This is also reflected in terms of the differences and in it's rms for both oscillations, independent of the computation method.

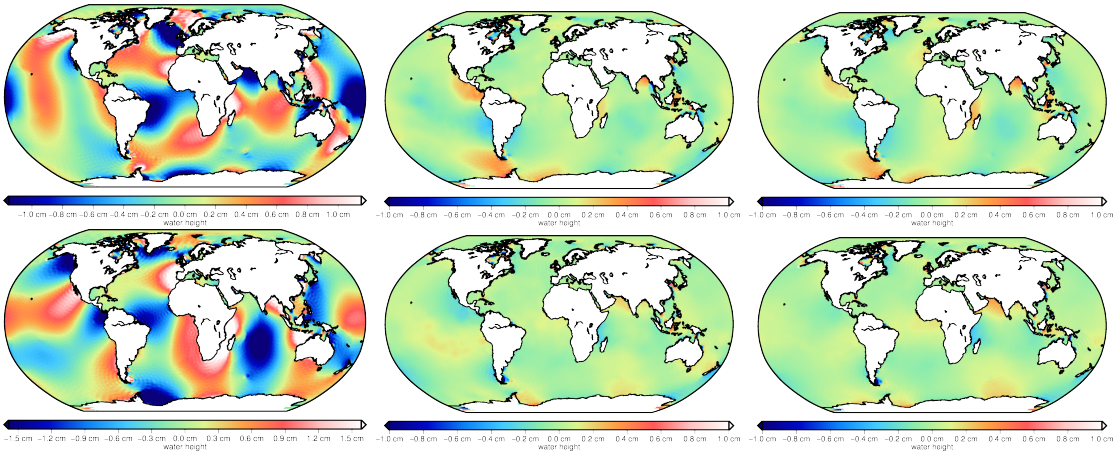

(a) collocation **(b)** FES2014 - lin. admittance **(c)** FES2014 - collocation

Figure 5.13: semi - diurnal tidal constituent T_2 estimated by least squares collocation in cosine (above) and sine (below) and their differences to FES2014 of the linear admittance apporach and LSC

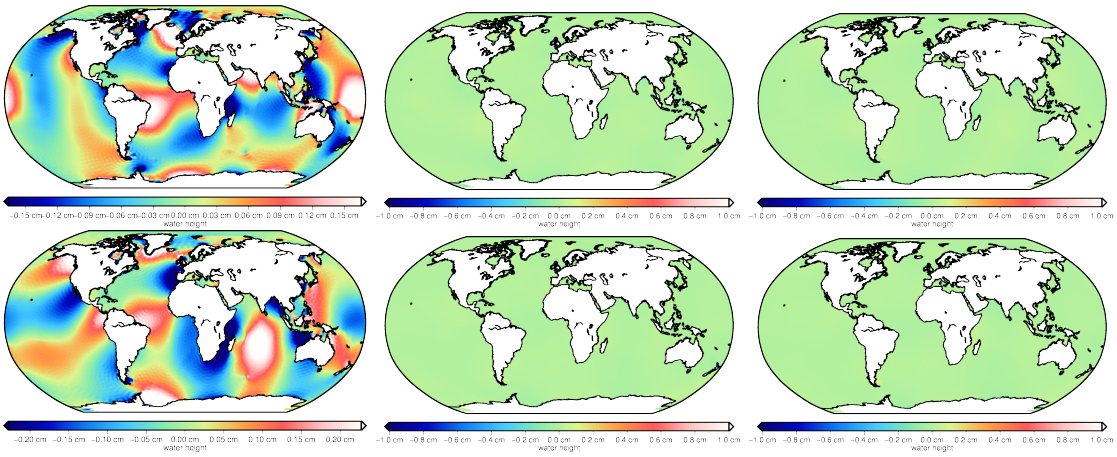

(a) collocation **(b)** FES2014 - lin. admittance **(c)** FES2014 - collocation

Figure 5.14: semi - diurnal tidal constituent R_2 estimated by least squares collocation in cosine (above) and sine (below) and their differences to FES2014 of the linear admittance apporach and LSC

6 Estimation of residual tidal constituents in terms of potential coefficients by GRACE

This section deals with the estimation of long-periodic, diurnal and semi-diurnal residual tidal constituents from GRACE observations to improve the EOT11a model. More than 15 years of observations are used in calculations by the short arc approach in the global gravity field model ITSG - Grace2016 [10]. The GRACE observations do not only consist of tidal residual signals. It's a co-estimated approach together with all gravity field variations from other mass redistributions, in order that, the ocean tide effect can be separated from other mass distributions. A benefit of estimating ocean tides with GRACE is - in addition to altimeter data, that it provides informations in the pole regions. [12, Rieser et al.].

Each tidal constituent has different tidal alias frequencies of GRACE, therefore those should be taken closer into account.

6.1 GRACE tidal alias frequencies

As mentioned before, it could be meaningful to have a closer look on GRACE tidal alias frequencies to clarify if it's possible to estimate tidal constituents by GRACE observations.

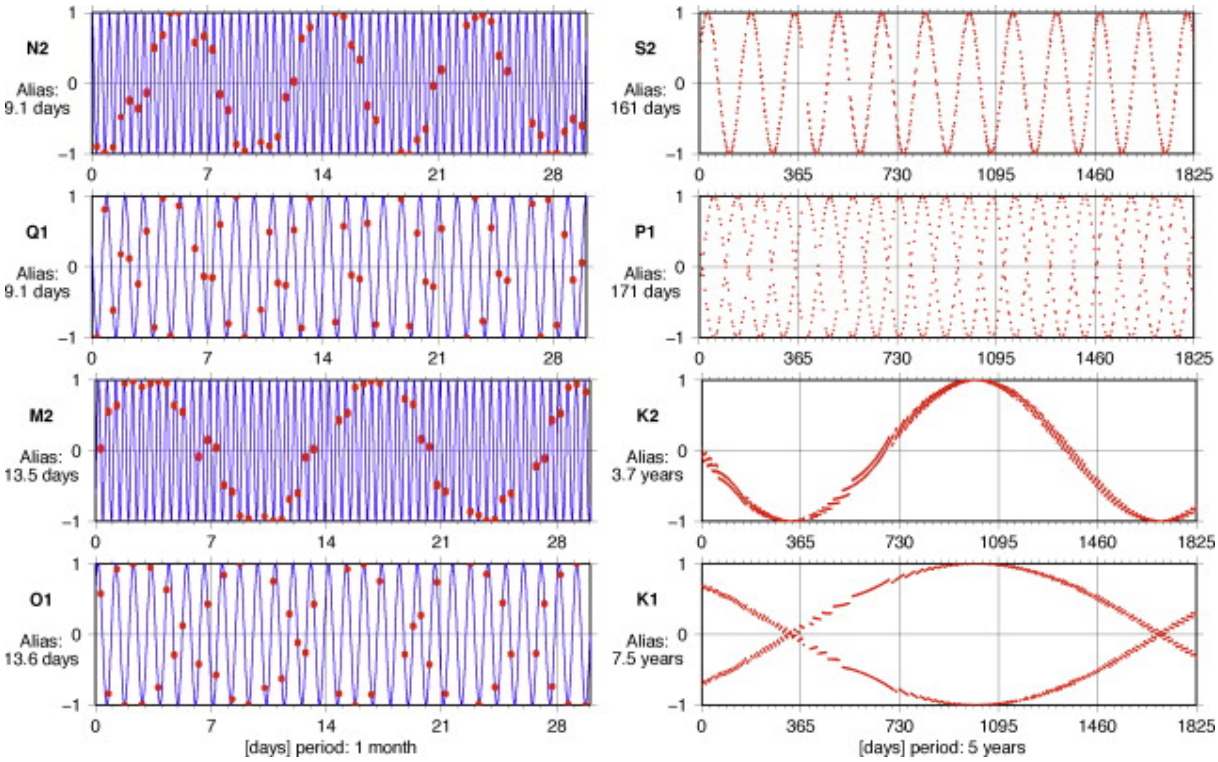

Figure 6.1: GRACE alias periods of different tidal constituents [12, Mayer-Gürr]

GRACE has no exact repeat orbit, so it is not possible to compute the aliasing frequencies of the different tidal constituents using closed formulas. An analysis of the real GRACE orbits is required. Therefore, the local sampling by GRACE during the time span from 2002 until 2016 are compared to the oscillations of the major tides.

The aliasing periods are listed in table 6.1 below.

Table 6.1: GRACE tidal alias frequencies [11]

Darwin notation	**Alias period [d]**
long period waves	
M_m	28
M_f	14
M_{tm}	9
diurnal waves	
Q_1	9.00
O_1	13.60
P_1	171.20
S_1	322.10
K_1	2725.40
semi-diurnal waves	
N_2	9.10
M_2	13.50
S_2	161.00
K_2	1362.70

It can be seen, that the tidal constituent K_1 has the highest aliasing period (7.48 y). Hence at least 8 years of GRACE observations are needed, to compute tides. Caused by a combined estimation together with the monthly solutions is possible.

6.2 Residual tidal constituents from GRACE

First investigations are done over the whole period of available observations from 2002 - 2016. The residual consituents differ in dependency of the frequency band. For instance the results in the long-periodic frequency band are very smooth and the main residuals can be seen in the pole regions and at coastal areas (see figure 6.2) .

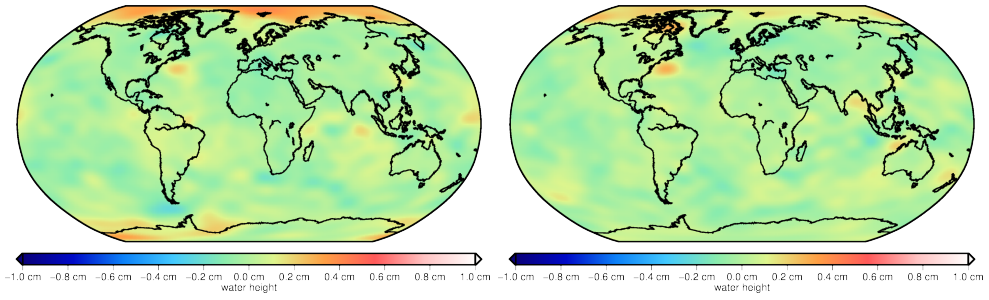

Figure 6.2: tidal constituent (M_f) estimated from GRACE observations during different time-spans (2002 - 2016) from degree 2 up to D/O 30 in terms of equivalent water heights in cosine (left) and sine (right)

Those residuals are reasonable, because for one thing the background model EOT11a is a pure altimetry model - that's why there is no data available at pole regions - and for another thing currents are an issue. In the other frequency bands, the residuals get higher and it looks like the results could be random - particular at the semi-diurnal tidal constituents (see figure 6.3).

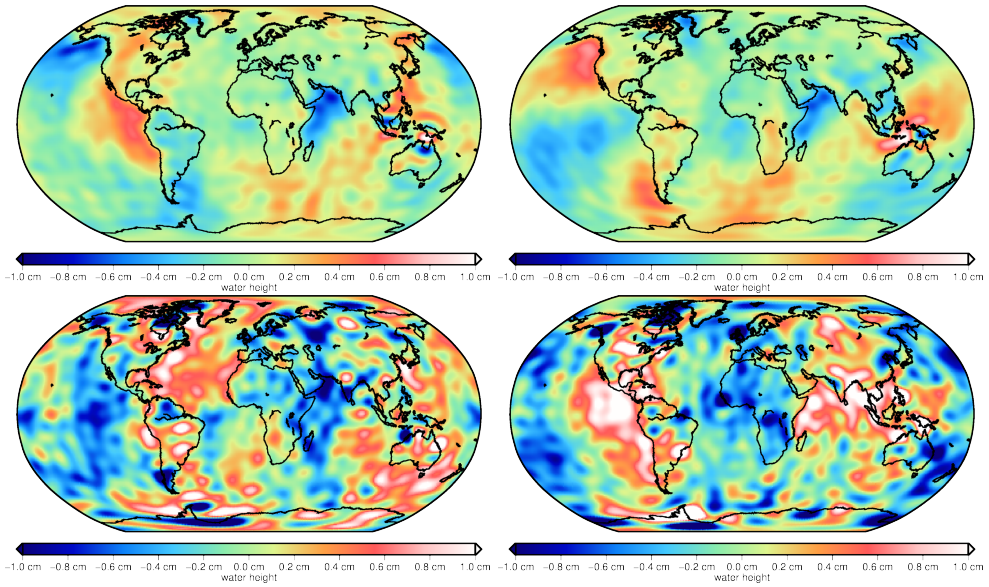

Figure 6.3: tidal constituents (S_1 and S_2) estimated from GRACE observations during 2002 - 2016 from degree 2 up to D/O 30 in terms of equivalent water heights in cosine (left block) and sine (right block)

The results of the semi-diurnal solar tidal constituent S_2 shows much signal/noise along the continents too. To validate the results of 14 years of GRACE observations above, the available dataset got split up in

- even/odd years,
- 2002 - 2008 and
- 2009 - 2016.

This is necessary to find out, if the results are signal or just noise/random. Three tidal constituents are illustrated below (figure 6.4 - 6.6) to show the signals behavior. All estimated residual tidal constituents can be seen in the appendix A.3.

The chosen time-spans consider the tidal aliasing and ensure that the combined estimation is possible.

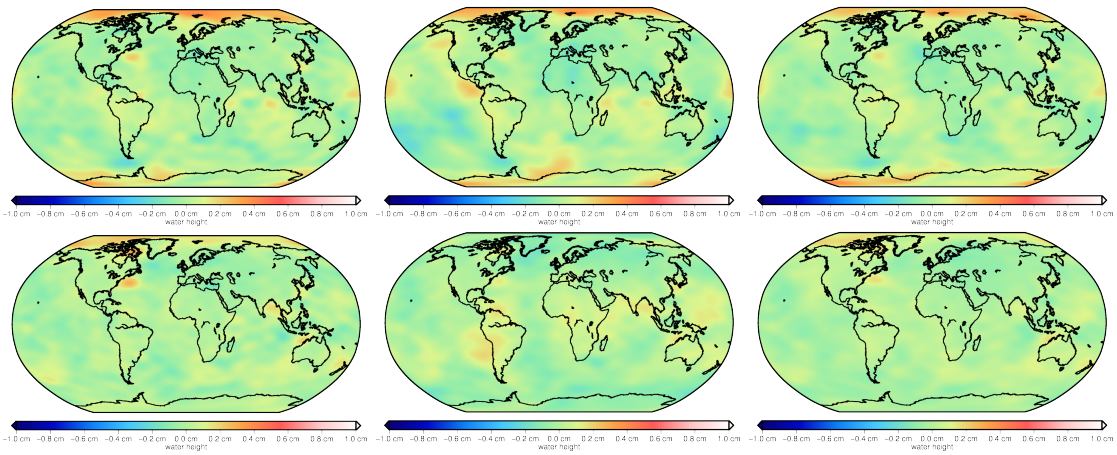

(a) 2002-2016 **(b)** 2009-2016 **(c)** odd years

Figure 6.4: tidal constituent (M_f) estimated from GRACE observations during different time-spans from degree 2 up to D/O 30 in terms of equivalent water heights in cosine (upper block) and sine (lowerblock)

Illustration 6.4 shows residuals estimated from 2002-2016, 2009-2016 and odd years of observations. Caused by similar behavior of the resiudals, although the input data got changed, it can foreshadowed, that the received residuals are actually signals, at least at the long-periodic frequency band.

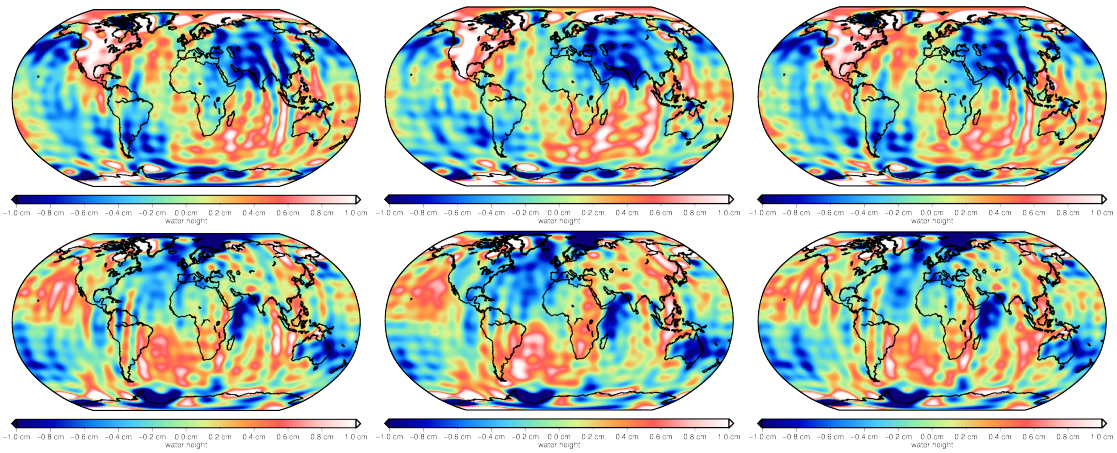

(a) 2002-2016 **(b)** 2009-2016 **(c)** odd years

Figure 6.5: tidal constituent (K_1) estimated from GRACE observations during different time-spans from degree 2 up to D/O 30 in terms of equivalent water heights in cosine (upper block) and sine (lowerblock)

Figure 6.5 shows the behavior of the residuals of the luni-solar diurnal tide K_1. Equally to the semi-diurnal tide S_2 - see illustration 6.3 - the results show inexplicable behavior over the continents. The question above, if it is signal or just random/noise, could be clarified, since the residuals behaviour does not change significant.

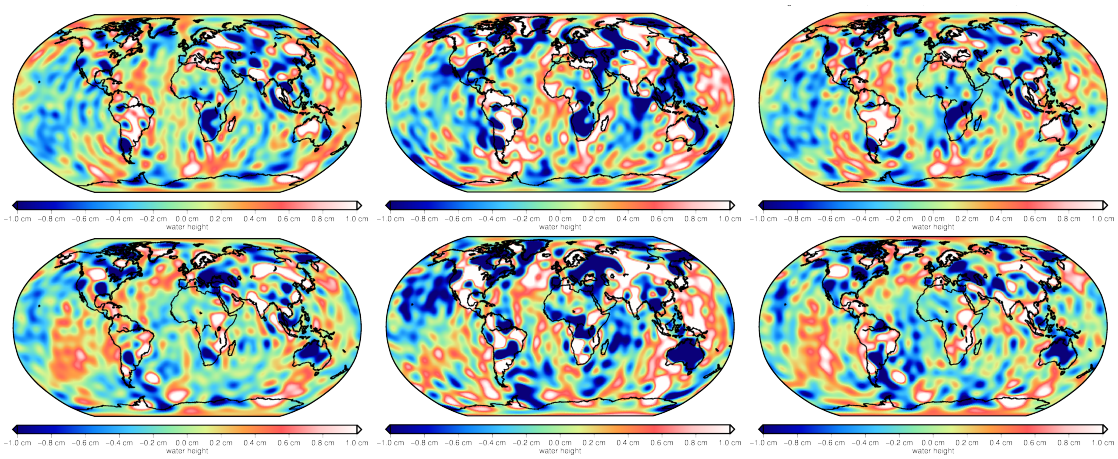

(a) 2002-2016 **(b)** 2009-2016 **(c)** odd years

Figure 6.6: tidal constituent (K_2) estimated from GRACE observations during different time-spans from degree 2 up to D/O 30 in terms of equivalent water heights in cosine (upper block) and sine (lowerblock)

Compared with the the other illustrated tidal residuals, the diurnal luni-solar tide K_2 shows the most random behaviour. The results does not change depending on the input-dataset.

Caused by this results another investigation will be done - estimating tidal constituents exclusive K_2 to see if this single tide sophisticates the other results.

estimating residual tides exclusive K_2 from GRACE observations (2009-2016)

The following subsection deals with the estimation of tidal constituents with GRACE obsverations exclusive K_2 to proof how the signals behaviour change.

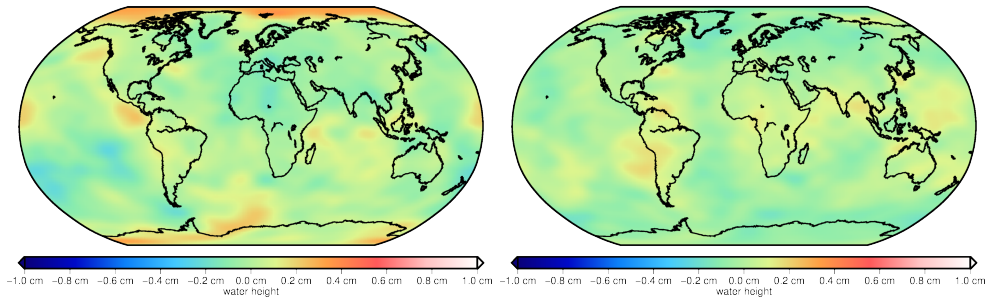

Figure 6.7: tidal constituent (M_f) estimated from GRACE observations during 2009 - 2016 from degree 2 up to D/O 30 in terms of equivalent water heights in cosine (left) and sine (right) with K_2 eliminated from normal equations

At first the long-periodic frequency band has been investigated, because it has the lowest noisy characteristics. As it can be seen in illustration 6.7, there are no changes in the result compared to figure 6.4.

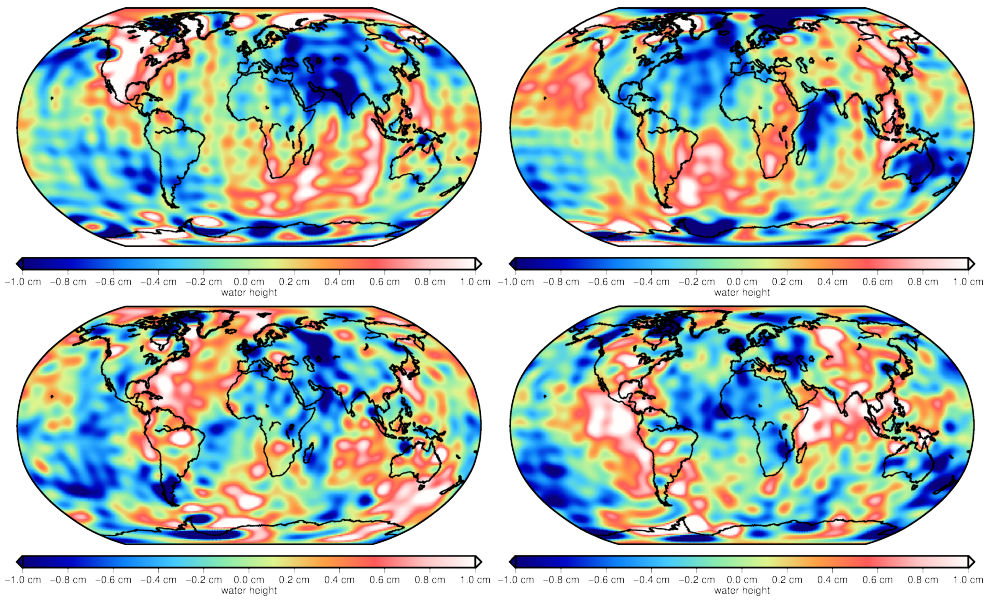

Figure 6.8: tidal constituents (M_f ,K_1 and S_2) estimated from GRACE observations during 2009 - 2016 from degree 2 up to D/O 30 in terms of equivalent water heights in cosine (left block) and sine (right block) with K_2 eliminated from normal equation

The figure shows the tidal constituents K_1 and S_2 estimated with eliminated K_2 tide. Compared to figures 6.5 and 6.3 there are no significant differences. It can be assumed, that the tidal constituent K_2 does not falsify the results.

Furthermore it can be said clearly, that the current signals - in form of residual tidal waves - are not just noise or random, because their behaviour is similar, no matter which combination of GRACE years observations are used as input for computations.

6.3 Validation of the residual constituents w.r.t to FES2014

Since the global ocean-tide model EOT11a is the background model for ocean tides, the results of this chapter are residuals to the EOT11a model up to degree 30^{th}. Those residuals get compared with the differences between the FES2014 and EOT11a model.

The illustrations below show the tidal constituent Q_1 derived by GRACE and for purpose of comparison the differences of the ocean tide models. It implies, that both residuals have the same magnitude and a quite similiar behaviour.

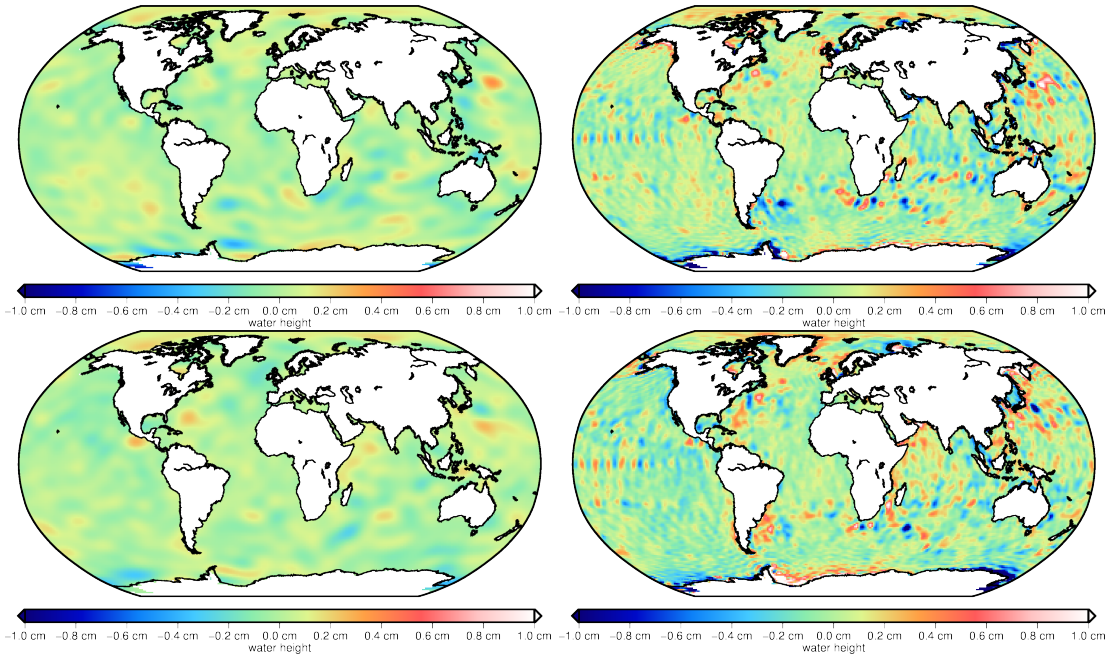

(a) residuals by GRACE **(b)** residuals of ocean tide models

Figure 6.9: residuals of the diurnal tidal constituent Q_1 from GRACE and the observed ocean tide models in cosine (above) and sine (below)

The results yield to the fact, that estimating tidal constituents from GRACE observations are meaningful and should be done to improve the existing model.

Because all other tidal constituents show the same results, just two more tidal constituents are shown exemplaric on the following page. The remaining ones can be seen in the appendix A.3.

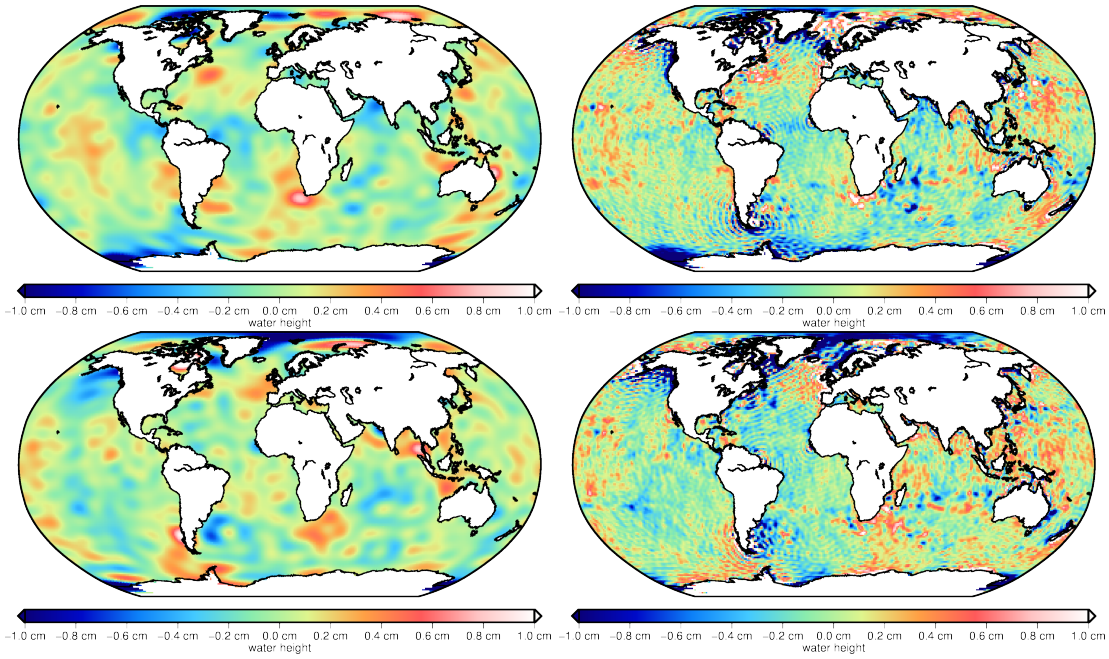

(a) residuals by GRACE **(b)** residuals of ocean tide models

Figure 6.10: residuals of the semi-diurnal tidal constituent N_2 from GRACE and the observed ocean tide models in cosine (above) and sine (below)

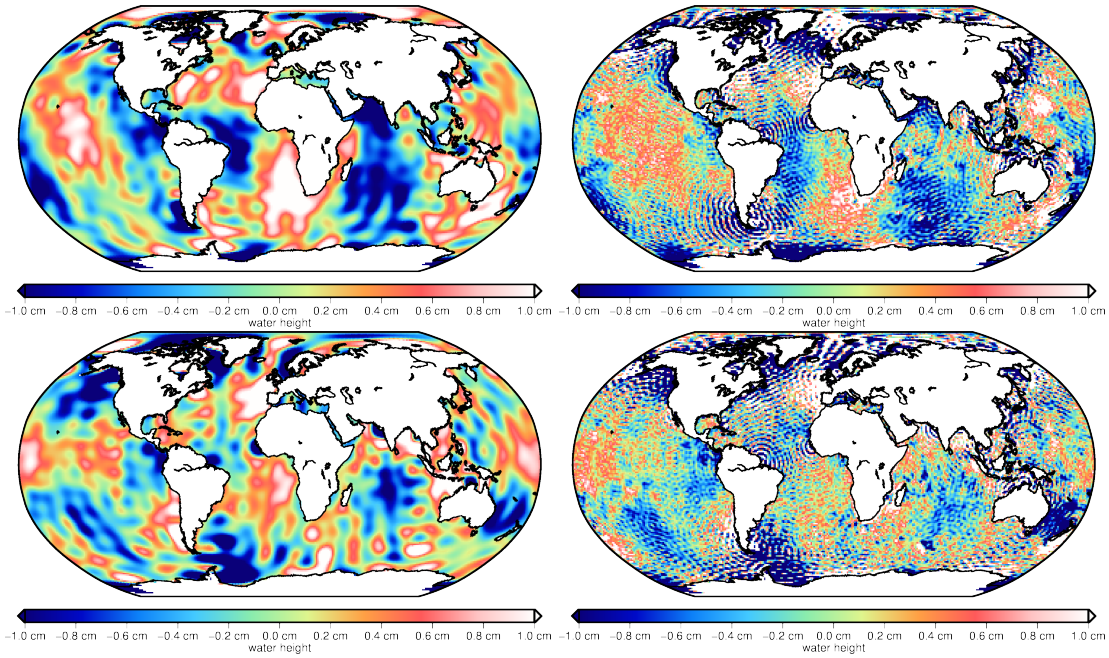

(a) residuals by GRACE **(b)** residuals of ocean tide models

Figure 6.11: residuals of the semi-diurnal tidal constituent M_2 from GRACE and the observed ocean tide models in cosine (above) and sine (below)

7 Summary and Outlook

The objectives of this thesis have been to validate the major tides of the global ocean tide model EOT11a w.r.t. to FES2014 and furhtermore with special respect to the satellite mission GRACE. The second goal of this current work was it to proof if the linear admittance apporach can be improved, since they are representing one of the main error sources of the latest gravity field model [22, ITSG-Grace2016].

In a first step, equivalent water heights are succesfully computed from the given tidal constituents for each global ocean tide model with the allocated software GROOPS. These first investigations show that the EOT11a model should be enhanced for the reason that in the pole regions are less altimeter data available. Moreover the differences compared to FES2014 are larger, since it uses an additional hydrodynamic model for modeling major ocean tides.

The second part of the thesis deals with different methods to determine minor tides. First off, different linear and quadratic admittance approaches are computed by changing the sampling points in form of the respective major tides. It turned out that detailed considerations of the origins of the respective tidal constituents yield to better results. Out of that reason, some minor tides got computed by least square collocation, to examine if the assumption of linearity inside the frequency band is proper. Therefore it was tested how a single minor tide changes, if one major tide gets excluded. The results show clearly, that all major tides do influence one single minor tide and that the approach of admittance should be reconsidered.

In a next step, the major tidal constituents are estimated of GRACE observations from 14 years. These residuals show the same behaviour as the differences between the EOT11a model and the FES2014. Hence it can be clearly said, that a thorough modeling of tidal constituent is fundamental and that GRACE can also see ocean tides, since there are so many years of observations available. To improve the current solution a combined estimation seems to be useful. Also a regional refinement could be considered.

If all available major tides are considered, the determination of minor tides by LSC show good results, even if the defined covariance function does not fit properly for all observed minor tides. More investigations on the analytical covariance are necessary, to be able to predict all minor tides automatically. Also the estimated weighted trend should be adjusted by considering the origins of the respective minor tides in more detail.

The adaption of the ocean tide model by regional refinement can be mentioned as an additional point of view.

List of Acronyms

CB	Celestial Body
DGFI	Deutsches Geodätisches Forschungsinstitut
DLR	Deutsches Zentrum für Luft- und Raumfahrt
EOT	Empirical Ocean Tide Model
EWH	equivalent water height
FES	Finite Element Solution
GPS	Global Positioning System
GRACE	Gravity Recovery and Climate Experiment
GROOPS	Gravity Field Object Oriented Programming System
GST	Greenwich Sideral Time
HW95	Hartmann and Wenzel Tidal catalog
LSC	Least Square Collocation
NASA	National Aeronautic Space Administration
NCDF	Network Common Data Format
RMS	Root Mean Square
SST	Satellite to Satellite Tracking
TGP	Tide Generating Potential

A APPENDIX

A.1 major tides of ocean tide models and their respective differences

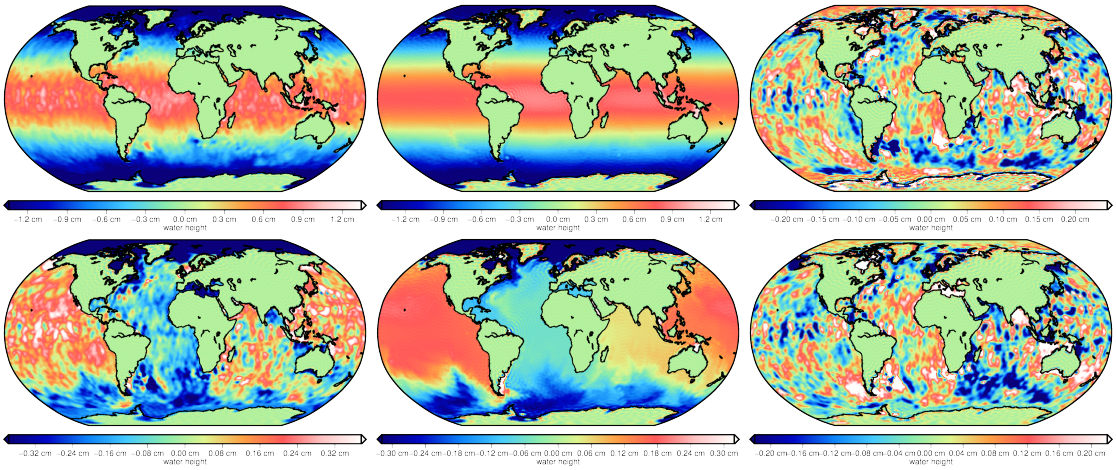

(a) EOT11a **(b)** FES2014 **(c)** differences

Figure A.1: tidal constituent (MM) derived by different ocean tide models in cosine and sine in terms of equivalent water heights

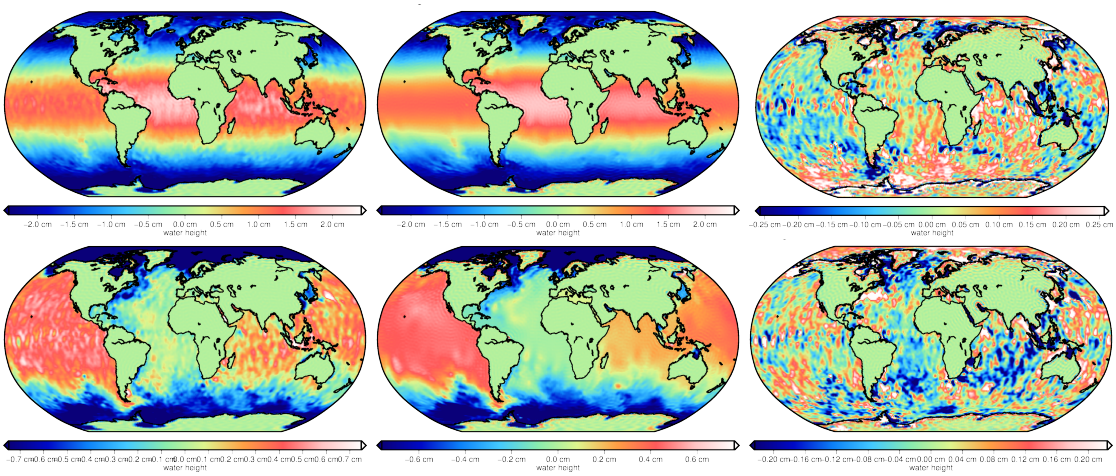

(a) EOT11a **(b)** FES2014 **(c)** differences

Figure A.2: tidal constituent (MF) derived by different ocean tide models in cosine and sine in terms of equivalent water heights

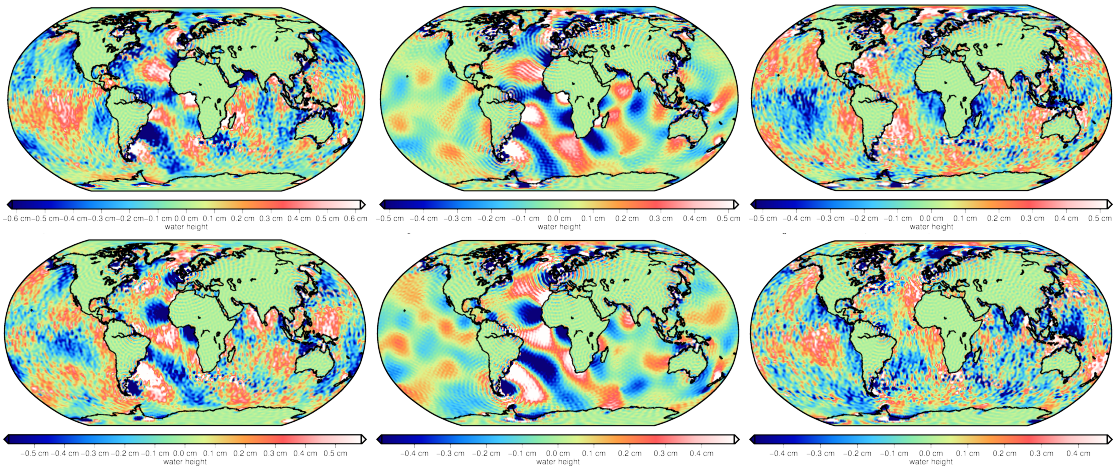

(a) EOT11a **(b)** FES2014 **(c)** differences

Figure A.3: tidal constituent (M_4) derived by different ocean tide models in cosine and sine in terms of equivalent water heights

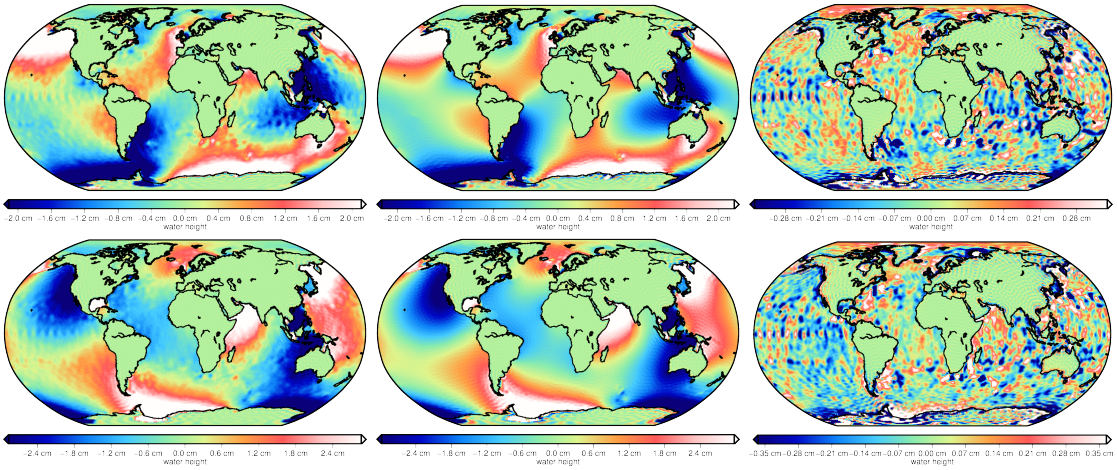

(a) EOT11a **(b)** FES2014 **(c)** differences

Figure A.4: tidal constituent (Q_1) derived by different ocean tide models in cosine and sine in terms of equivalent water heights

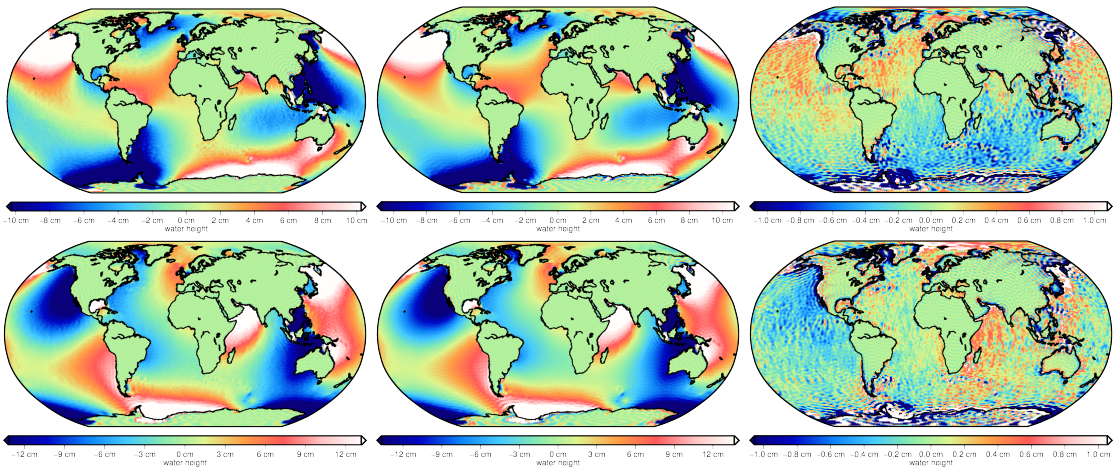

(a) EOT11a **(b)** FES2014 **(c)** differences

Figure A.5: tidal constituent (O_1) derived by different ocean tide models in cosine and sine in terms of equivalent water heights

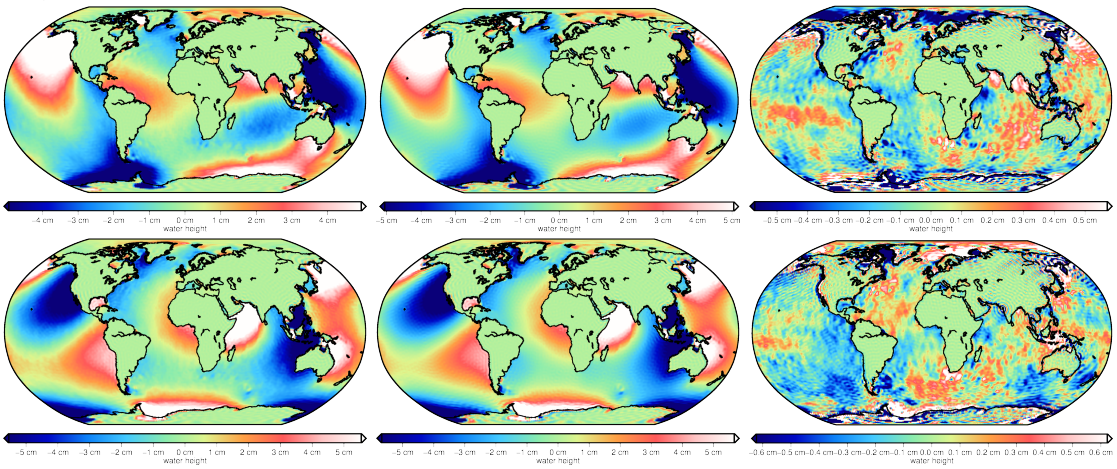

(a) EOT11a **(b)** FES2014 **(c)** differences

Figure A.6: tidal constituent (P_1) derived by different ocean tide models in cosine and sine in terms of equivalent water heights

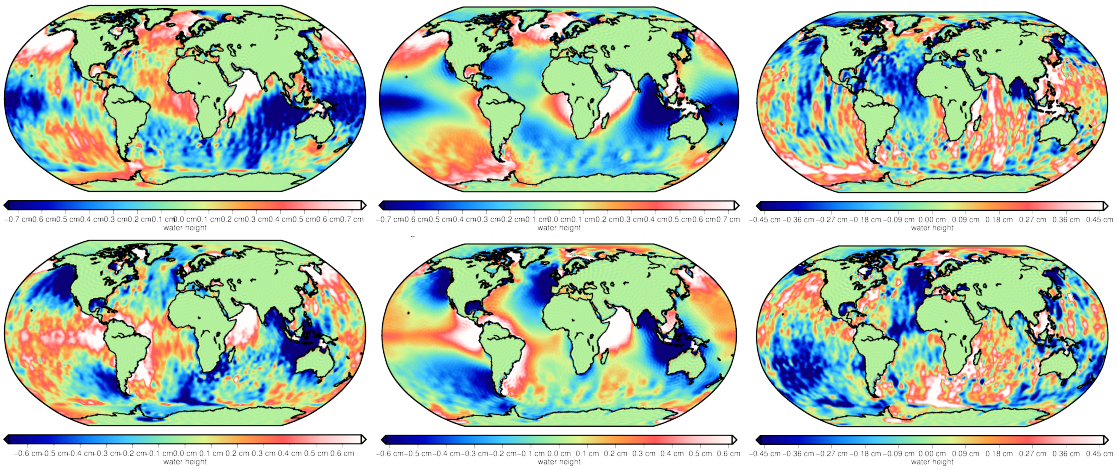

(a) EOT11a **(b)** FES2014 **(c)** differences

Figure A.7: tidal constituent (S_1) derived by different ocean tide models in cosine and sine in terms of equivalent water heights

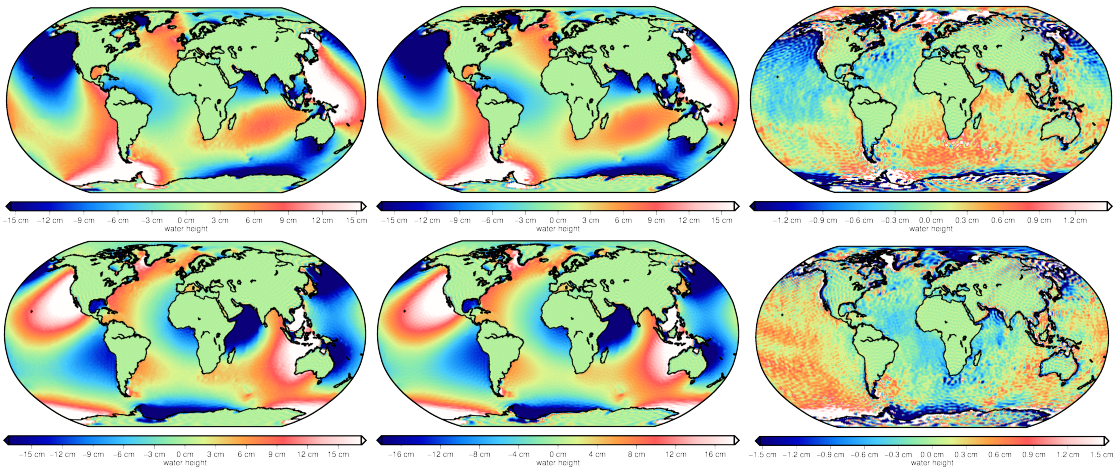

(a) EOT11a **(b)** FES2014 **(c)** differences

Figure A.8: tidal constituent (K_1) derived by different ocean tide models in cosine and sine in terms of equivalent water heights

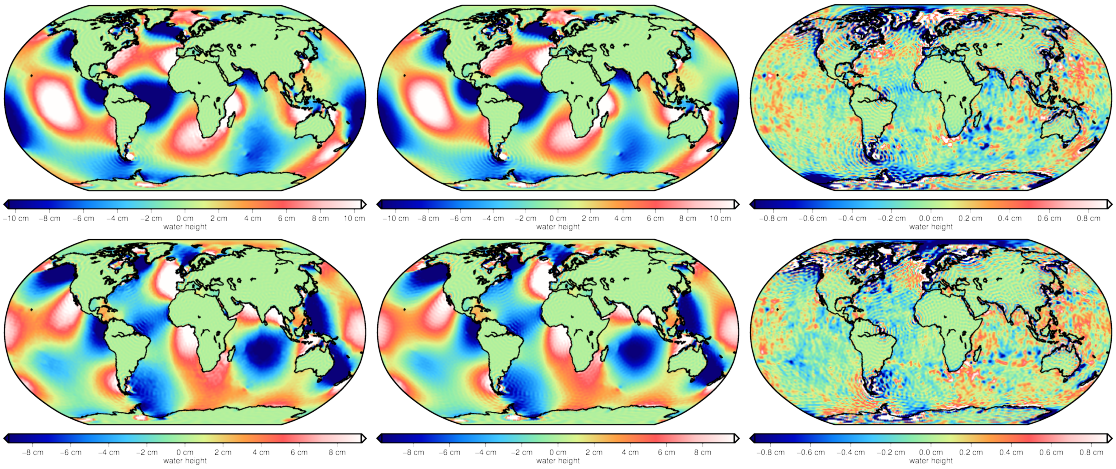

(a) EOT11a **(b)** FES2014 **(c)** differences

Figure A.9: tidal constituent (N_2) derived by different ocean tide models in cosine and sine in terms of equivalent water heights

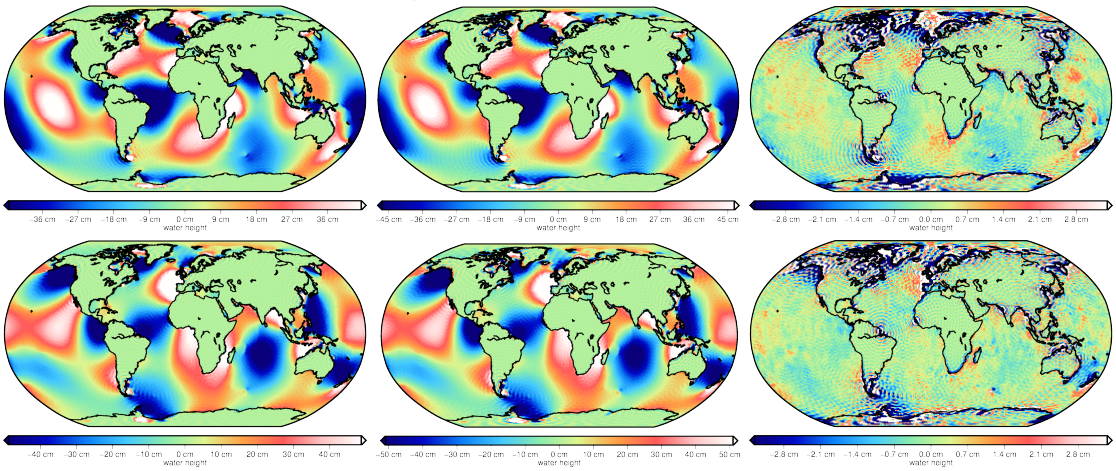

(a) EOT11a **(b)** FES2014 **(c)** differences

Figure A.10: tidal constituent (M_2) derived by different ocean tide models in cosine and sine in terms of equivalent water heights

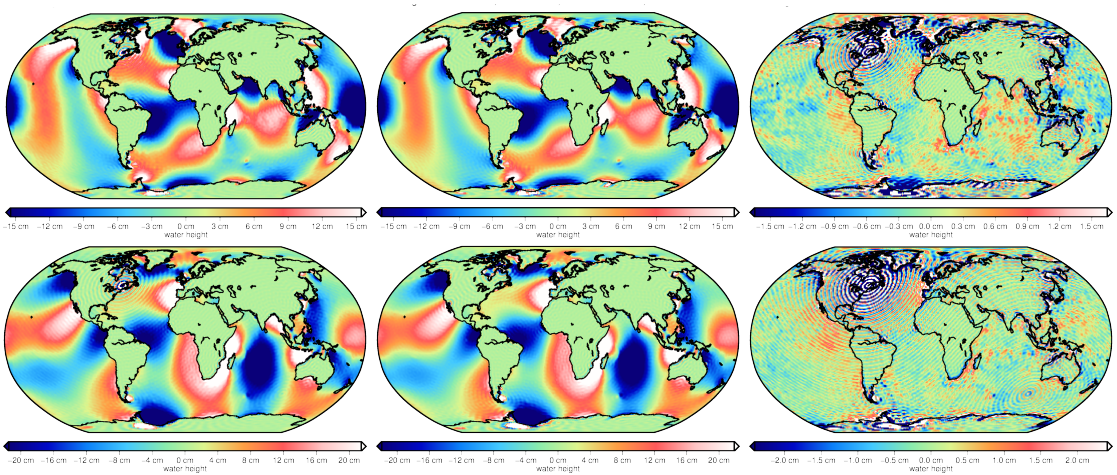

(a) EOT11a **(b)** FES2014 **(c)** differences

Figure A.11: tidal constituent (S_2) derived by different ocean tide models in cosine and sine in terms of equivalent water heights

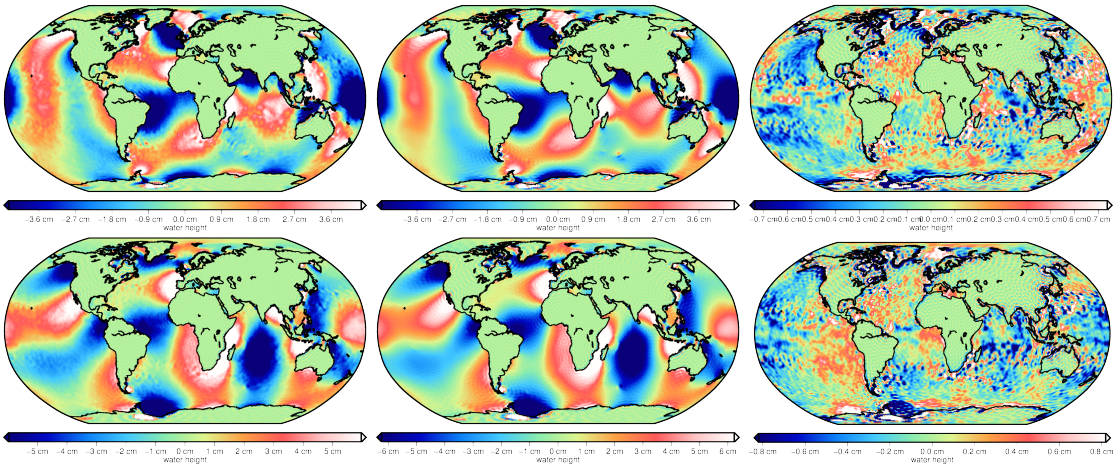

(a) EOT11a **(b)** FES2014 **(c)** differences

Figure A.12: tidal constituent (K_2) derived by different ocean tide models in cosine and sine in terms of equivalent water heights

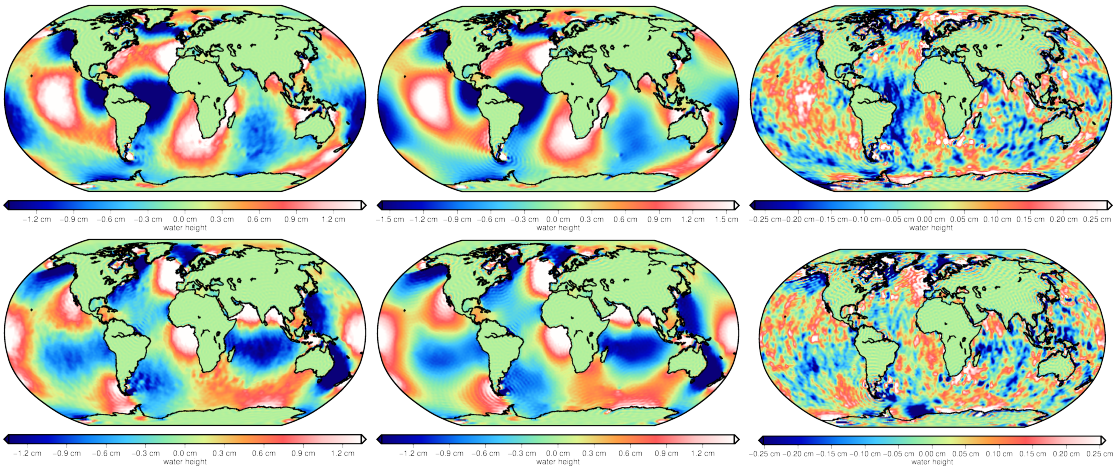

(a) EOT11a **(b)** FES2014 **(c)** differences

Figure A.13: tidal constituent (K_2) derived by different ocean tide models in cosine and sine in terms of equivalent water heights

A.2 minor tides linearly interpolated with FES2014 potential coefficients

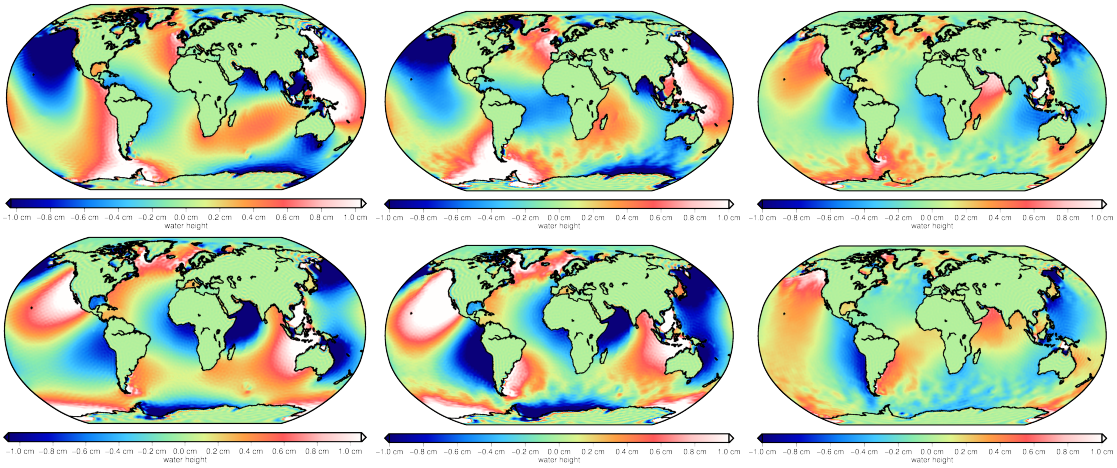

(a) admittance **(b)** FES2014 **(c)** differences

Figure A.14: diurnal constitutent J_1 derived by linear admittance from EOT11a with FES2014 main tides potential coefficients, from FES2014 main tides potential coefficients and their differences in cosine (upper block) and sine (lower block)

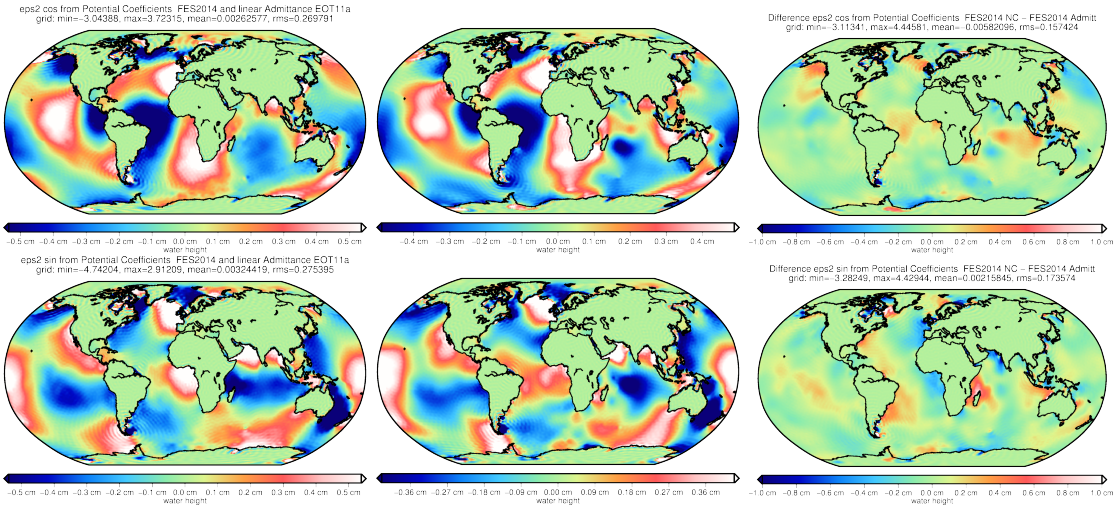

(a) admittance **(b)** FES2014 **(c)** differences

Figure A.15: semi-diurnal constitutent ϵ_2 derived by linear admittance from EOT11a with FES2014 main tides potential coefficients, from FES2014 main tides potential coefficients and their differences in cosine (upper block) and sine (lower block)

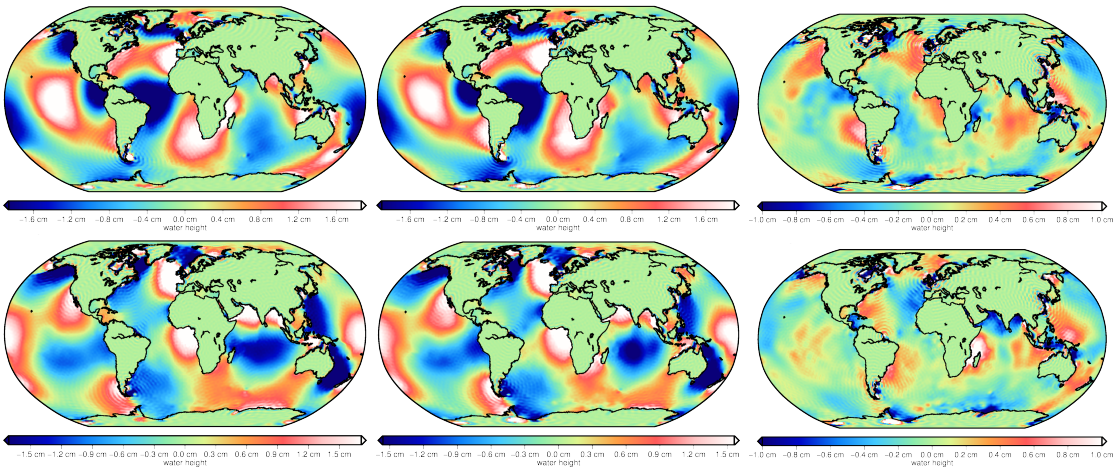

(a) admittance **(b)** FES2014 **(c)** differences

Figure A.16: semi-diurnal constitutent μ_2 derived by linear admittance with FES2014 main tides potential coefficients, from FES2014 main tides potential coefficients and their differences in cosine (upper block) and sine (lower block)

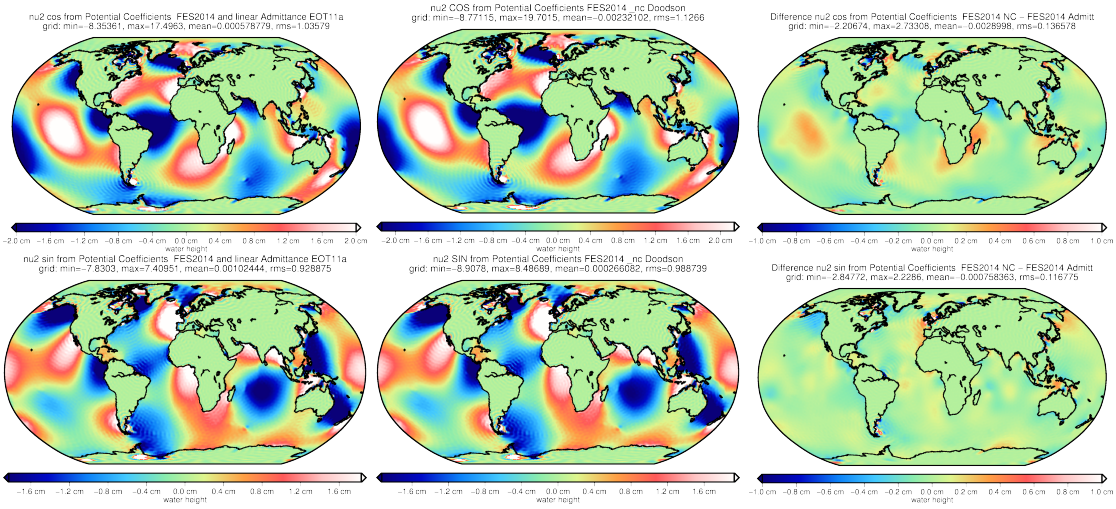

(a) admittance **(b)** FES2014 **(c)** differences

Figure A.17: semi-diurnal constitutent ν_2 derived by linear admittance with FES2014 main tides potential coefficients, from FES2014 main tides potential coefficients and their differences in cosine (upper block) and sine (lower block)

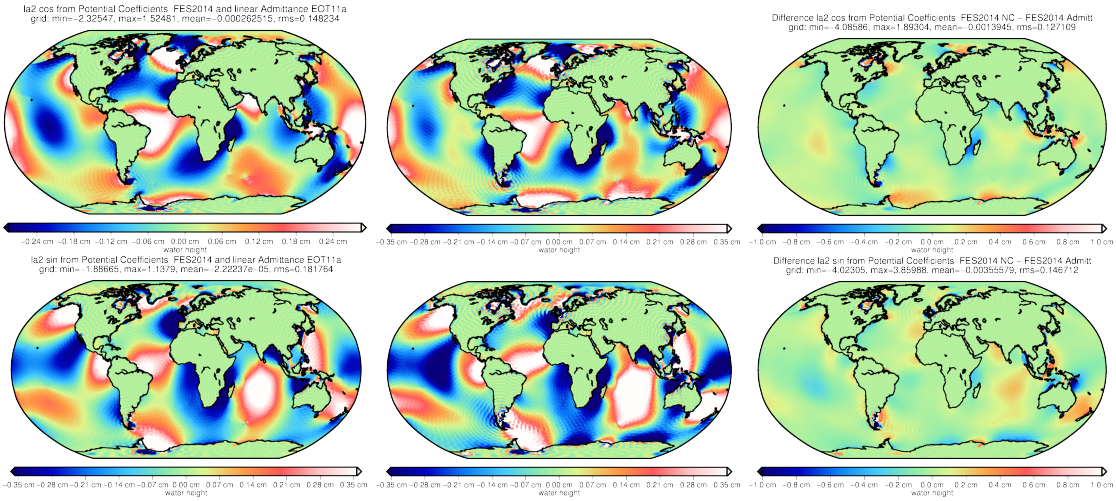

(a) admittance **(b)** FES2014 **(c)** differences

Figure A.18: semi-diurnal constitutent λ_2 derived by linear admittance with FES2014 main tides potential coefficients, from FES2014 main tides potential coefficients and their differences in cosine (upper block) and sine (lower block)

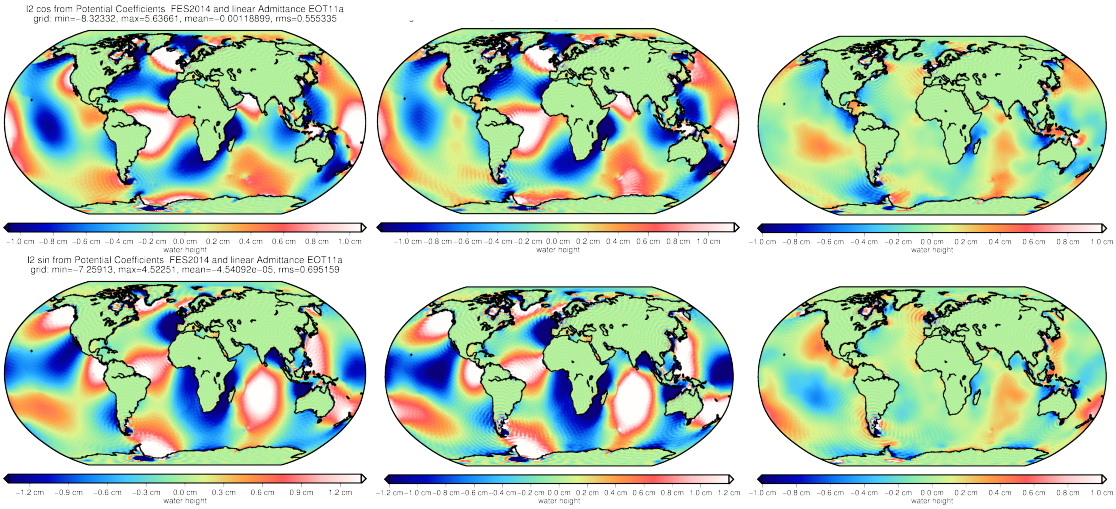

(a) admittance **(b)** FES2014 **(c)** differences

Figure A.19: semi-diurnal constitutent L_2 derived by linear admittance with FES2014 main tides potential coefficients, from FES2014 main tides potential coefficients and their differences in cosine (upper block) and sine (lower block)

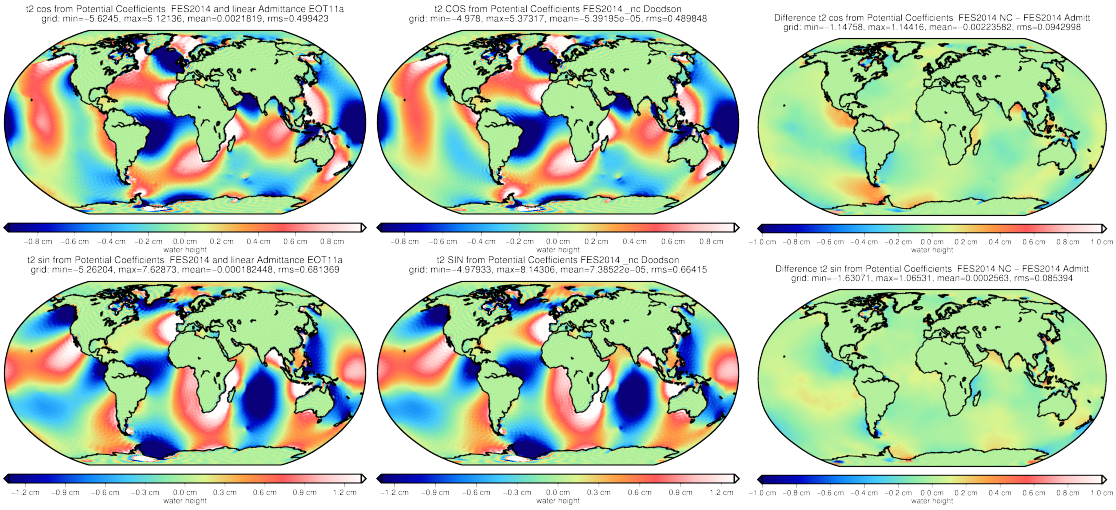

(a) admittance **(b)** FES2014 **(c)** differences

Figure A.20: semi-diurnal constitutent T_2 derived by linear admittance with FES2014 main tides potential coefficients, from FES2014 main tides potential coefficients and their differences in cosine (upper block) and sine (lower block)

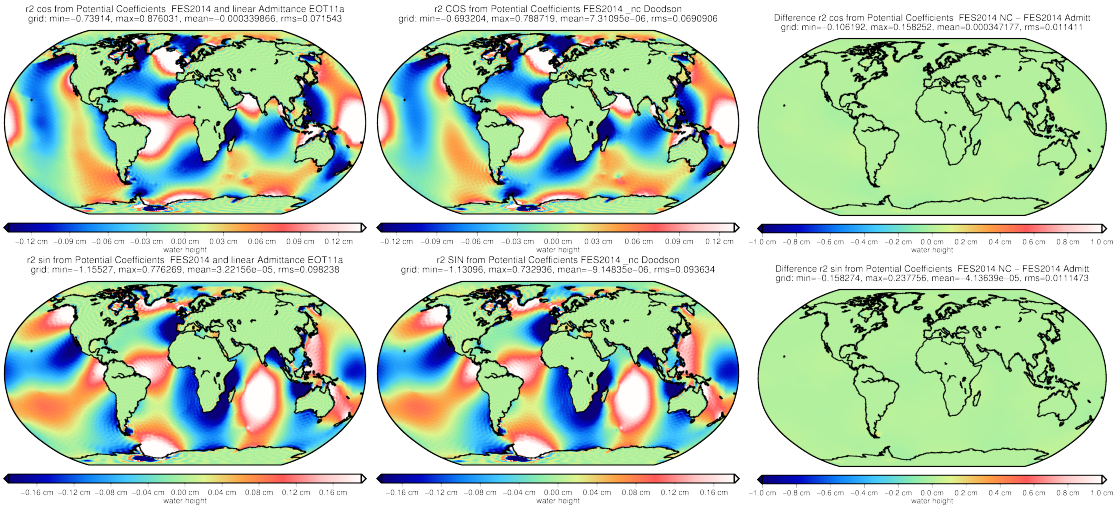

(a) admittance **(b)** FES2014 **(c)** differences

Figure A.21: semi-diurnal constitutent T_2 derived by linear admittance with FES2014 main tides potential coefficients, from FES2014 main tides potential coefficients and their differences in cosine (upper block) and sine (lower block)

A.3 residual tidal constituents estimated from GRACE observations (2002-2016)

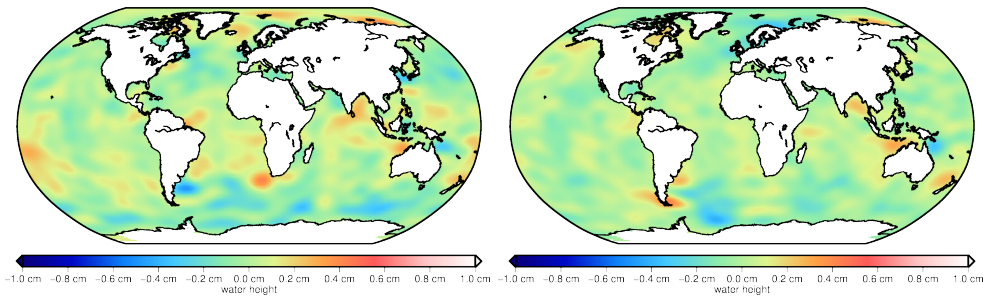

Figure A.22: residual tidal constituents (MM) estimated from GRACE observations during 2002 - 2016 from degree 2 up to D/O 30 in terms of equivalent water heights in cosine (left block) and sine (right block)

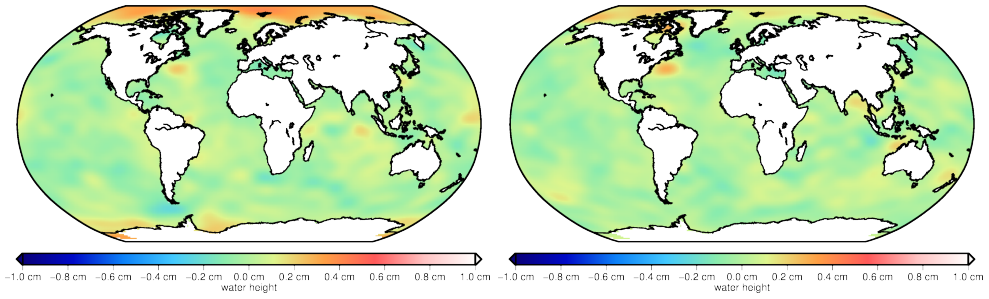

Figure A.23: residual tidal constituents (MF) estimated from GRACE observations during 2002 - 2016 from degree 2 up to D/O 30 in terms of equivalent water heights in cosine (left block) and sine (right block)

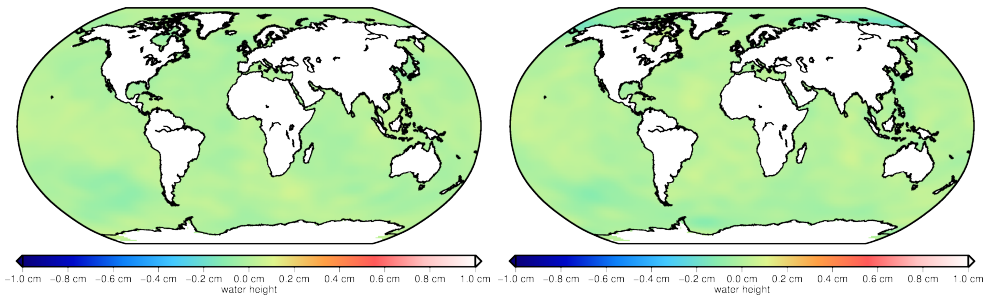

Figure A.24: residual tidal constituents (MTM) estimated from GRACE observations during 2002 - 2016 from degree 2 up to D/O 30 in terms of equivalent water heights in cosine (left block) and sine (right block)

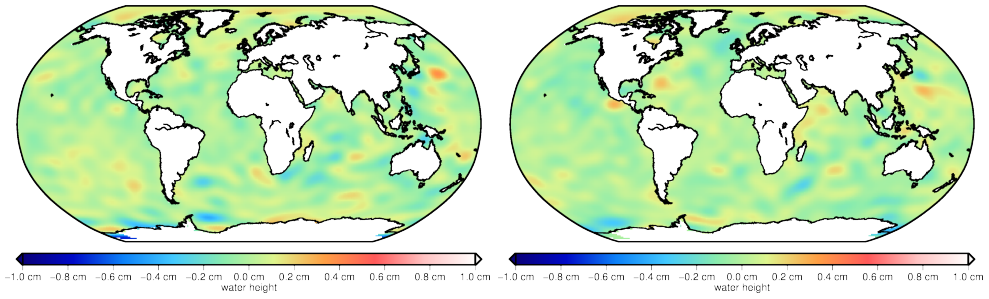

Figure A.25: residual tidal constituents (Q_1) estimated from GRACE observations during 2002 - 2016 from degree 2 up to D/O 30 in terms of equivalent water heights in cosine (left block) and sine (right block)

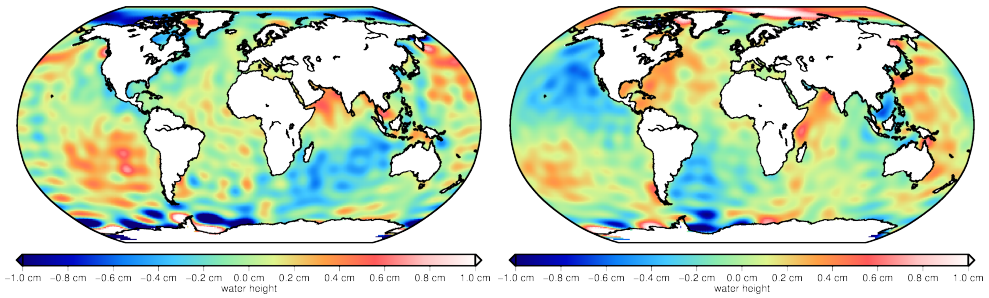

Figure A.26: residual tidal constituents (O_1) estimated from GRACE observations during 2002 - 2016 from degree 2 up to D/O 30 in terms of equivalent water heights in cosine (left block) and sine (right block)

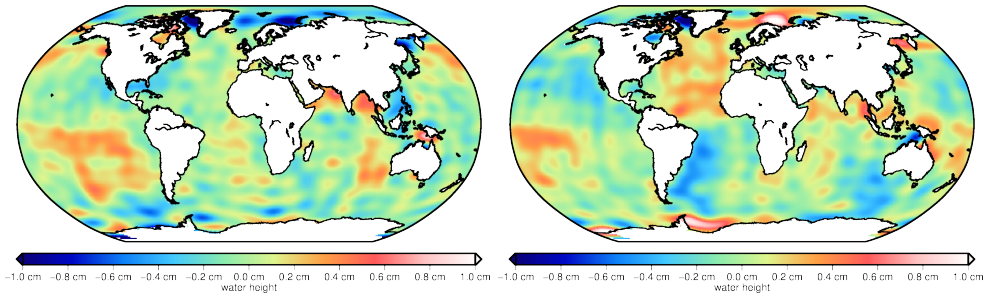

Figure A.27: residual tidal constituents (P_1) estimated from GRACE observations during 2002 - 2016 from degree 2 up to D/O 30 in terms of equivalent water heights in cosine (left block) and sine (right block)

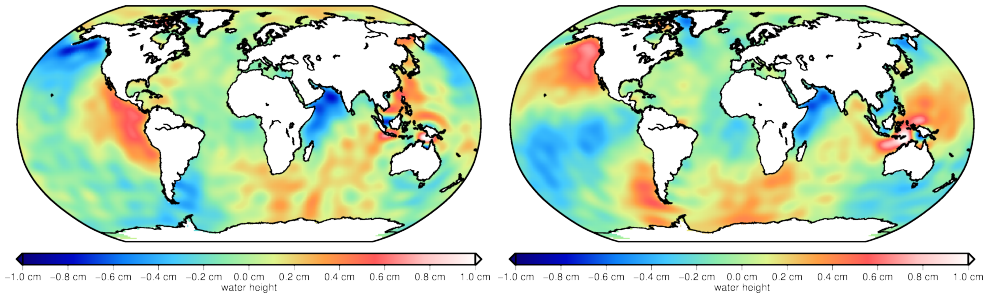

Figure A.28: residual tidal constituents (S_1) estimated from GRACE observations during 2002 - 2016 from degree 2 up to D/O 30 in terms of equivalent water heights in cosine (left block) and sine (right block)

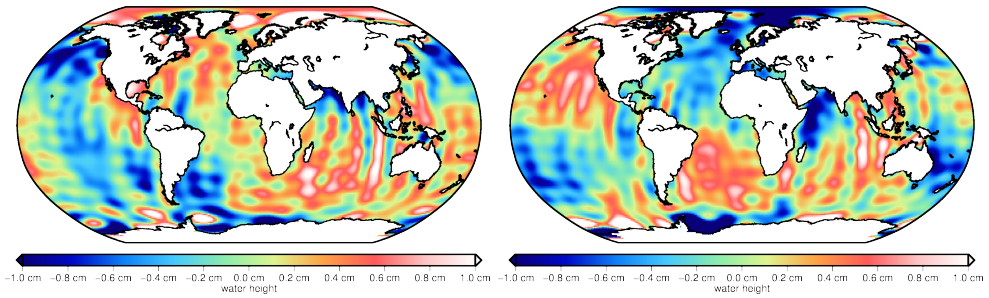

Figure A.29: residual tidal constituents (S_1) estimated from GRACE observations during 2002 - 2016 from degree 2 up to D/O 30 in terms of equivalent water heights in cosine (left block) and sine (right block)

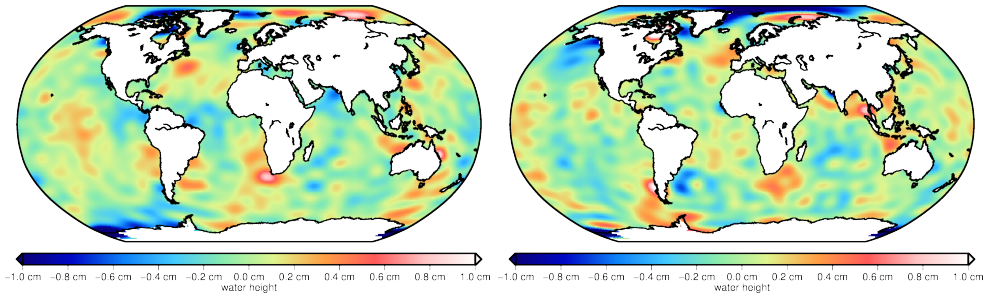

Figure A.30: residual tidal constituents (N_2) estimated from GRACE observations during 2002 - 2016 from degree 2 up to D/O 30 in terms of equivalent water heights in cosine (left block) and sine (right block)

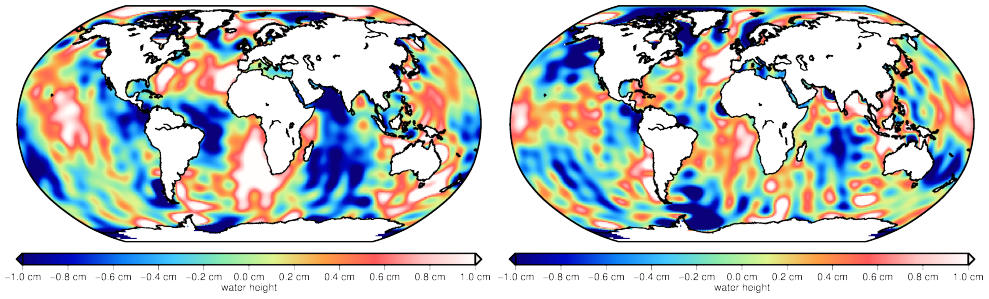

Figure A.31: residual tidal constituents (M_2) estimated from GRACE observations during 2002 - 2016 from degree 2 up to D/O 30 in terms of equivalent water heights in cosine (left block) and sine (right block)

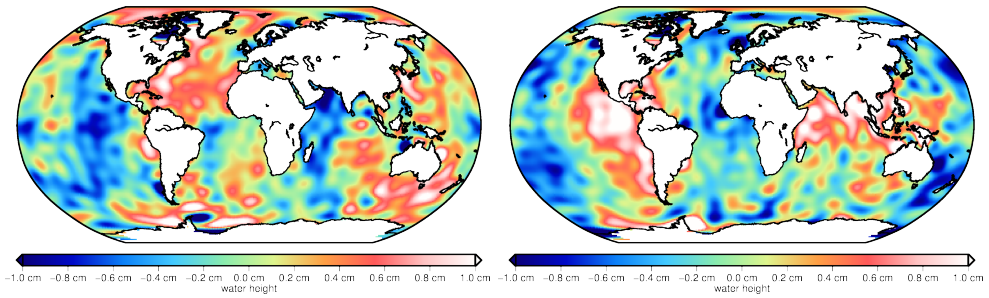

Figure A.32: residual tidal constituents (S_2) estimated from GRACE observations during 2002 - 2016 from degree 2 up to D/O 30 in terms of equivalent water heights in cosine (left block) and sine (right block)

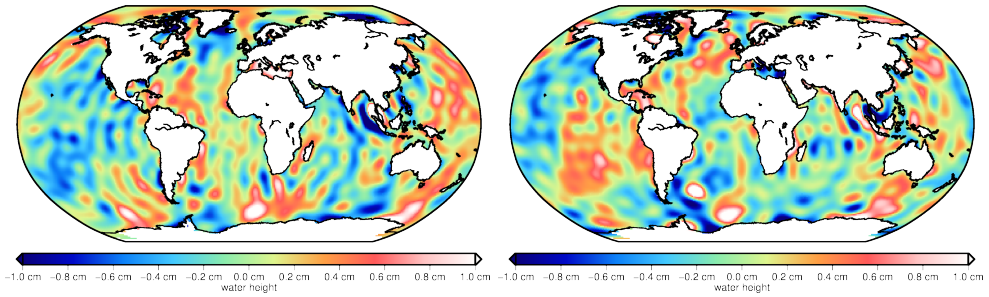

Figure A.33: residual tidal constituents (K_2) estimated from GRACE observations during 2002 - 2016 from degree 2 up to D/O 30 in terms of equivalent water heights in cosine (left block) and sine (right block)

List of Figures

List of Tables

References

[1] Allein D. J., (2012) *TUGOm Tidal ToolBox. CNES/CLS, LEGOS. France.*

[2] Baur O., (2012) *Lecture Notes of GGOS. TU Graz.*

[3] Baur O., (2002) *Ozeangezeitenlösungen aus Bahnstörungen erdnaher Satelliten. Diplomarbeit, Geodätisches Institut der Universität Stuttgart.*

[4] Cartwright D. E., (1978) *Oceanic Tides. Insitute of Oceanographic Sciences, Bidston, Birkenhead, England.* .

[5] Doodson A.T. (1921) *The Harmonic Development of the Tide Generating Potential. Proceedings of the Royal Society of London. Series A. Volume 100, Issue 704* .

[6] Dow J. M. (1988), *Ocean Tides and Tectonic Plate Motions from Lageos. Deutsche Geodätische Kommission, Reihe C(344)*

[7] Hartmann T., Wenzel H.-G., (1995) *The HW95 Tidal Potential Catalogue. Bulletin d'Informations Marees Terrestres* .

[8] Hofmann-Wellenhof B., Moritz H. (1971) *Physical Geodesy.*

[9] Madzak Matthias (2016) *Short periodic ocean tide variations in Earth rotationg, geowissenschaftliche Mitteilung, Heft Nr.97*

[10] Mayer-Gürr T.; Behzadpour S., Ellmer M., Kvas A., Klinger B., Zehentner N. (2016) *ITSG-Grace2016 - Monthly and Daily Gravity Field Solutions from GRACE. GFZ Data Services. http://doi.org/10.5880/icgem.2016.007.*

[11] Mayer-Gürr,T., (2014) *Lecture Notes of Geophysics and Geodynamics. TU Graz.*

[12] Mayer-Gürr,T., Savcenko R., Bosch W., Daras I., Flechtner F. Dahle Ch. (2011) *Ocean tides from satellite altimetry and GRACE. Journal of Geodynamics.*

[13] Mayer-Gürr,T., (2006) *Gravitationsfeldbestimmung aus der Analyse kurzer Bahnbögen am Beispiel der Satellitenmissionen CHAMP und GRACE. Dissertation Universität Bonn*

[14] Moritz H. (1980) *Advanced Physical Geodesy. Karlsruhe: Wichtmann*

[15] Na S., Baek J. (2011) *Computation of the Load Love Number and the Load Green's Function for an Elastic and Spherically Symmetric Earth. Journal of the Korean Physical Society, Vol. 58, No. 5*

[16] Petit G., Luzum B. (2010), *IERS Conventions. IERS Technical Note No. 36. Verlag des Bundesamts für Kartographie und Geodäsie, Frankfurt am Main*

[17] Rieser D., Mayer-Gürr T., Savcenko R., Bosch W., Wünsch J., Dahle C., Flechtner F., (2011) *The ocean tide model EOT11a in spherical harmonics representation . Technical Note. Special Priority Program SPP125 'Mass transport and mass distribution in the system Earth' funded by the Deutsche Forschungsgemeinschaft (DFG).*

[18] Roosbeek F. (1994), *RATGP95: a harmonic development of the tide-generating potentiail using an analytical method. Geophysical Journal International, Vol.126*

[19] Savcenko R., Bosch W. (2012) *EOT11a - Empirical ocean tide model from multi-mission satellite altimetry. DGFI Report No.89*

[20] Schureman P. (1971), *Manual of harmonic analysis and prediction of tides, Special Publication No.98, U.S.: Department of Commerce, Coast and geodetic survey*

[21] Torge W. (2001), *Geodesy. Third completely revised and extended editon. Walter de Gruyter Verlag*

[22] Tapley, B. D., S. Bettadpur, M. Watkins, and C. Reigber (2004) *The gravity recovery and climate experiment: Mission overview and early results. Geophysical Research Letters 31, pp. 9607–+..*

[23] United Kingdom Hydrographic Office, (2006) *Harmonic Constants Product Specification. United Kingdom Hydrographic Office.*

[24] Wilhelm H., Zürn W-, Wenzel H.-G., (1997) *Tidal Phenomena.Lecture Notes in Earth Sciences, Springer Verlag .*